TECHNISCHE UNIVERSITÄT MÜNCHEN

- WISSENSCHAFTSZENTRUM WEIHENSTEPHAN -
LEHRSTUHL FÜR BIOTECHNOLOGIE DER NUTZTIERE

THE ROLE OF EGFR / KRAS DOWNSTREAM TARGETS MEK, EGR1 AND KLF5 IN PANCREATIC CANCER INITIATION AND PROGRESSION

THOMAS K. K. BRIEL

Vollständiger Abdruck der von der Fakultät Wissenschaftszentrum Weihenstephan für Ernährung, Landnutzung und Umwelt der Technischen Universität München zur Erlangung des akademischen Grades eines

DOKTORS DER NATURWISSENSCHAFTEN

genehmigten Dissertation.

Vorsitzender:	Univ.-Prof. Dr. H. Luksch
Prüfer der Dissertation:	1. Univ.-Prof. A. Schnieke, PhD
	2. apl. Prof. Dr. J. Th. Siveke

Die Dissertation wurde am 07.07.2014 bei der Technischen Universität München eingereicht und durch die Fakultät Wissenschaftszentrum Weihenstephan für Ernährung, Landnutzung und Umwelt am 17.12.2014 angenommen.

In der Wissenschaft gleichen wir alle nur den Kindern, die am Rande des Wissens hie und da einen Kiesel aufheben, während sich der weite Ozean des Unbekannten vor unseren Augen erstreckt.

Sir Isaac Newton

ABSTRACT

Pancreatic ductal adenocarcinoma (PDAC) is one of the most aggressive tumours known and incurable to this day. Hence, understanding key signalling pathways of PDAC development is critical for identification of potential therapy approaches. Recently, EGFR was found to be essential for $KRAS^{G12D}$ driven MEK activation, thus *Egfr* ablation blocks PDAC initiation as a result of abolished MEK - ERK signalling. This work was focussed on MEK as well as on two target genes of the MEK - ERK pathway, EGR1 and KLF5, and investigated their specific role during PDAC initiation and progression.

The impact of MEK was elucidated by characterising mice with pancreas-specific expression of dominant active MEK1DD. Here, sustained MEK activity enhances early PDAC precursor lesion formation. Long-term studies revealed that lesion progression is halted at an age of three to six months, thus *Mek1DD* mice do not develop tumour during their life span. Consequently, it was shown that MEK - ERK signalling alone is not sufficient for progression to PDAC, suggesting a necessity of additional factors, such as mutated P53, ultimately driving precursor lesions towards tumour formation.

EGR1, previously reported as being cancer related and a direct downstream target of the MEK - ERK pathway in other tissues, was characterised in various mouse models. Not only was the mentioned mode of regulation verified within the pancreas, but also could it be shown that EGR1 expression is closely related to early metaplastic events - in mice as well as in men. While $Egr1^{KO}$ pancreata were healthy even after long-term analysis, *Egr1* ablation led to accelerated PDAC formation in a $Kras^{G12D}$-based genetic mouse model. During the search for mechanisms causing these tumour suppressing characteristics, it was shown that both EGFR and Cytokeratin 19 are directly regulated via EGR1 in the pancreas. The latter one was found coexpressed with Amylase in normal acinar tissue during several experimental setups as a direct result of an *Egr1* knockout. Given this coexpression of acinar and ductal markers, these cells were suggested to represent an intermediate state, consequently identifying increased cellular plasticity caused by *Egr1* knockout as one central putative mechanism driving PDAC formation in an activating factor expressing environment.

The transcription factor KLF5 was investigated as a putative mediator of EGR1. Contrary to what has been reported in other murine tissues, KLF5 is not a target of EGR1 in the pancreas. However, regulation of KLF5 via the EGFR - MEK - ERK pathway could be verified and expression dynamics in PDAC precursor lesions suggest that KLF5 may be involved in ductal differentiation.

ZUSAMMENFASSUNG

Das duktale Adenokarzinom (PDAC) ist einer der aggressivsten bekannten Tumore und bis heute unheilbar. Ein tieferes Verständnis der Hauptregulationswege der PDAC Entwicklung ist somit unabdingbar für die Identifikation möglicher Therapieansätze. EGFR wurde kürzlich als essentiell für die $KRAS^{G12D}$ vermittelte MEK Aktivierung beschrieben - folgerichtig blockiert eine *Egfr* Deletion die PDAC Initiation. Die vorliegende Arbeit fokussiert sich auf MEK sowie auf zwei weitere Mitglieder des MEK - ERK Signalweges, EGR1 und KLF5, und untersucht deren spezifische Rolle während der PDAC Initiation und Progression.

Der Einfluss von MEK wurde durch die Charakterisierung von Mäusen untersucht, welche das dominantaktive MEK1DD Protein pankreasspezifisch exprimieren. Die permanente MEK Aktivität beschleunigte die Entstehung früher Vorläuferläsionen von PDAC. Langzeitstudien zeigten, dass die Fortschreitung der Läsionen nach drei bis sechs Monaten zum Stillstand kommt, also *Mek1DD* Mäuse während ihres Lebens keine Tumore entwickeln. Somit wurde gezeigt, dass die MEK - ERK Signalübermittlung nicht für die PDAC Entstehung ausreicht, sondern zusätzliche Faktoren, wie etwa mutiertes P53, hierfür nötig sind.

EGR1, bereits zuvor mit Krebs in Verbindung gebracht und als ein direktes Ziel des MEK - ERK Signalweges beschrieben, wurde eingehend in mehreren Mausmodellen charakterisiert. Es wurde nicht nur die zuvor genannte Art der Regulation im Pankreas bestätigt, sondern auch gezeigt, dass die EGR1 Expression eng mit frühen metaplastischen Ereignissen verbunden ist - in der Maus wie im Menschen. Während $Egr1^{KO}$ Pankreata auch nach Langzeitanalysen gesund waren, führte eine Deletion von EGR1 in einem $Kras^{G12D}$-basierten Mausmodell zu beschleunigter PDAC Entstehung. Auf der Suche nach Mechanismen dieser Effekte konnte gezeigt werden, dass EGFR und Cytokeratin 19 im Pankreas direkt durch EGR1 reguliert werden. Letzteres wurde in vielen experimentellen Aufbauten als direkte Folge einer *Egr1* Deletion in normalen Azini mit Amylase koexprimiert vorgefunden. Diese Koexpression azinärer und duktaler Marker ließ auf einen Zwischenzustand schließen und somit wurde eine erhöhte zelluläre Plastizität als ein möglicher, zentraler Mechanismus der PDAC Entstehung identifiziert.

Der Transkriptionsfaktor KLF5 wurde als möglicher Mittler von EGR1 untersucht. Entgegen dessen, was für andere Organe veröffentlicht wurde, wird KLF5 im Pankreas nicht durch EGR1 reguliert. Jedoch wurde eine Regulation von KLF5 durch den EGFR - MEK - ERK Signalweg bestätigt und die Expressionsdynamik in PDAC Vorläuferläsionen legt nahe, dass KLF5 eng mit duktaler Differenzierung verbunden sein könnte.

TABLE OF CONTENTS

LIST OF FIGURES

LIST OF TABLES

ABBREVIATIONS

A	adenine
ABC	avidin-biotin complex
ADM	acinar-ductal metaplasia
AFL	atypical flat lesions
&	and
AP	acute pancreatitis
APS	ammonium persulphate
approx.	approximately
ATP	adenosine triphosphate
BCA	bicinchoninic acid
bp	basepair(s)
BPE	bovine pituitary extract
BSA	bovine serum albumin
C	cytosine
Ca	calcium
CAAC	centroacinar-acinar compartment
cDNA	complementary deoxyribonucleic acid
CK19	Cytokeratin 19
Cl	chloride
CO_2	carbon dioxide
CP	crossing point
Cre	Causes Recombination
Cu	copper
Cys	cysteine
°C	degree Celsius
Da	Dalton
DAB	diaminobenzidine
DAPI	diamidinophenylindole
ddH_2O	double destilled water
DMEM	Dulbecco`s Modified Eagle`s Medium
DMSO	dimethyl sulfoxide
DNA	deoxyribonucleic acid
dNTP	deoxyribonucleotide triphosphate
E	embryonic day
E. coli	*escherichia coli*
EDTA	ethylenediaminetetraacetic acid
EGF	Epidermal Growth Factor
EGFP	Enhanced Green Fluorescent Protein
EGFR	Epidermal Growth Factor Receptor
EGR1	Early Growth Response 1
EMT	epithelial to mesenchymal transition

ERK	Extracellular Signal Regulated Kinase
et al.	*et alii*
EtOH	ethanol
FCS	fetal calf serum
g	gram / gravitational acceleration
G	guanine
GDP	guanosine diphosphate
GTP	guanosine triphosphate
h	hour(s)
H	hydrogen
H_2O	water
His	histidine
HRP	horseradish peroxidase
HSP90	Heat Shock Protein 90
i.p.	intraperitoneal
IPMN	intraductal papillary-mucinous neoplasm
k	kilo
kb	kilo basepairs
KLF5	Krüppel-Like Factor 5
KRAS	Kirsten Rat Sarcoma Viral Oncogene Homolog
L	liter(s)
LB	lysogeny broth
LiCl	lithium chloride
*lox*P	locus of crossing over, bacteriophage P1
m	milli ($\cdot 10^{-3}$) / meter(s)
M	mega ($\cdot 10^{6}$) / molar
µ	micro ($\cdot 10^{-6}$)
MCN	mucinous cystic neoplasm
MEK	Mitogen Activated Protein Kinase Kinase
Mg	magnesium
min	minute(s)
MUC5	Mucin 5
n	nano ($\cdot 10^{-9}$)
NaCl	sodium chloride
NaOH	sodium hydroxide
NDLB	non-denaturing lysis buffer
NEAA	non-essential amino acids
NES	nuclear export signal
NLS	nuclear localisation signal
NP-40	Nonidet P-40 octyl phenoxypolyethoxylethanol
o/n	over night
p	piko ($\cdot 10^{-12}$) / phosphorylated
P48	Tumour Protein 48
P53	Tumour Protein 53

P110	Tumour Protein 110
PanIN	pancreatic intraepithelial neoplasia
PBS	phosphate buffered saline
PBS-T	phosphate buffered saline with Triton X-100
PCR	polymerase chain reaction
PCNA	proliferating cell nuclear antigen
PDA	pancreatic ductal adenocarcinoma
%	percent
PFA	paraformaldehyde
pH	*potentia hydrogenii*
polyA	poly adenosine
PCNA	proliferating cell nuclear antigen
PFA	paraformaldehyde
PTF1A	Pancreas Transcription Factor 1 Subunit Alpha
qPCR	quantitative real-time polymerase chain reaction
RIPA	radio immunoprecipitation assay
RNA	ribonucleic acid
rpm	rounds per minute
RT	room temperature
RT-PCR	reverse transcriptase polymerase chain reaction
SBTI	soybean trypsin inhibitor
SDS	sodium dodecyl sulphate
sec	second(s)
ssDNA	single stranded deoxyribonucleic acid
SUMO	small ubiquitin-like modifier
T	thymine
TAE	tris-acetate-EDTA
TBS	tris buffered saline
TBS-T	tris buffered saline with Triton X-100
TEMED	tetramethylethylenediamine
TGFα	Transforming Growth Factor Alpha
tris	tris(hydroxymethyl)aminomethane
U	unit
V	volt

1 INTRODUCTION

1.1 THE PANCREAS

1.1.1 Morphology and Function

The pancreas is a hormone and enzyme secreting organ and part of the human gastrointestinal tract (figure 1.1). It is located in the abdominal cavity adjacent to the duodenum and spleen, and can be macroscopically differentiated into two areas. The broad, duodenum-linked part is designated as the pancreatic head, whereas the part connected to the spleen is denominated as the pancreatic tail (Pan and Wright, 2011). On the cellular level, the pancreas can be subdivided into two major domains, the endocrine and the exocrine pancreas. The endocrine part consists of the islets of Langerhans, which hold five different cell types: glucagon-secreting α-cells, insulin-secreting β-cells, somatostatin-releasing δ-cells, ghrelin-producing ε-cells and pancreatic polypeptide-secreting PP-cells. These hormones are secreted into surrounding blood vessels and regulate glucose homeostasis (Edlund, 2002; Prado *et al.,* 2004). The exocrine part on the other hand consists of acinar cells, which are arranged in

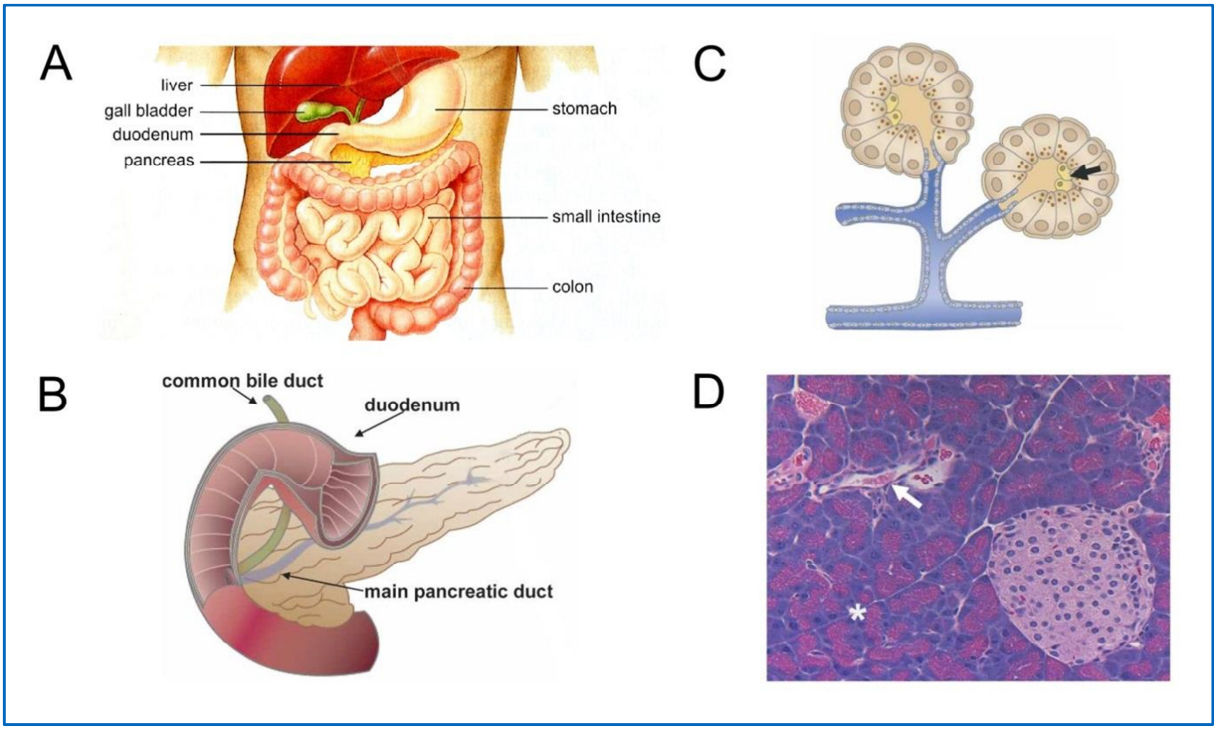

Figure 1.1: The pancreas. (A) The human gastrointestinal tract, schematic (from: Campbell and Reece, 2006). **(B)** Anatomy of the pancreas, with adjacent duodenum and common bile duct, schematic. **(C)** Acinar subunit, schematic. The figure illustrates acini and related ducts; the arrow denotes centroacinar cells. **(D)** Histology of a murine wild type pancreas. An islet of Langerhans can be seen on the right side; the asterisk denotes acini, the arrow points to a duct (B – D adapted from: Hezel, 2006).

digestive enzymes secreting clusters. These enzymes are transported to the duodenum through ducts pervading the pancreas and participate in nutrient digestion; duct cells themselves also actively secrete mucins and bicarbonate (Slack, 1995). Hence, the pancreas is an important compartment of the digestive system and essential for maintenance of many metabolic functions. However, given its central role, genetic alterations within pancreatic cells often give rise to severe illnesses such as diabetes, pancreatitis or pancreatic cancer.

1.1.2 Organogenesis

The basis of pancreatic organogenesis is laid very early in embryonic development. On the molecular level, a variety of complex genetic interdependencies take place which are often bound to a specific point of time. Expression of proteins in specific cell types and at strictly defined stages of development is critical; hence, these molecular mechanisms are highly conserved throughout vertebrates (McCracken and Wells, 2012). In several species it has been shown that NODA1, a main endoderm-promoting factor, plays a central role during early developmental events. Its gradient decides whether a cell lineage will form endoderm or exoderm, thus promoting endoderm fate if NODA1 is highly expressed (Kubo *et al.,* 2004; Shen, 2007). The endoderm itself is subsequently patterned as anterior and posterior, forming the foregut (figure 1.2). The posterior part of the foregut gives rise to several organs, among these liver and pancreas. In the mouse, important pathways exhibiting posterior effects are WNT, FGF and BMP (Wells and Melton, 2000). While embryonic development advances, the fate of distinct cell domains is decided by the expression of key regulators, thus giving rise to the different organs. During this process, the pancreatic buds develop from both the ventral and dorsal foregut, induced by differing mechanisms (figure 1.3). Important hallmarks of dorsal pancreatic budding are the repression of *Sonic Hedgehog*, which exhibits a pancreas inhibiting effect (Hebrok *et al.,* 1998; Mfopou *et al.,* 2007) and the induction of *Ptf1a*, an important pancreas

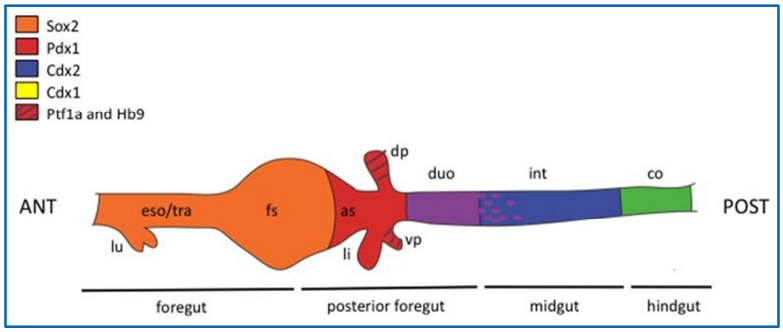

Figure 1.2: Anterior and posterior patterning of the digestive tract. Expression of transcription factors is illustrated by specific colours. Purple indicates coexpression of PDX1 and CDX2, green coexpression of CDX1 and CDX2. Abbreviations: ANT: anterior; POST: posterior; as: antral stomach; co: colon; dp: dorsal pancreas; duo: duodenum; eso: esophagus; fs: forestomach; int: intestine; li: liver; lu: lung; tra: trachea; vp: ventral pancreas (from: Moody *et al.,* 2009).

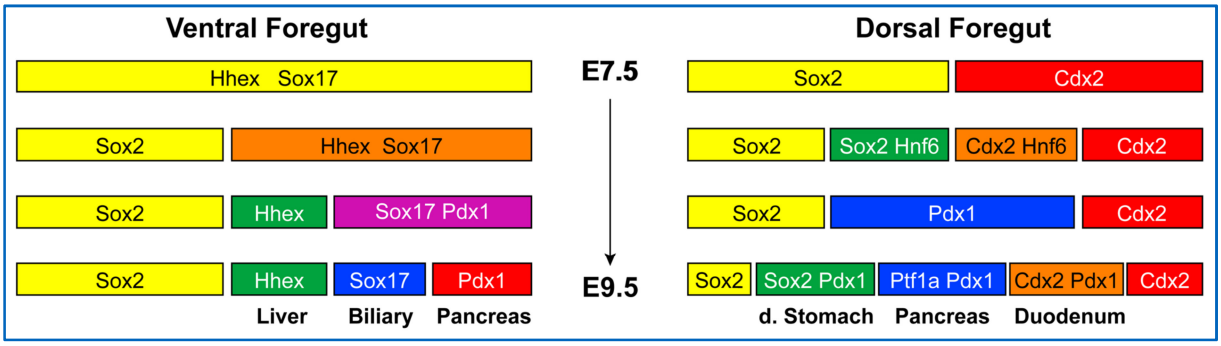

Figure 1.3: Lineage segregation in the ventral and dorsal foregut from E7.5 to E9.5. *Pdx1* expression drives progenitor cells to pancreatic differentiation in both the ventral and dorsal foregut. Additional *Ptf1a* expression is necessary in the dorsal foregut (from: McCracken and Wells, 2012).

promoting factor (Yoshitomi and Zaret, 2004). The cell fate within the ventral foregut is mainly defined by expression of *Hhex* (Bort *et al.,* 2004) and pancreas budding is promoted by expression of *Pdx1* (McCracken and Wells, 2012). The development of the murine pancreas takes place from approx. E9.5 (embryonic day 9.5) on, at which the dorsal foregut endoderm begins to thicken and the ventral pancreatic anlage begins to form. The pancreatic developmental stage between E9.5 and E12.5 is designated as the primary transition, which is characterised by proliferation of pancreatic progenitor cells, microlumen formation and rotation of the gut tube, which approximates the dorsal and ventral pancreatic buds (Kopp *et al.,* 2011; Pan and Wright, 2011). Subsequently, the epithelium is segregated into "tip" and "stalk" domains, which coevally defines the fate of the pancreatic progenitor cells (figure 1.4). The cells within the "tip" become multipotent pancreatic progenitor cells, while the "stalk" harbours endocrine and duct progenitor cells (Zhou *et al.,* 2007). From approx. E13.5 to E16.5, the epithelium undergoes the second transition, a phase of extensive differentiation processes. The multipotent progenitor cells located at the "tip" give now rise to acinar cells, while the progenitor cells at the "stalk" give rise to ducts as well as to endocrine cells via a process designated as epithelial to mesenchymal transition (EMT; Rukstalis and Habener, 2007). Thus, by the end of this phase, all three pancreatic cell lineages have evolved, which further expand by continued differentiation of progenitors and mitosis of differentiated cells. This process retains after birth until the mice have reached their mature size (Desai *et al.,* 2007).

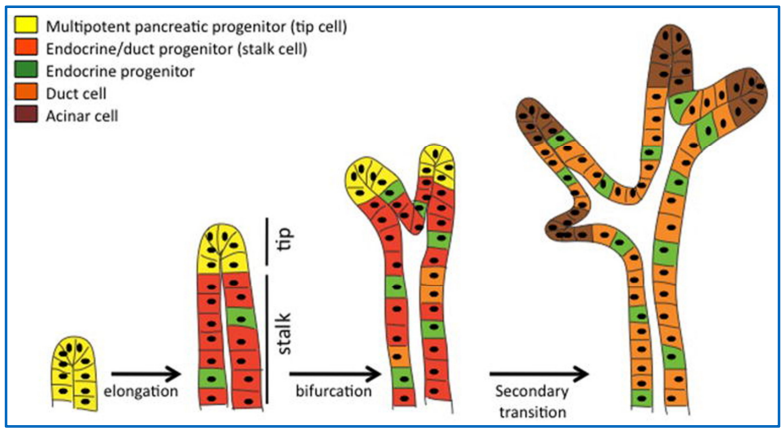

Figure 1.4: The location of pancreatic progenitor cells during morphogenesis. Cells at the "tip" (yellow) become acinar cells (brown), while endocrine and duct progenitors (red) at the "stalk" form endocrine (green) and duct (orange) cells (from: Moody *et al.,* 2009).

1.2 PANCREATIC CANCER AND PRECURSORS

1.2.1 Acute Pancreatitis

Acute pancreatitis (AP) is an inflammatory disease of the exocrine pancreas. Symptoms are abdominal pain, tenderness in the upper abdomen, more than 3-fold elevated levels of digestive enzymes in serum or urine, as well as AP typical ultrasonographic or radiologic abnormalities (Otsuki, 2013). Mild cases can be cured by intravenous rehydration, while severe cases may require surgical interventions. Depending on the severity of the disease, AP can be lethal even if treated (Kota *et al.,* 2013). The most common causes are gallstones (approx. 38 %) and alcohol (approx. 36 %), but also diabetes mellitus, smoking, lysosomal or autophagic dysfunction and, if in combination with other factors, a prolonged fatty and protein rich diet can lead to AP (Wang, 2009; Sadr-Azodi *et al.,* 2012; Barreto *et al.,* 2012). Furthermore, there is evidence that genetic risk factors may also contribute to AP, such as premature trypsinogen activation caused by gain-of-function mutations in the trypsinogen gene *Prss1*, or by loss-of-function mutations in the pancreatic trypsinogen inhibitor gene *Spink1* as well as in the trypsin degrading enzyme gene *Ctrc* (Larusch and Whitcomb, 2012). On the cellular level, AP leads to acinar cell damage (figure 1.5), release of digestive enzymes, migration of neutrophils into damaged tissue and other inflammatory events (Schoenberg *et al.,* 1995). The human disease can be mimicked in murine models by induction of AP via treatment with cerulein, a cholecystokinin analogue. Intraperitoneal (i.p.) administration of cerulein leads to transient interstitial pancreatitis within one hour after the first injection, with a fast recovery of the damaged tissue if the treatment is stopped (Adler *et al.,* 1979). Furthermore, it has been shown that cerulein induced AP significantly enhances the formation of both acinar-ductal metaplasia (ADM) and pancreatic ductal adenocarcinoma (PDAC), thus being an important model for studying underlying molecular events crucial for development of early pancreatic cancer precursors (Carrière *et al.,* 2009; Morris *et al.,* 2010).

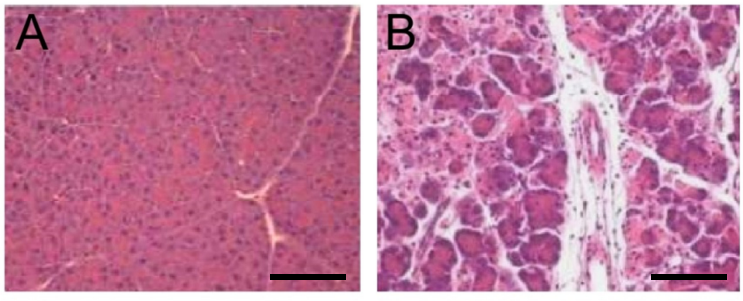

Figure 1.5: Acute pancreatitis. (A) Histology of a murine wild type pancreas. **(B)** Histology of a murine wild type pancreas treated with 12 hourly injections of 50 µg/kg bodyweight of cerulein intraperitoneal. The mouse was sacrificed one hour after the last injection. The pancreas exhibits acinar cell destruction and necrosis. Scale bar represents 50 µm (adapted from: Weylandt *et al.,* 2008).

1.2.2 Acinar-Ductal Metaplasia

Conversion or replacement of one differentiated cell type with another is referred to as metaplasia. During acinar-ductal metaplasia (ADM), pancreatic acinar cells undergo genetic reprogramming and transdifferentiate to pancreatic duct cells (figure 1.6 B), which is believed to be an important step towards forming precursor lesions of pancreatic cancer (Means, 2005). ADM can be initiated by a variety of factors, such as inflammatory events like acute and chronic pancreatitis as well as genetic mutations (Reichert and Rustgi, 2011). In this regard, both murine model organisms and studies using *ex vivo* acinar explants provide important insights into mechanisms underlying ADM formation. For example, it has been shown that the TGFα / EGFR pathway is critical during ADM formation (Song *et al.,* 1999; Means *et al.,* 2003). There is furthermore strong evidence that ADM can give rise to pancreatic intraepithelial neoplasia. Thus, genetic alterations found in ADM are of particular interest for investigating molecular mechanisms leading to formation of these lesions (Reichert and Rustgi, 2011).

1.2.3 Pancreatic Intraepithelial Neoplasia

Pancreatic intraepithelial neoplasia (PanIN) represents the most common precursor lesion of PDAC and is believed to derive from pancreatic ducts or acinar cells which underwent ADM (Morris *et al.,* 2010; Aichler *et al.,* 2012). Normal pancreatic duct cells exhibit cuboidal appearance and possess round nuclei (figure 1.6 A). During transition to PanIN lesions, size, shape and polarity of these cells change dramatically, depending on the lesion´s grade. PanIN1A lesions have a columnar shape; the cytosol is enlarged and contains mucin, which accumulates in the cytoplasm (figure 1.6 C). If these lesions become papillary, they are designated as PanIN1B, yet maintaining their cellular polarity and nuclear shape (figure 1.6 D). Beginning moderate nuclear atypia and a loss of polarity are hallmarks of higher grade PanIN2 lesions (figure 1.6 E), whereas significant nuclear atypia and a complete loss of polarity can be observed in PanIN3 lesions (figure 1.6 F; Hingorani *et al.,* 2003). Not only histological abnormalities, but also genetic alterations accumulate as these lesions advance. One of the earliest and most common mutations occurs within the proto-oncogene *Kras*, which can be detected in approx. 36 % of PanIN1A, 44 % of PanIN1B and 87 % of PanIN2-3 lesions (Löhr *et al.,* 2005). Since PanIN lesions contain considerable amounts of mucin, they can be detected via Alcian blue staining, which reacts with mucins in general

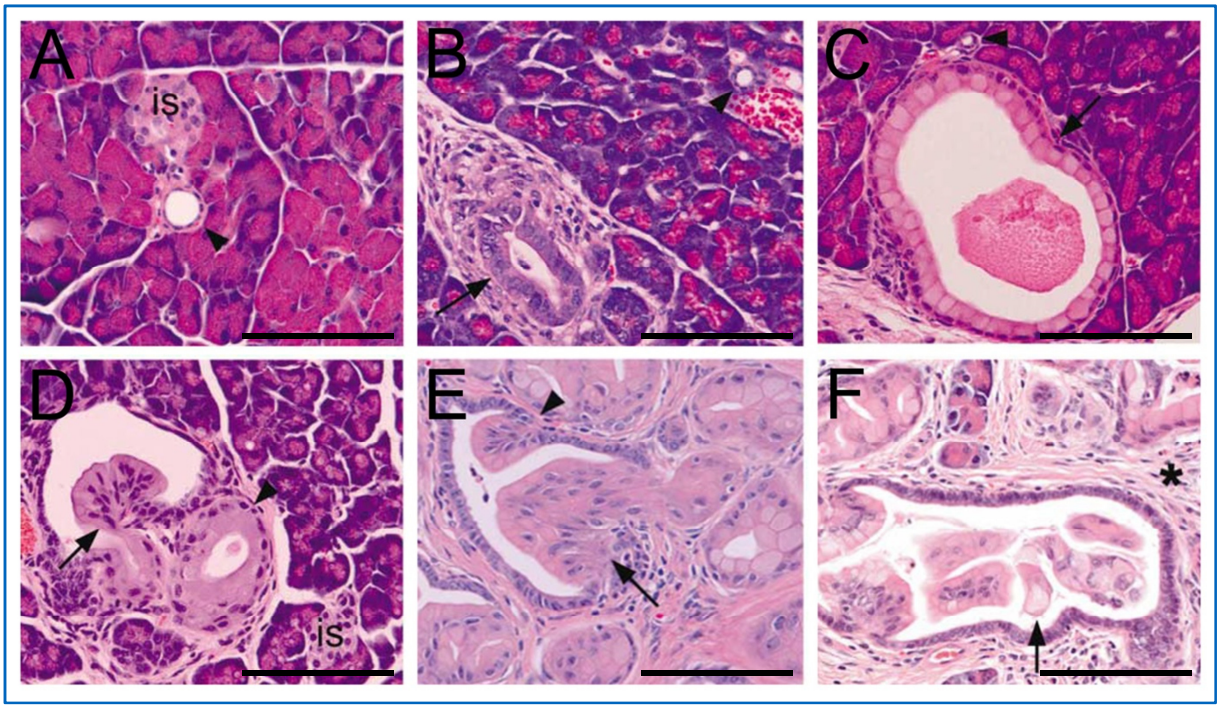

Figure 1.6: ADM and PanIN lesions. (A) Wild type pancreas with a normal pancreatic duct (arrowhead). **(B)** ADM (arrow) and an adjacent normal pancreatic duct (arrowhead). **(C)** PanIN1A with columnar shape and enlarged cytosol (arrow) and an adjacent normal pancreatic duct (arrowhead). **(D)** PanIN1B exhibiting papillary architecture (arrow) and an adjacent PanIN1A lesion (arrowhead). **(E)** PanIN2 with a more significant loss of polarity and moderate nuclear atypia (arrow) and a PanIN1B lesion within the same duct (arrowhead). **(F)** PanIN3 lesion with complete loss of cellular polarity and significant nuclear atypia (arrow) with surrounding fibroinflammatory reaction (asterisk). The abbreviation "is" denotes islets of Langerhans, scale bar represents 50 µm (adapted from: Hingorani *et al.,* 2003).

(Albores-Saavedra *et al.,* 2008). A specific protein present within some mucins is Mucin 5, a protein detectable in both PanIN lesions and PDAC, exhibiting increasing expression the more the lesions advance (Rachagani *et al.,* 2011). In addition, PanIN lesions can be stained for Claudin 18, a protein situated within the cell membrane (Sanada *et al.,* 2010).

1.2.4 Pancreatic Cancer

Pancreatic cancer is one of the most aggressive and chemo-resistant cancers known today, thus one of the most challenging. Being the focus of immense research activities, numerous underlying events as well as genetic mutations leading to pancreatic cancer have been identified and studied through the last decades. However, it remains an uncurable disease, with approx. 15,940 deaths in 2011 in Germany (Statistisches Bundesamt, 2014). Due to its various possible origins, pancreatic cancer can be classified into multiple subtypes (Mulkeen *et al.,* 2006). The most common type is pancreatic ductal adenocarcinoma (PDAC; figure 1.7), which represents approx. 85 % of all cases, thus being the fourth leading cancer related death cause in the USA (Warshaw and Fernández-del Castillo, 1992; Hezel, 2006).

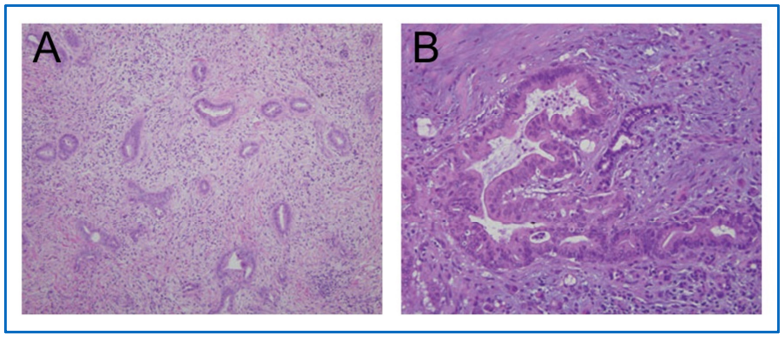

Figure 1.7: Infiltrating murine pancreatic adenocarcinoma. (A) Low-power photography. **(B)** High-power photography (from: Maitra and Hruban, 2008).

Patients diagnosed with PDAC exhibit a mean survival of less than 6 months, and the 5 year survival rate is between 3 % and 5 %. Hence, it is critical to diagnose PDAC at an early stage, which today is rarely the case. At the time of diagnosis, approx. 80 % of patients do already exhibit an advanced disease and only approx. 10 % can be resected successfully (Kedia *et al.,* 2013). Surgical interventions often do not lead to extended life expectancies, though (Yeo *et al.,* 2002). PDAC is a micrometastatic disease, therefore spreading fast to the lymphatic system as well as to the liver and leading to metastasis even after resection. Precursor lesions are hard to detect, given their small size as well as the retroperitoneal location of the pancreas. In addition, patients usually exhibit a late onset of symptoms (Hingorani *et al.,* 2003). The most frequent causes of PDAC are advanced age, smoking, chronic pancreatitis, diabetes and obesity, each contributing towards genetic mutations (Everhart and Wright, 1995; Fuchs *et al.,* 1996; Gapstur *et al.,* 2000; Michaud *et al.,* 2001). It has been shown that more than 90 % of PDACs exhibit a mutated *Kras* gene, while approx. 50 % hold a mutation in the *P53* gene (Hezel, 2006). Accordingly, it has been shown in murine model organisms that $Kras^{G12D}$ mutation is sufficient for both mimicking human PDAC as well as many of its precursor lesions and that an additional *P53* mutation accelerates this effect (Hingorani *et al.,* 2005). Adjacent to PanINs, other PDAC precursor lesions exist, such as intraductal papillary-mucinous neoplasm (IPMN) and mucinous cystic neoplasm (MCN). Both exhibit a duct-like shape, which has led to the conclusion that PDAC arises mainly from pancreatic ducts (Maitra and Hruban, 2008). Recently, it has been proposed that atypical flat lesions (AFL) may represent an additional precursor lesion, originating from the centroacinar-acinar compartment (CAAC) via ADM (Aichler *et al.,* 2012). However, the particular cell type of origin remains unclear and is still in focus of current research.

1.3 MODELS OF PANCREATIC CANCER DEVELOPMENT

1.3.1 Transgenic Mice

Numerous severe diseases known today remain uncurable, some due to the lack of efficient therapeutics, some as a result of insufficient knowledge. Pancreatic cancer has failed to be cured with the use of conventional chemotherapeutics (Steele *et al.,* 2013). In addition, many questions about the development of pancreatic cancer still have to be addressed. It has become necessary to create animal model organisms capable of closely mimicking the human course of disease. Hence, an optimal animal model organism should be both physiologically and genetically as close to humans as possible. Primates meet these requirements, but their use in research is accompanied with major moral reservations. Porcine models are much more suitable, given that pigs are used as productive animals and food source, thus causing few reservations within the population to using them for medical research. Due to the fact that porcine organ size is comparable to that of humans, they provide benefits in clinical trials (Flisikowska *et al.,* 2013). For basic research, however, mainly murine models are used today because of their easy handling, cheap stock breeding and short generation time. The most common method of generating genetically modified mice is the knockout or overexpression of specific genes. Subsequently, the molecular and cellular phenotype is analysed in order to elucidate the function of the gene of interest. However, many genes involved in carcinogenesis and other diseases are critical for normal cellular development and growth. A molecular dysregulation as a result of an overexpression or deletion of these genes can therefore be lethal, especially if the genetic modification is active within the whole body. For example, *Kras* is essential for foetal development, and expression of a non-functional protein in the whole organism would lead to prenatal death (Koera *et al.,* 1997). Hence, the genetic modification is often restricted to a particular tissue by using the Cre/*loxP* system.

The Cre/*loxP* system is a site specific recombination system, which is based on the recombination enzyme Cre (“causes recombination”) from the bacteriophage P1 (Sternberg and Hamilton, 1981). This protein recognizes a sequence referred to as *loxP* site (“locus of crossover in P1”; figure 1.8 A), consisting of 34 base pairs (bp) including two inverted repeats with a length of 13 bp each and an additional 8 bp long, asymmetric core region (Abremski *et al.,* 1986). The Cre protein binds two *loxP* sites simultaneously, catalysing a recombination event between both core regions involved. During this process, a DNA double strand break is induced, followed by a subsequent ligation of the two core regions. The result depends on the orientation of the *loxP* sites; if they are orientated in the same direction, the

recombination leads to an excision of the enclosed ("floxed") sequence (figure 1.8 B). If they are oriented in the opposite direction, the sequence will become inverted (Van der Weyden *et al.,* 2002). This process is both highly specific and reliable. In addition, no cofactors are required, thus making the Cre/*loxP* system a widely used method today (Hadjantonakis *et al.,* 2008). The sequence floxed is often a poly adenosine (polyA), which acts as a stop signal during translation. If cloned upstream of a mutated gene, this particular gene of interest will only be translated if a Cre protein is expressed within the same cell, excising the polyA. The tissue specificity is achieved by introducing a *Cre* gene into the model organism which is under the control of a tissue specific promoter. For pancreas restricted expression, the endogenous *Ptf1a* promoter is widely used, replacing the existing *Ptf1a* gene with the *Cre* sequence (Hingorani *et al.,* 2003). *Ptf1a* is approx. expressed from E9 on and is critical for pancreatic cell fate decision. Hence, a homozygous loss of *Ptf1a* leads to an absent pancreas and death of the mouse shortly after birth (Kawaguchi *et al.,* 2002). In adult mice, *Ptf1a* expression is restricted to acinar cells. Due to the fact that *Ptf1a* is critical for survival, only heterozygous expression of Cre is feasible but sufficient (Hingorani *et al.,* 2003).

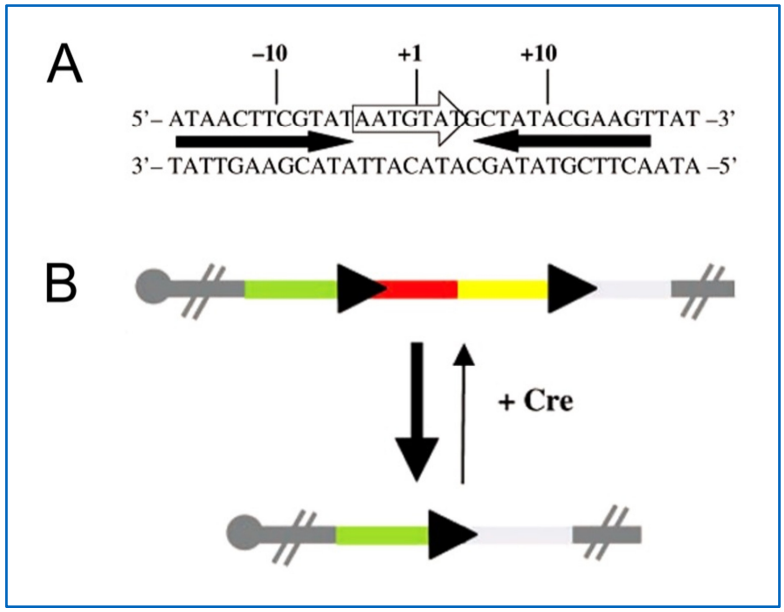

Figure 1.8: The Cre/*loxP* system. (A) Sequence of the *loxP* site, consisting of two inverted repeats (black arrows) and a core sequence (white arrow). **(B)** Recombination between two equally orientated *loxP* sites leads to an excision of the enclosed sequence (adapted from: van der Weyden *et al.,* 2002).

1.3.2 *Ex Vivo* Acinar Explants

Murine model organisms are most suitable for long term studies and provide insights into both tissue organisation and crosstalk in the context of a specific genetic background. However, pairing and maintaining of animals is time consuming and expensive. Cultures of either immortalised or cancer derived cells are cheap, easy to handle and, given the fast proliferation rate of most cell lines, provide the possibility to perform experiments with high

frequency. A major drawback to cultured lines is the fact that each cell line represents only one type of cell out of a whole organ, neglecting tissue specific signalling as well as cell - cell interactions. In addition, immortalised or cancer cell lines often lose the ability to transdifferentiate and are insensitive to many agents or stimuli (Ulrich *et al.,* 2002).

Ex vivo acinar explants represent a compromise between both approaches. Using this technique, acini of fresh pancreatic tissue are isolated and cultured for a limited period of time, mimicking their environment by collagen embedding (Sphyris *et al.,* 2005). The acinar cells remain organised in clusters, preserving their ability to interact through the exchange of factors or via direct cell - cell contact. Furthermore, the explants are neither immortalized nor harbour unknown accumulated mutations as cancer derived cell lines do, thus responding to stimuli in a much more physiological way. Due to the fact that *ex vivo* acinar explants from an adult mouse provide enough material for several experimental setups, fewer mice have to be sacrificed. Acinar explants retain their ability to transdifferentiate to duct like structures (figure 1.9), thus providing the possibility to investigate underlying mechanisms of ADM development *in vitro*. Explants of wild type pancreata have been shown to start transdifferentiation approx. five to seven days after isolation as a result of growth factors present within the applied medium. This process can be accelerated by adding additional growth factors to the culture medium, such as EGF or TGFα, leading to a beginning transdifferentiation two to three days after isolation (Heid *et al.,* 2011). Agents such as inhibitors can be added alternatively or simultaneously, providing the possibility of investigating their impact on ADM development without the need of treating animals (Ardito *et al.,* 2012). Hence, *ex vivo* acinar explants represent a reliable, time saving technique, suitable to test hypotheses within a few days, simultaneously being much closer to animal models than cell culture experiments.

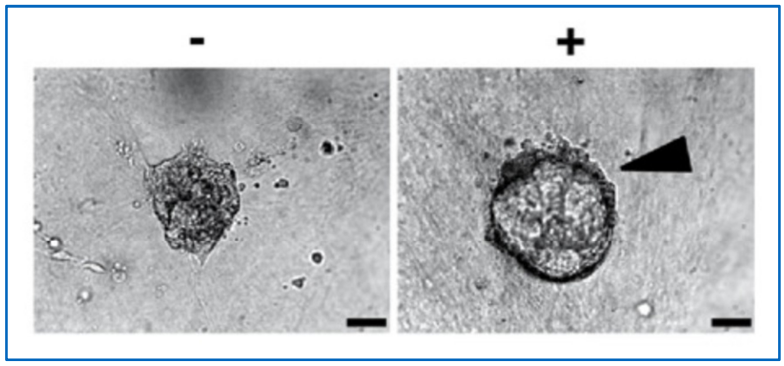

Figure 1.9: *Ex vivo* acinar explants. Bright field microscopy of explants of a six weeks old wild type mouse, without (-) and with (+) treatment with TGFα. The arrowhead denotes a transdifferentiated duct like structure, scale bar represents 50 µm (from: Heid *et al.,* 2011).

1.4 THE EGFR - ERK PATHWAY IN PANCREATIC CANCER

1.4.1 Epidermal Growth Factor Receptor

The epidermal growth factor receptor (EGFR) is a receptor tyrosine kinase and belongs to a family of four ERBB proteins. It has a size of approx. 170 kDa and is capable of forming heterodimers with ERBB family members as well as with other proteins. As it is a transmembrane protein, EGFR is mainly located within the cell membrane, where it can be activated through several ligands (Han and Lo, 2012). Two of the best characterized ligands are the epidermal growth factor (EGF) and transforming growth factor alpha (TGFα), both exhibiting strong structural and functional similarities to each other (Derynck *et al.,* 1984; Navolanic *et al.,* 2003). These bind to the extracellular binding domain of EGFR, initiating a conformation change of the intracellular domain, followed by recruitment of special adapter proteins, such as the growth factor receptor bound protein 2 (GRB2) or other Src homology 2 (SH2) domain containing proteins (Avraham and Yarden, 2011). The adapter proteins mediate activation of numerous downstream pathways, among these the RAS - MEK - ERK cascade as well as the PI3K - AKT - mTOR pathway (figure 1.10).

Coevally upon activation, EGFR is internalised into the cell via early endosomes, a process which is dynamin dependent. Subsequently, the protein is recycled to the cell membrane,

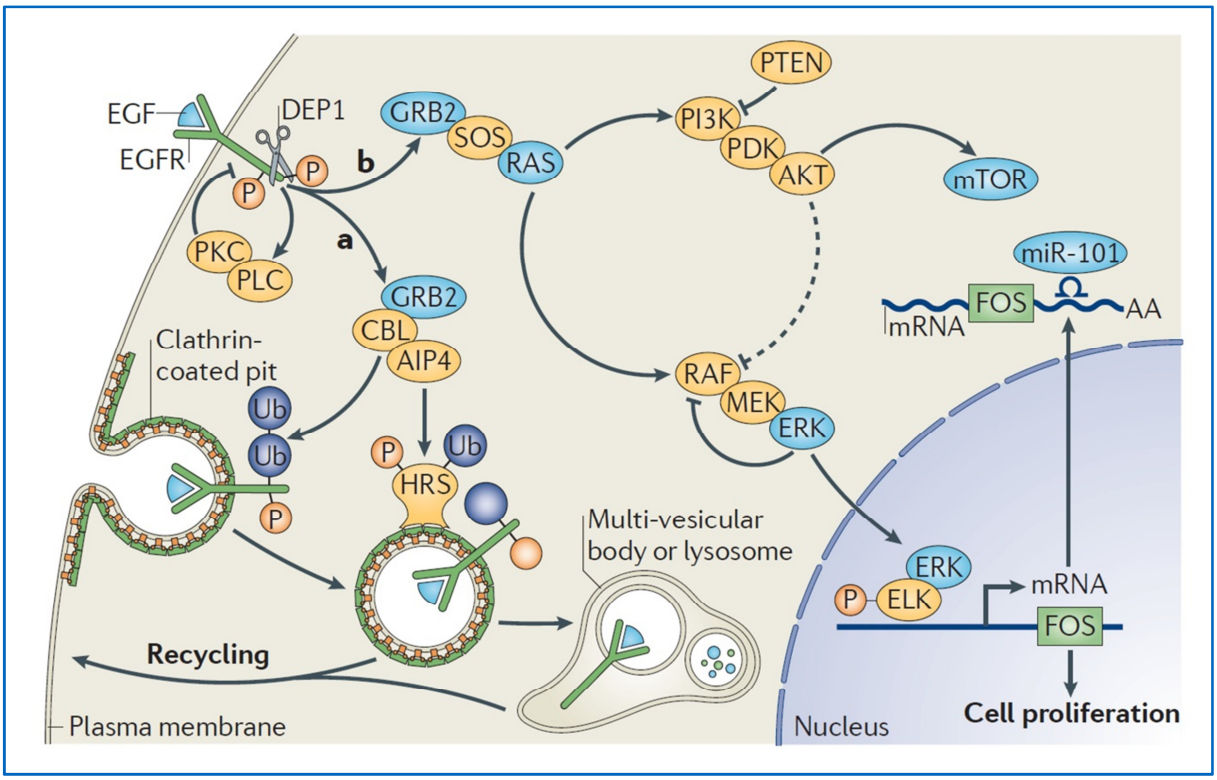

Figure 1.10: The epidermal growth factor receptor and its downstream pathways. EGFR regulates both the RAS - MEK - ERK and PI3K - AKT - mTOR pathway. Once activated, the receptor is internalised into the cell via endosomes and either recycled, degraded or transported into the nucleus (from: Avraham and Yarden, 2011).

degraded or transported into the nucleus (Grant and Donaldson, 2009). Since it possesses no DNA binding domain, EGFR cannot directly act as a transcription factor within the nucleus. It has been shown though that EGFR recruits co-regulators such as STAT3 which mediate transcription (Lo *et al.,* 2005). In addition, EGFR is capable of retaining its tyrosine kinase activity within the nucleus, phosphorylating the proliferating cell nuclear antigen (PCNA), for example (Wang *et al.,* 2006). During embryonic development, *Egfr* is essential; a whole body knockout in mice leads to postnatal death within the first eight days (Miettinen *et al.,* 2004), whereas tissue specific knockout in the pancreas has no obvious effect on pancreatic development (Ardito *et al.,* 2012). The importance of EGFR in terms of tumourigenesis and development of precursor lesion has been highlighted by the fact that expression levels of EGFR are elevated in many tumours, including PDAC (Fjällskog *et al.,* 2003). In addition, its ligand TGFα was also found highly expressed in both neoplastic tissues and cell lines derived from human cancers. In mice, it has been shown that sustaining expression of TGFα under the control of the pancreas specific elastase promoter leads to a significantly increased size of the pancreas and induced both fibrosis and ADM (Sandgren *et al.,* 1990). This effect was abolished by an additional tissue specific knockout of *Egfr* in these mice. Moreover, similar results were obtained concerning the $Kras^{G12D}$ expressing mouse model, where an additional *Egfr* knockout led to a complete rescue of the wild type phenotype, thus blocking initiation of PDAC as well as its precursor lesions (Ardito *et al.,* 2012).

1.4.2 The KRAS – MEK – ERK Signalling Cascade

One of the most important downstream targets of EGFR is KRAS, a well-studied proto-oncogene (Logsdon and Ji, 2009). It belongs to the RAS family of guanosine triphosphate (GTP) binding proteins, consisting of HRAS, NRAS and KRAS (Karreth and Tuveson, 2009). The impact of RAS and its downstream pathways on cancer development and progression has been investigated extensively. All three family members were found to be mutated in human cancers, with approx. 15 % harbouring a mutated NRAS and approx. 1 % harbouring a mutated HRAS protein. However, KRAS is the most common mutated protein, present in more than 90 % of all human tumours (Downward, 2003). Activation of KRAS takes place via the SHC/GRB2/SOS complex, recruited by EGFR (figure 1.11). This complex catalyses an exchange of the KRAS bound guanosine diphosphate (GDP) for GTP, leading to a confirmation change of the KRAS protein (McCubrey *et al.,* 2007). Activated KRAS subsequently recruits and phosphorylates RAF, a serine / threonine kinase. During this

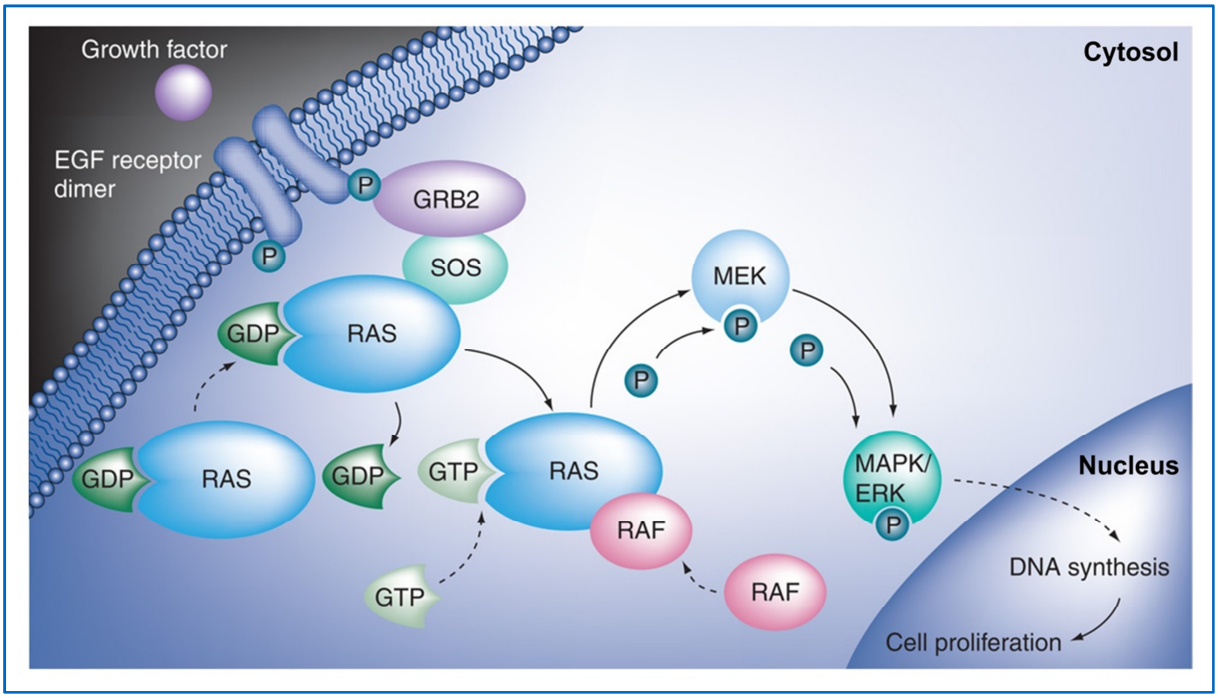

Figure 1.11: EGFR dependent, GRB2/SOS mediated activation of RAS. Downstream signal transduction takes place via phosphorylation cascades and leads to activation of transcription factors in the nucleus (from: Kim *et al.,* 2011).

process, the GTP bound by KRAS is dephosphorylated to GDP, resulting in a deactivation of the KRAS protein. The now active RAF phosphorylates MEK, the mitogen-activated protein kinase kinase (Alessi *et al.,* 1994). The main downstream target of MEK is the extracellular-signal-regulated kinase (ERK), which is also activated via phosphorylation. ERK itself is capable of translocating into the nucleus where it can phosphorylate many different transcription factors, such as c-JUN, c-MYC or ELK1. It can furthermore activate the S6 ribosomal protein kinase, a downstream target of the PI3K - AKT - mTOR pathway (Steelman *et al.,* 2004). In total, more than 160 targets of ERK have been identified so far, predominantly regulating cell cycle progression and apoptosis (McCubrey *et al.,* 2007).

In murine models, the most frequently used approach for mimicking human malignancies is the endogenous expression of a mutated, permanently active $KRAS^{G12D}$ protein, thus providing physiological expression levels. By using a floxed transcriptional stop signal upstream of the mutated gene, the expression can be furthermore performed in a tissue specific manner (Karreth and Tuveson, 2009). $KRAS^{G12D}$ was shown to be sufficient for induction of both tumours and precursor lesions in several organs, such as lung (Jackson *et al.,* 2001) and pancreas (Hingorani *et al.,* 2003). In addition, continued $KRAS^{G12D}$ expression is critical for tumour maintenance in PDAC, thus leading to tumour regression if the expression is abandoned (Collins *et al.,* 2012). $KRAS^{G12D}$ mice exhibit elevated levels of pERK, indicating a highly enhanced activity of the RAS - MEK - ERK pathway. It has been

shown that an inhibition of MEK in the $KRAS^{G12D}$ mouse model leads to reduced pERK levels, accompanied with a strong reduction of both metaplasia and neoplasia *in vitro* and *in vivo* (Ardito *et al.,* 2012). These results highlight the importance of the RAS - MEK - ERK pathway for PDAC precursor formation. However, given the high number of possible downstream targets, it is yet unknown which transcription factors in particular are mediating these events, a question which still remains to be addressed.

1.4.3 Early Growth Response 1

The early growth response 1 (EGR1) protein belongs to a family of four DNA binding transcription factors, which are denoted as EGR1, 2, 3 and 4. It has a size of approx. 80 kDa and holds three Cys_2His_2 zinc finger motives, granting the ability to bind DNA (Milbrandt, 1987). The motif recognized by EGR1 is a 9 bp sized, GC rich target site, exhibiting the consensus sequence GCG(G/T)GGGCG (Liu *et al.,* 1998). EGR1 also holds a nuclear localisation signal (NLS), hence the protein is mainly situated in the nucleus (Bhattacharyya *et al.,* 2013). However, in most normal tissues EGR1 is expressed very low or undetectable, except in cells of the brain (Beckmann *et al.,* 1997). A whole body knockout of *Egr1* in mice leads to no severe phenotype; homozygous deficient females are infertile, though, due to atrophied regenerative organs (Lee *et al.,* 1995). Several events result in a considerable upregulation of EGR1, such as hypoxia, oxidative stress, cytokines, mechanical injury and ultraviolet radiation (Bhattacharyya *et al.,* 2013). Furthermore, it has been shown that TGFβ increases EGR1 expression in human fibroblasts (Bhattacharyya *et al.,* 2008) and in murine TGFβ expressing fibrosis models; an additional *Egr1* knockout leads to a blockage of fibrosis formation in these mice (Lee *et al.,* 2004). The regulation of *Egr1* mainly takes place via the ERK - ELK1 pathway (figure 1.12; Midgley and Khachigian, 2004; Khachigian, 2006; Hasan and Schafer, 2008), though EGR1 is also capable of self-regulating its expression. This process is mediated via NAB2, which is positively regulated by EGR1. NAB2 itself represses *Egr1*, resulting in a negative feedback loop (Ehrengruber *et al.,* 2000). Some downstream target genes affected by EGR1 are *P53*, *Pten* and *Klf5* (Krones-Herzig *et al.,* 2003; Nandan *et al.,* 2004; Gitenay and Baron, 2009). Furthermore, it has been shown that EGR1 also regulates EGFR by binding directly to the *Egfr* promoter, thus leading to reduced EGFR expression if EGR1 is inhibited (Chen *et al.,* 2006a).

The effects of EGR1 during cancer progression are diverse and strongly depending on the type of cancer examined. In the gastric cancer cell lines AGS and TMK1, *Egr1* knockdown

led to a decreased migration and invasion ability of these cells. Accordingly, over-expression of EGR1 in the cell line SGC7901 led to increased β-Catenin levels and higher proliferation. Gastric tumours exhibit a correlation between EGR1 expression and both tumour size and survival (Myung *et al.,* 2013; Sun *et al.,* 2013). Similar results were obtained for prostate cancer, where an additional *Egr1* knockout in existing tumour models results in prolonged survival (Abdulkadir *et al.,* 2001). However, two of the main tumour suppressor genes downstream of EGR1, *P53* and *Pten*, are deleted or inactive in most prostate cancers (Gitenay and Baron, 2009). Several other studies reported converse results, though. In murine skin cancer models, knockout of *Egr1* results in accelerated tumour progression (Krones-Herzig *et al.,* 2005) and EGR1 expression was shown to suppress leukaemia as well (Gibbs *et al.,* 2008). Hence, EGR1 is closely related with cancer progression; its tumour promoting or suppressing effects are highly tissue depending, though. Within the pancreas, the influence of EGR1 expression during tumourigenesis still has to be revealed.

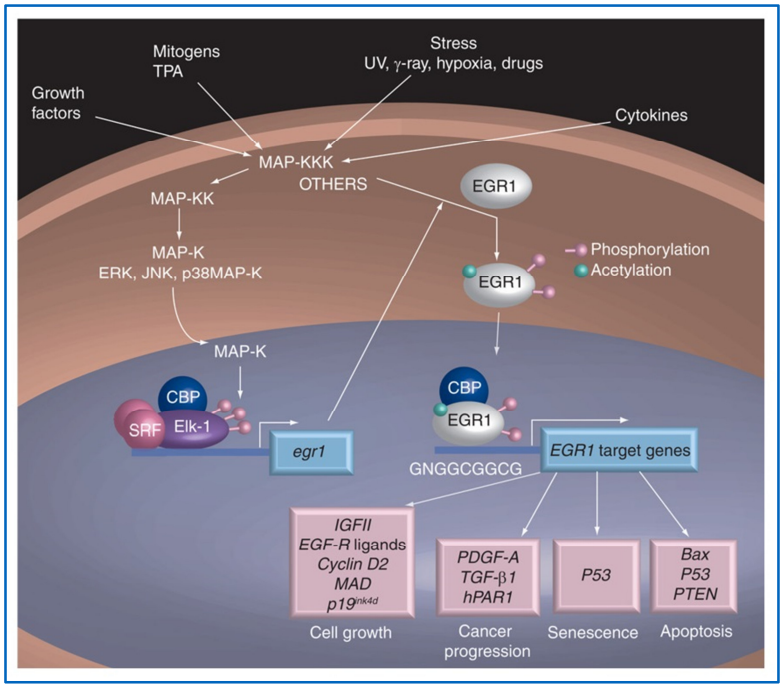

Figure 1.12: *Egr1* regulation and downstream targets. *Egr1* is situated downstream of the MEK – ERK pathway. By regulating numerous downstream targets, EGR1 effects cell growth, senescence, apoptosis and cancer progression (from: Gitenay and Baron, 2009).

1.4.4 Krüppel-Like Factor 5

The krüppel-like factor 5 (KLF5) is a DNA binding transcription factor and belongs to a family of approx. 20 KLF proteins (Dong and Chen, 2009). All family members are homologs to the gene *Krüppel*, which was first identified in *Drosophila melanogaster*, where a deletion of this gene led to a "crippled" phenotype (McConnell *et al.,* 2007). In mice, *Klf5* is essential during embryonic development, for example in terms of skeletal growth, cardiovascular remodelling or adipocyte differentiation. Consequently, a homozygous whole body knockout of *Klf5* is lethal early during embryogenesis (Shindo *et al.,* 2002; Oishi *et al.,* 2005). The

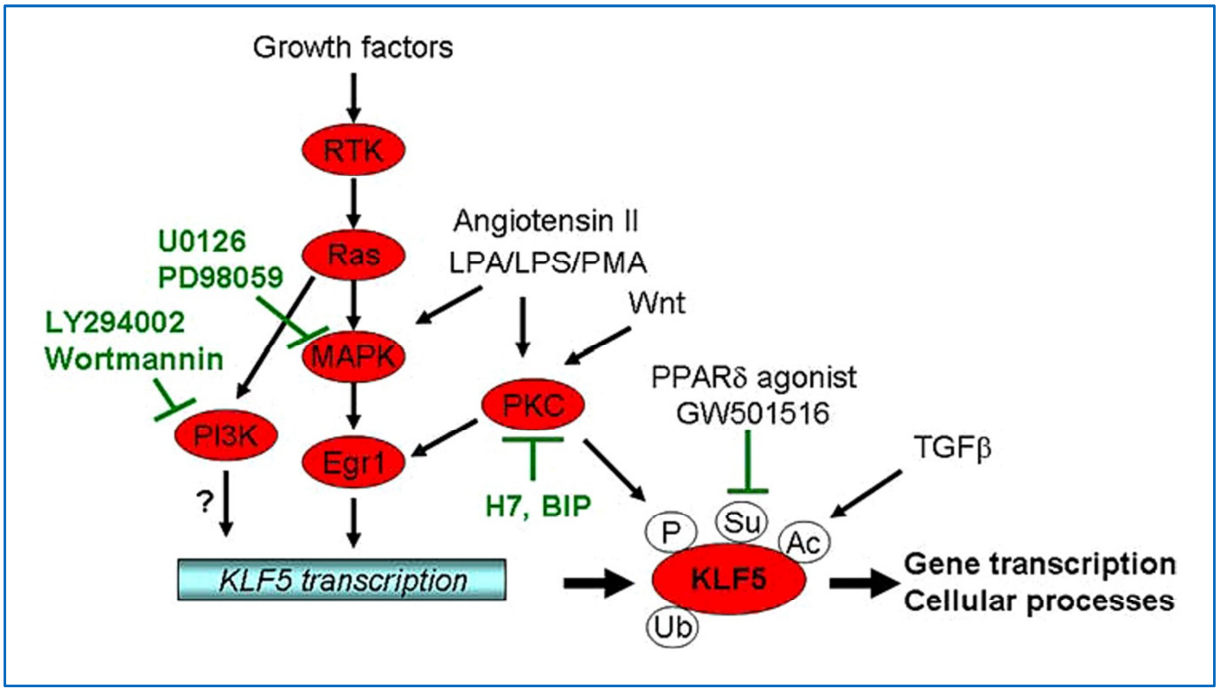

Figure 1.13: Pathways involved in *Klf5* regulation. *Klf5* expression and activity is influenced by numerous factors on both the transcriptional and posttranscriptional level (from: Dong and Chen, 2009).

KLF5 protein exhibits a size of approx. 50 kDa, and pulse chase assays revealed that it has a half-life of approx. 1.5 h (Chen *et al.,* 2005). It holds several conserved Cys_2His_2 zinc finger motives and is capable of binding both CACCC and GC rich target sequences, though it has no specific consensus binding site (Sogawa *et al.,* 1993; Dong and Chen, 2009). Furthermore, a small ubiquitin-like modifier (SUMO) binding site which promotes nuclear localisation and a nuclear export signal (NES) which facilitates cytosolic localisation are situated within the protein as well, suggesting that KLF5 assumes tasks in both domains (Du *et al.,* 2008). Hence, KLF5 is involved in the regulation of numerous genes and pathways, such as WNT (Taneyhill and Pennica, 2004) and TGFβ (Adam *et al.,* 2000). It also participates in the RAS - MEK - ERK pathway (figure 1.13), since KLF5 becomes downregulated if either EGFR or MEK is inhibited, which was shown in both murine oesophageal keratinocytes (Yang *et al.,* 2007) and the embryonic fibroblast cell line NIH3T3 (Nandan *et al.,* 2004). Furthermore, an EGR1 binding site was detected within the *Klf5* promoter (Kawai-Kowase *et al.,* 1999). It has been shown that KLF5 also directly binds to the *Egfr* promoter, thus elevating EGFR levels and activating the MEK - ERK pathway if overexpressed, suggesting a self-regulating feedback loop (Yang *et al.,* 2007).

Within the gastrointestinal tract, both KLF4 and KLF5 are well investigated, even though they exhibit opposite functions. KLF4 has been shown to be expressed mainly in differentiated, non-dividing epithelial cells of the gut. In addition, overexpression in NIH3T3 cells led to growth arrest of these cells (Shields *et al.,* 1996). KLF5 on the other hand

promoted proliferation and transformation in many experimental setups. It is expressed in highly proliferative tissues such as basal oesophagus, epidermis of the skin and crypts of the gut (Conkright *et al.,* 1999; Ohnishi *et al.,* 2000). In NIH3T3 cells, an overexpression of KLF5 resulted in higher proliferation, which was also shown in the bladder cancer cell line TSU-Pr1 (Chen *et al.,* 2006b). It mediates transforming effects of HRAS and activation of the proliferation promoting CyclinB1 / CDC2 complex (Sun *et al.,* 2001; Nandan *et al.,* 2004). In addition, it increases cell survival by inhibiting apoptosis and elevating expression of survivin (Zhu *et al.,* 2006). Moreover, *Klf5* is an important cancer related gene and has been shown to exhibit both tumour promoting and, in some cases, tumour suppressing characteristics, suggesting that some functions may be context and especially tissue depending (Dong and Chen, 2009). In both $Kras^{V12G}$ and $Kras^{V12G};Apc^{Min}$ derived tumours of the colon, KLF5 is highly expressed *in vitro* and *in vivo*. Furthermore, $Kras^{V12G};Apc^{Min};Klf5^{+/-}$ mice, which hold a heterozygous whole body knockout of *Klf5*, were shown to develop tumours of both less number and size, simultaneously exhibiting reduced expression levels of β-Catenin, KI67 and Cyclin D1 (Nandan *et al.,* 2008; Nandan *et al.,* 2010), thus underlining its potential role as a key player in intestinal tumour progression.

1.5 OBJECTIVES

Activating *Kras* mutations are thought to be key drivers of cancer initiation and progression. In genetically engineered mouse models, expression of $KRAS^{G12D}$ leads to activation of the MEK – ERK pathway and is sufficient to induce both ADM and PanIN lesions, which eventually further progress to PDAC. Recently, it has been shown that EGFR is essential for $KRAS^{G12D}$ dependent PDAC initiation and progression as well as for sustained MEK – ERK activity in the murine pancreas. This work focuses on revealing the specific role of MEK during development of PDAC as well as its precursor lesions and investigates two downstream targets of the MEK – ERK pathway, EGR1 and KLF5.

The impact of MEK on PDAC initiation and progression shall be elucidated via pancreas specific expression of MEK1DD, a constitutively active form of the MEK protein. MEK1DD expressing mice are to be analysed at different stages of life on both the molecular and histological level and should furthermore be compared to $Kras^{G12D}$ and $P110\alpha^{H1047R}$ mouse models.

In order to gain further insights into the MEK – ERK pathway, the transcription factor EGR1, a protein known to exhibit either tumour suppressing or oncogenic effects in a tissue and context specific manner, shall be investigated. For this purpose, a detailed expression analysis of EGR1 in several ADM mouse models should be performed. In addition, the influence of EGR1 on ADM and PanIN development ought to be analysed via a full knockout of EGR1 in established PDAC genetically engineered mouse models.

KLF5 is a cancer related target of the MEK – ERK pathway and has been reported to be downstream of EGR1. The expression of KLF5 should be investigated in the pancreas of several murine ADM models as well as in $Egr1^{KO}$ mice.

This detailed analysis of the RAS – MEK – ERK – EGR1 pathway aims at understanding its role during PDAC initiation and progression. Hence, this work should provide insights into major signalling pathways which might lead to the identification of new therapy targets for PDAC treatment.

2 MATERIALS AND METHODS

2.1 MATERIALS

2.1.1 Software

Application Suite Advanced Fluorescence 2.6
© 2012 Leica Microsystems GmbH

AxioVision 3.1.2.1
© 2003 Carl Zeiss Vision GmbH

Axio Vision LE 4.8.2.0
© 2010 Carl Zeiss MicroImaging GmbH

ImageJ 1.47
Open Source Software (Wayne Rasband)

LightCycler® 480 1.5.0
© 2008 Roche GmbH

MatInspector 3.1
© 2014 Genomatix Software GmbH

NanoDrop 2000 1.4.1
© 2009 Thermo Scientific Inc.

Primer3Plus Web Interface
http://www.primer3plus.com
Open Source Software (Untergasser *et al.*, 2007)

Prism 5.0
© 2007 GraphPad Software Inc.

Vector NTI 10.3.1
© 2007 Invitrogen Corporation

2.1.2 Equipment

Amersham™ Hyper Processor	GE Healthcare GmbH, München, D
Amersham™ Hyperfilm™ ECL	GE Healthcare GmbH, München, D
ASP300S	Leica GmbH, Solms, D
AxioCam HRc	Carl Zeiss GmbH, Göttingen, D
AxioCam MRm	Carl Zeiss GmbH, Göttingen, D
Axio Imager.A1	Carl Zeiss GmbH, Göttingen, D
Axiovert 200M	Carl Zeiss GmbH, Göttingen, D
Cell Culture Canted Neck Flask 25 / 75 / 150 cm²	Corning Inc., NY, USA
Cell Culture Cluster 6-Well	Corning Inc., NY, USA
Cell Culture Cluster 48-Well	Corning Inc., NY, USA
Cell Culture Dish	Corning Inc., NY, USA
Cell scraper	Corning Inc., NY, USA
Cellstar® 5 ml / 10 ml / 25 ml	Greiner Bio One GmbH, Frickenhausen, D
Centrifuge 5702 R	Eppendorf GmbH, Hamburg, D
Centrifuge 5810	Eppendorf GmbH, Hamburg, D
Cryo tubes	Sarstedt GmbH, Nürnbrecht, D
DAB staining kit	Vector Labs Inc., Burlingame, USA
DNeasy Blood & Tissue Kit	Qiagen GmbH, Hilden
EG 1150 H	Leica GmbH, Solms, D
Falcon Tubes 14 ml	Becton Dickinson & Co., Sparks, USA
Falcon Tubes 15 ml	Greiner GmbH, Frickenhausen, D
Falcon Tubes 50 ml	Greiner GmbH, Frickenhausen, D
Gel Documentation System	Bio-Rad GmbH, München, D
GeneAmp® PCR System 9700	Applied Biosystems GmbH, Darmstadt, D
Hera Cell 240	Heraeus GmbH, Hanau, D
Hera Freeze	Heraeus GmbH, Hanau, D
Hera Safe	Heraeus GmbH, Hanau, D
Hereaus Function Line	Heraeus GmbH, Hanau, D
Immobilon® transfer membrane	Merck Millipore KG, Darmstadt, D
Inkubator TH/KS 15	Edmund Bühler GmbH, Hechingen, D
KAPA Express Extraction	KAPA Biosciences Inc., Boston, USA
KAPA2G Fast HS Genotyping Mix	KAPA Biosciences Inc., Boston, USA
LightCycler® 480	Roche GmbH, Grenzach-Wyhlen, D

LightCycler® 480 SYBR Green I Master Kit	Roche GmbH, Grenzach-Wyhlen, D
Lipofectamine® 2000	Invitrogen GmbH, Karlsruhe, D
Mastercycler	Eppendorf GmbH, Hamburg, D
Maxwell® 16	Promega GmbH, Mannheim, D
Maxwell® 16 LEV simplyRNA Tissue Kit	Promega GmbH, Mannheim, D
Microm HM 355S	Thermo Scientific Inc., Waltham, USA
Mini Protean Gel System	Bio-Rad GmbH, München, D
Multiskan FC	Thermo Scientific Inc., Waltham, USA
NanoDrop 2000	Thermo Scientific Inc., Waltham, USA
Neubauer improved counting chamber	Marienfeld GmbH, Königshofen, D
Nylon mesh 100 µm	BD Biosciences Inc., New Jersey, USA
Objective EC Plan-Neofluar 10x 0.3	Carl Zeiss GmbH, Göttingen, D
Objective EC Plan-Neofluar 20x 0.5	Carl Zeiss GmbH, Göttingen, D
Objective EC Plan-Neofluar 20x 0.4 Ph2	Carl Zeiss GmbH, Göttingen, D
Objective EC Plan-Neofluar 40x 1.3 Oil Ph3	Carl Zeiss GmbH, Göttingen, D
Pierce® ABC Solution kit	Thermo Scientific Inc., Waltham, USA
Pierce® BCA Protein Assay kit	Thermo Scientific Inc., Waltham, USA
Pierce® LDH Cytotoxicity Assay kit	Thermo Scientific Inc., Waltham, USA
pJET1.2/blunt Cloning Kit	Fermentas GmbH, St. Leon-Rot, D
Power Pac™ Basic	Bio-Rad GmbH, München, D
Primus 96 Plus	MWG Biotech GmbH, Ebersberg, D
PureYield™ Plasmid Midiprep Kit	Promega GmbH, Mannheim, D
PureYield™ Plasmid Miniprep Kit	Promega GmbH, Mannheim, D
Reaction Tubes	Sarstedt GmbH, Nürnbrecht, D
RedTaq® Ready Mix™ PCR Reaction Mix	Sigma-Aldrich GmbH, Steinheim, D
Scalpel	Feather Safety Razor Co. Ltd., Osaka, J
Silentcrusher M	Heidolph GmbH, Schwabach, D
Sonopuls UW2070	Bandelin Electronic GmbH, Berlin, D
Stripettor™ Plus	Corning Inc., NY, USA
Sub-Cell® GT Electrophoresis Chambers	Bio-Rad GmbH, München, D
Superfrost® Plus Slides	Thermo Scientific Inc., Waltham, USA
TCS SP5	Leica GmbH, Solms, D
ThermoForma Steri-Cycle CO_2	Thermo Scientific Inc., Waltham, USA
Wizard® SV Gel and PCR Clean-Up System	Promega GmbH, Mannheim, D

2.1.3 Chemicals and Enzymes

Acetone	Merck KG, Darmstadt, D
Agarose	Biozym Scientific GmbH, Oldendorf, D
Alcian Blue	Sigma-Aldrich GmbH, Steinheim, D
Amersham™ ECL™	GE Healthcare GmbH, München, D
Amphotericin B	Sigma-Aldrich GmbH, Steinheim, D
Ampicillin	Sigma-Aldrich GmbH, Steinheim, D
Antarctic phosphatase	New England Biolabs GmbH, Frankfurt, D
Antigen Unmasking Solution	Vector Labs Inc., Burlingame, USA
APS	Sigma-Aldrich GmbH, Steinheim, D
β-mercaptoethanol	Sigma-Aldrich GmbH, Steinheim, D
Blue Loading Buffer	Peqlab GmbH, Erlangen, D
Bovine serum albumin	Carl Roth GmbH, Karlsruhe, D
BPE	Corning Inc., NY, USA
Bromphenol blue	Sigma-Aldrich GmbH, Steinheim, D
Cerulein	Sigma-Aldrich GmbH, Steinheim, D
Collagen	BD Biosciences Inc., New Jersey, USA
Collagenase VIII	Sigma-Aldrich GmbH, Steinheim, D
cOmplete Protease Inhibitor Cocktail	Roche GmbH, Grenzach-Wyhlen, D
DMEM	Life Technologies Corp., NY, USA
DMSO	Sigma-Aldrich GmbH, Steinheim, D
Dulbecco´s PBS	Biochrom GmbH, Berlin, D
Dulbecco´s PBS, cell culture grade	Life Technologies Corp., NY, USA
EDTA	Sigma-Aldrich GmbH, Steinheim, D
Endonucleases	New England Biolabs GmbH, Frankfurt, D
Eosin	Carl Roth GmbH, Karlsruhe, D
Ethanol 70 % / 96 % / 99,8 %	Otto Fischar GmbH, Saarbrücken, D
Ethidium bromide	Carl Roth GmbH, Karlsruhe, D
FCS	Life Technologies Corp., NY, USA
Formaldehyde	Merck KG, Darmstadt, D
G418	AppiChem GmbH, Darmstadt, D
Gelatine	Sigma-Aldrich GmbH, Steinheim, D
Glacial acetic acid	Merck KG, Darmstadt, D
Glutaraldehyde	Carl Roth GmbH, Karlsruhe, D

Glycerine	Carl Roth GmbH, Karlsruhe, D
Glycine	Sigma-Aldrich GmbH, Steinheim, D
Goat serum	Sigma-Aldrich GmbH, Steinheim, D
GoTaq™ DNA Polymerase	Promega GmbH, Mannheim, D
Hämalaun	Merck KG, Darmstadt, D
Hydrogen peroxide	Carl Roth GmbH, Karlsruhe, D
Isopropanol	Merck KG, Darmstadt, D
Klenow Fragment	New England Biolabs GmbH, Frankfurt, D
Lithium chloride	Carl Roth GmbH, Karlsruhe, D
Lysogeny Broth (Luria)	Carl Roth GmbH, Karlsruhe, D
Lysogeny Broth (Miller)	Carl Roth GmbH, Karlsruhe, D
Magnesiumchloride hexahydrate	Carl Roth GmbH, Karlsruhe, D
McCoy´s Medium	Sigma-Aldrich GmbH, Steinheim, D
Methanol	Merck KG, Darmstadt, D
N,N-dimethylformamide	Merck KG, Darmstadt, D
Non-Essential Amino Acids	Life Technologies Corp., NY, USA
NP40	USB Corp., Cleveland, USA
Nucleotide Solution Mix	Fermentas GmbH, St. Leon-Rot, D
Oligonucleotides	Promega GmbH, Mannheim, D
Pen/Strep	Life Technologies Corp., NY, USA
PeqGOLD DNA Ladder Mix	Peqlab GmbH, Erlangen, D
Paraformaldehyde	EM Sciences Inc., Hatfield, USA
Phusion™ High-Fidelity DNA Polymerase	Thermo Scientific Inc., Waltham, USA
Potassium hexacyanoferrat (II) trihydrate	Merck KG, Darmstadt, D
Potassium hexacyanoferrat (III)	Merck KG, Darmstadt, D
Precision Plus Protein™ All Blue Standard	Bio-Rad GmbH, München, D
Protein A Agarose / Salmon Sperm DNA	Merck Millipore KG, Darmstadt, D
Proteinase K	Roche GmbH, Grenzach-Wyhlen, D
RA1 lysis buffer	Macherey-Nagel GmbH, Düren, D
RNase A	Fermentas GmbH, St. Leon-Rot, D
Roti® Histol	Carl Roth GmbH, Karlsruhe, D
Rotiphorese® Gel	Carl Roth GmbH, Karlsruhe, D
SBTI	Sigma-Aldrich GmbH, Steinheim, D
Selenium X	Life Technologies Corp., NY, USA

Skim milk powder	Sigma-Aldrich GmbH, Steinheim, D
Sodium acetate	Carl Roth GmbH, Karlsruhe, D
Sodium chloride	Sigma-Aldrich GmbH, Steinheim, D
Sodium deoxycholate	Sigma-Aldrich GmbH, Steinheim, D
Sodium dodecyl sulphate	Carl Roth GmbH, Karlsruhe, D
SuperScript® II Reverse Transcriptase	Invitrogen GmbH, Karlsruhe, D
SuperSignal® West Fempto	Thermo Scientific Inc., Waltham, USA
T4 Ligase	New England Biolabs GmbH, Frankfurt, D
T4 Polynucleotide Kinase	New England Biolabs GmbH, Frankfurt, D
TEMED	Carl Roth GmbH, Karlsruhe, D
Tris	Carl Roth GmbH, Karlsruhe, D
Tris HCl	Carl Roth GmbH, Karlsruhe, D
Triton X-100	Sigma-Aldrich GmbH, Steinheim, D
Trypsin	Life Technologies Corp., NY, USA
Tween20	Carl Roth GmbH, Karlsruhe, D
VECTASHIELD® mounting medium	Vector Labs Inc., Burlingame, USA
Waymouth´s medium	Genaxxon Bioscience GmbH, Ulm, D

2.1.4 Buffers and Solutions

Acinar explants solution I	McCoy´s medium, 0.1 % BSA, 4 µg/ml SBTI
Acinar explants solution II	McCoy´s medium, 0.1 % BSA, 4 µg/ml SBTI, 150 µg/ml Collagenase VIII
Blot buffer	14.4 g glycine, 3 g tris, 200 ml methanol, ad 1000 ml ddH_2O
Elution buffer	10 mM tris pH 8.0, 1 mM EDTA, 1 % SDS
High Salt buffer	500 mM NaCl, 20 mM tris pH 8.0, 2 mM EDTA, 1 % NP-40, 0.1 % SDS
L2 buffer	50 mM tris pH 8.0, 5 mM EDTA, 1 % SDS, cOmplete Protease Inhibitor Cocktail
Laemmli buffer	20 % glycerine, 10 % β-mercaptoethanol, 4 % SDS, 0.004 % bromphenol blue, 0.125 tris HCl, pH 6.8

LiCl buffer	250 mM LiCl, 20 mM tris pH 8.0, 1 mM EDTA, 0.5 % NP-40, 0.5 % sodium deoxycholate
Low Salt buffer	10 mM tris pH 8.0, 1 mM EDTA
Lower Tris	181.7 g tris, 0.4 % SDS, ad 1 L ddH_2O, pH 8.8
NDLB buffer	137 mM NaCl, 20 mM tris pH 8.0, 2 mM EDTA, 10 % glycerine, 1 % NP-40, cOmplete Protease Inhibitor Cocktail
PBS-T	Dulbecco`s PBS, 1 % Triton X-100
RIPA buffer	150 mM NaCl, 50 mM tris pH 8.0, 1 % NP-40, 0.5 % sodium deoxycholate, 0.1 % SDS, cOmplete Protease Inhibitor Cocktail
Running buffer	190 mM glycine, 25 mM tris, 0.1 % SDS, pH 8.3
Separating gel	3.33 ml ddH_2O, 2.67 ml Rotiphorese® Gel 30, 2 ml Lower Tris, 15 µl TEMED, 15 µl 10 % APS
Stacking gel	3.15 ml ddH_2O, 1.25 ml Upper Tris, 0.6 ml Rotiphorese® Gel 30, 15 µl TEMED, 15 µl 10 % APS
TAE buffer	100 ml EDTA 0.5 M, 57.1 ml glacial acetic acid, 242 g tris, ad 1000 ml ddH_2O, pH 8.0
TBS	150 mM NaCl, 50 mM tris HCl pH 7.4
TBS-T	TBS, 0.05 % Tween 20
Upper Tris	60.6 g tris, 0.4 % SDS, ad 1 L ddH_2O, pH 6.8

2.1.5 Culture Media

Acinar explants medium	Waymouth´s medium, 0.1 % BSA, 4 µg/ml SBTI, 50 µg/ml BPE, 1 % Selenium X, 0.2 % Pen/Strep, 0.1 % FCS, 0.25 µg/ml Amphotericin B
$DMEM_{FCS + NEAA + P/S}$	DMEM medium, 10 % FCS, 1 % Non-Essential Amino Acids, 1 % Pen/Strep
$DMEM_{Cryo}$	70 % DMEM medium, 20 % FCS, 10 % DMSO
$DMEM_{G418}$	$DMEM_{FCS + NEAA + P/S}$ medium, 500 µg/ml G418
LB_{fluid}	Lysogeny broth, Luria fluid culture medium (Luria and Burrous, 1957): 10 g Trypton, 5 g yeast extract, 0.5 g NaCl, pH 7.2, ad 1000 ml ddH_2O
LB_{solid}	Lysogeny broth, Miller solid culture medium (Miller, 1972): 10 g Trypton, 5 g yeast extract, 10 g NaCl, pH 7.2, 15 g agarose, ad 1000 ml ddH_2O
LB_{amp}	$LB_{fluid/solid}$, 100 mg/L ampicillin

2.1.6 Vectors

The following vectors were used during this work and were provided by other institutions. The particular vector maps are documented in the appendix.

pCAG-MS	Expression vector used for negative controls; P CAG, amp^R (Shindo *et al.,* 2002; University of Tokyo).
pCAG-MS-Klf5	pCAG-MS vector containing the *Klf5* mRNA sequence for overexpression (Shindo *et al.,* 2002; University of Tokyo).
pCAGGS-Cherry-Neo	Contains the *cherry* gene under the control of the CAGGS promoter; P CAGGS, *cherry*, *β-globin* pA, P SV40, neo^R, amp^R (Chair of Livestock Biotechnology, TUM).

2.1.7 Primers

Primer	Sequence
ChIP CK19 for 1	CGT GAC ATG TTG GCA GTA GC
ChIP CK19 rev 1	TGC AAA TAT GGG CTC TTT CC
ChIP CK19 for 2	AGG GGA GAG GTA GGA GCA GA
ChIP CK19 rev 2	CCC TCA CCT GTG GCT TTT TA
ChIP CK19 for 3	GCA CAT CCC ATT GAT TCC TT
ChIP CK19 rev 3	GAG GCC ATG GAA ACT TGT CT
ChIP EGFR for 1	CTC CTC CTC TTC GCT CCT CT
ChIP EGFR rev 1	TGC CCA GAC GTC TAG TTA GC
ChIP EGFR for 2	CGG AGT CCC CTC AGA AAT TA
ChIP EGFR rev 2	CCT TGG CCA CCA CTA GAC AA
Cre001	ACC AGC CAG CTA TCA ACT CG
Cre002	TTA CAT TGG TCC AGC CAC C
Cre003	CTA GGC CAC AGA ATT GAA AGA TCT
Cre004	GTA GGT GGA AAT TCT AGC ATC ATC C
mG_Egr1_common	GGG CAC AGG GGA TGG GAA TG
mG_Egr1_wt	AAC CGG CCC AGC AAG ACA CC
mG_Egf1_mut	CTC GTG CTT TAC GGT ATC GC
mG_Kras_wt_UP1	CAC CAG CTT CGG CTT CCT ATT
mG_Kras_URP_Lp1	AGC TAA TGG CTC TCA AAG GAA TGT A
mG_Kras_mut_UP	CCA TGG CTT GAG TAA GTC TGC
mG_Mek1DD_mut	TTG TTC GGA TCC ATA ACT TCG
mG_Mek1DD_comm	AAG GGA GCT GCA GTG GAG TA
mG_Mek1DD_wt	CCG AAA ATC TGT GGG AAG TC
mG_p110a_UP	AAA GTC GCT CTG AGT TGT TAT
mG_p110a_MUT	GCG AAG AGT TTG TCC TCA ACC
mG_p110a_WT	GGA GCG GGA GAA ATG GAT ATG
$p53^{R172H}$-wt-For	AGC CTT AGA CAT AAC ACA CGA ACT
$p53^{R172H}$-mut-For	GCC ACC ATG GCT TGA GTA A
$p53^{R172H}$-uni-Rev	CTT GGA GAC ATA GCC ACA CTG
mqAmylase for	TGG TCA ATG GTC AGC CTT TTT C
mqAmylase rev	CAC AGT ATG TGC CAG CAG GAA G
mqCK19 for	ACC CTC CCG AGA TTA CAA CCA
mqCK19 rev	GGC GAG CAT TGT CAA TCT GT
mqCyclophilin for	ATG GTC AAC CCC ACC GTG T
mqCyclophilin rev	TTC TGC TGT CTT TGG AAC TTT GTC
mqEgfr for	GTC TGC CAA GGC ACA AGT AAC
mqEgfr rev	CAC CTC CTG GAT GGT CTT TAA
mqEgr1 for	CCA CAA CAA CAG GGA GAC CT
mqEgr1 rev	ACT GAG TGG CGA AGG CTT TA
mqKlf5 for	GGA TCT GGA GAA GCG ACG TA
mqKlf5 rev	CCC GTA TGA GTC CTC AGG TG
ms_Egfr_Fw2	AAG GTC GGA ACC TCT GAG ACG
ms_Egfr_Rv1	CAG AGA GAT CTC CAC ACT TCC
p48-Cre487 F	GTC CAA TTT ACT GAC CGT ACA CCA A
p48-as1642 R	CCT CGA AGG CGT CGT TGA TGG ACT GCA
TGFα for	GGC TTT TTG ACA ACG CTA TG
TGFα rev	TGA GAG GTC ATA GAC GTT GC

Table 2.1: List of primers.

2.1.8 Antibodies

Antibody	Product No.	Manufacturer	Species	Dilution Western Blot	Dilution Immunohistology
Acetyl Histone H4	06-866	Millipore	rabbit	-	-
AKT (phospho Thr 308)	2965S	Cell Signaling	rabbit	-	1:200
Alexa Fluor 488 α-Goat	A11055	Invitrogen	donkey	-	1:500
Alexa Fluor 488 α-Rabbit	A21206	Invitrogen	donkey	-	1:500
Alexa Fluor 568 α-Rat	A11077	Invitrogen	goat	-	1:500
AMY	sc-12821	Santa Cruz	goat	1:500	-
AMY	A8273	Sigma	rabbit	-	1:200
β-Actin	A2228	Sigma	mouse	1:20000	-
Biotinylated α-Mouse IgG	BA-9200	Vector Labs	goat	-	1:500
Biotinylated α-Rabbit IgG	BA-1000	Vector Labs	goat	-	1:500
Biotinylated α-Rat IgG	BA-4000	Vector Labs	rabbit	-	1:500
CK19	m0888	DSHB	rat	1:500	1:100
CLDN18	700178	Invitrogen	rabbit	-	1:200
ECL™ α-Mouse IgG	NA931V	GE Healthcare	sheep	1:10000	-
ECL™ α-Rabbit IgG	NA934V	GE Healthcare	donkey	1:10000	-
EGFR	06-847	Millipore	rabbit	1:1000	-
EGR1	4153S	Cell Signaling	rabbit	1:500	1:500
ERK1	sc-93	Santa Cruz	rabbit	1:1000	-
ERK2	sc-154	Santa Cruz	rabbit	1:1000	-
ERK1/2 (phospho)	9106S	Cell Signaling	mouse	1:1000	-
ERK1/2 (phospho)	4376S	Cell Signaling	rabbit	-	1:200
HSP90	sc-7947	Santa Cruz	rabbit	1:1000	-
KLF5	07-1580	Millipore	rabbit	1:500	1:500
MUC5	ms-145-P1	NeoMarkers	mouse	-	1:200

Table 2.2: List of antibodies.

2.1.9 Bacterial and Mammalian Cell Lines

Escherichia coli — OneShot®TOP10; Genotype: F^- mcrA Δ(mrr-hsdRMS-mcrBC) Φ80lacZΔM15 ΔlacX74 recA1 araD139 Δ(araleu)7697 galU galK rpsL (StrR) endA1 nupG (Life Technologies GmbH)

266-6 — Murine pancreatic acinar cell tumour derived cell line (Ornitz *et al.,* 1985)

2.1.10 Mouse Strains

The following mouse strains were commercially purchased, provided by other institutions or crossed internally. Wild type control mice were either C57BL/6J mice or transgenic mice with Cre recombinase dependend, conditional mutations but without Cre expression.

Strain	Genotype	Reference
C57BL/6J	-	Paigen *et al.,* 1985
$Egfr^{\Delta Panc}$	$Ptf1a^{+/Cre};Egfr^{fl/fl}$	Natarajan *et al.,* 2007
$Egr1^{KO}$	$Egr1^{-/-}$	Lee *et al.,* 1995
$Kras^{G12D}$	$Ptf1a^{+/Cre};Kras^{+/LSL\text{-}G12D}$	Hingorani *et al.,* 2003
$Kras^{G12D};Egfr^{\Delta Panc}$	$Ptf1a^{+/Cre};Kras^{+/LSL\text{-}G12D};Egfr^{fl/fl}$	Ardito *et al.,* 2012
$Kras^{G12D};Egr1^{KO}$	$Ptf1a^{+/Cre};Kras^{+/LSL\text{-}G12D};Egr1^{-/-}$	Unpublished
Mek1DD	$Ptf1a^{+/Cre};R26^{+/LSL\text{-}Mek1DD}$	Srinivasan *et al.,* 2009
$Mek1DD;Egfr^{\Delta Panc}$	$Ptf1a^{+/Cre};R26^{+/LSL\text{-}Mek1DD};Egfr^{fl/fl}$	Unpublished
$Mek1DD;P53^{R172H}$	$Ptf1a^{+/Cre};R26^{+/LSL\text{-}Mek1DD};P53^{+/LSL\text{-}P53R172H}$	Unpublished
$P110\alpha^{H1047R}$	$Ptf1a^{+/Cre};R26^{+/LSL\text{-}p110\alpha H1047R}$	Eser *et al.,* 2013
$P53^{R172H}$	$Ptf1a^{+/Cre};P53^{+/LSL\text{-}P53R172H}$	Hingorani *et al.,* 2005
Ptf1aCre	$Ptf1a^{+/Cre}$	Nakhai *et al.,* 2007
Tgfα	*Ela-Tgfα*	Sandgren *et al.,* 1990
$Tgf\alpha;Egfr^{KO}$	$Ela\text{-}Tgf\alpha;Ptf1a^{+/Cre};Egfr^{fl/fl}$	Ardito *et al.,* 2012
$Tgf\alpha;Egr1^{KO}$	$Ela\text{-}Tgf\alpha;Egr1^{-/-}$	Unpublished

Table 2.3: List of mouse strains.

2.2 METHODS

2.2.1 Isolation and Modification of Nucleic Acids

2.2.1.1 Isolation of Plasmid DNA from *E. coli*

Plasmid DNA was isolated using the Promega PureYield™ Plasmid Miniprep System and the Promega PureYield™ Plasmid Midiprep System, depending on the amount of DNA required. Both kits are based on the alkaline lysis previously described (Sambrook and Russell, 1989) and use silica membrane columns for DNA binding. These allow following washing steps in order to eliminate salts and cell fragments, and the DNA can be subsequently eluted directly from the column with ddH_2O. Therefore, silica membrane columns provide clean samples for sensitive downstream applications. For restriction analysis and size control of vectors, the PureYield™ Plasmid Miniprep System was used. Here, the transformed *E. coli* bacteria were cultured on a shaker o/n at 37 °C and 230 rpm and 2 ml aliquots out of 5 ml cultures were used for the preparations. When higher amounts of DNA were needed, for example for transformations, transfections or sequencing, a Midi-Prep was performed using the PureYield™ Plasmid Midiprep System. Here, 150 ml culture batches were used. The isolations were carried out as described in the particular technical manual and the plasmid DNA was subsequently stored at - 20 °C.

2.2.1.2 Isolation of Plasmid DNA from Agarose Gels

For isolation of a certain DNA fragment from a mixture of differently sized fragments, for example after a PCR or a digest of a vector, or for removing residual buffer, primers and enzymes in an isolate, the samples were separated by agarose gel electrophoresis. The desired fragment was identified by size markers and cut out of the gel with a scalpel. Subsequently, the enclosed DNA was isolated using the Promega Wizard® SV Gel and PCR Clean-Up System as described in the technical manual. The samples were stored at - 20 °C.

2.2.1.3 Isolation of Genomic DNA from Mammalian Tissues

Genomic DNA was needed for genotyping of mice used during this work. Generally, the genomic DNA was isolated from the tail tip of the particular mouse using the KAPA Biosciences KAPA Express Extraction kit. Here, the tail tip was lysed in 100 µl of lysis

solution, containing 88 µl of ddH_2O, 10 µl of lysis buffer and 2 µl of Proteinase K. The sample was incubated for 10 min at 75 °C and the enzyme was subsequently heat inactivated for 5 min at 95 °C. The sample was mixed via vortexing for 10 sec and directly used for genotyping or stored at - 20 °C. If mice which had already been sacrificed had to be re-genotyped, frozen tissue pieces were used for genomic DNA isolation. For this purpose, the Qiagen DNeasy Blood & Tissue Kit was used as described in the technical manual. Subsequently, the sample was used directly for genotyping or stored at - 20 °C.

2.2.1.4 Isolation of Total RNA from Mammalian Cells and Tissues

Total RNA was isolated from both mammalian cells and tissues. For isolation from cells grown in monolayers, the medium was removed and the cells were washed twice with Dulbecco`s PBS. Subsequently, 350 µl of Macherey-Nagel RA1 lysis buffer was added and the cells were scratched down the cell culture flask with a cell scratcher. If cells were grown in suspension cultures, they were sedimented via spinning for 5 min at 430 x g and the supernatant was removed. The cell pellet was washed twice with PBS and 350 µl of RA1 lysis buffer was added. In both cases, the sample was subsequently mixed via pipetting and directly used for RNA isolation or frozen at - 80 °C. For isolation of total RNA from mammalian tissues, three small pieces of different areas were cut out of a fresh organ and 350 µl of RA1 lysis buffer were added. The sample was shredded using the Heidolph Silentcrusher M shredder and directly used for RNA isolation or frozen at - 80 °C. The RNA of both cells and tissues was isolated using the Promega Maxwell® 16 Instrument and the Maxwell® 16 LEV simplyRNA Tissue Kit. The isolation was carried out as described in the technical manual and the RNA was subsequently stored at - 80 °C.

2.2.1.5 Restriction Digest of DNA

Plasmid DNA was digested for size control of vectors or for cloning purposes. Bacterial endonucleases were used for digestion, which bind to a specific DNA target sequence and catalyse a hydrolysis of phosphodiester bonds. This leads to blunt or sticky ends exhibiting a specific overhanging sequence depending on the enzyme used. All endonucleases used during this work were purchased from NEB and were used with the appropriate buffers. For restriction of 1 µg of DNA, 1 U of enzyme and a buffer concentration of 1 x were used. The reaction batches were prepared following the manufacturer´s protocol.

2.2.1.6 Ligation of DNA

DNA fragments arisen from a restriction can be reconnected if the concerning fragments have blunt or complementary sticky ends with terminal phosphate groups. This reaction can be catalysed by a ligase and is energy dependent. The ligase hydrolyses adenosine triphosphate (ATP) and uses the energy from this exothermic reaction to esterify a 3' hydroxyl and a 5' phosphate group of two terminal nucleotides. In this work, the NEB T4 ligase and the appropriate ligase buffer were used. For the reactions, the vector and the insert were added at a ratio of 1:3 and incubated for 1 h at RT or o/n at 16 °C. The reaction batches were prepared following the manufacturer´s protocol.

2.2.1.7 Blunting of Single Stranded DNA Overhangs

If blunt ends were needed for ligation, the single stranded DNA (ssDNA) overhangs emerged from restriction digestions were filled up using the NEB DNA Polymerase I Klenow fragment. This polymerase synthesizes complementary DNA strands of ssDNA, but has lost 5'→3' exonuclease activity. The reaction was performed for 15 min at 25 °C and was stopped by incubating the samples for 20 min at 75 °C. The reaction batches were prepared following the manufacturer´s protocol.

2.2.1.8 Hydrolysis of Terminal Phosphate Groups

After linearizing a vector via digestion with only one restriction enzyme, its two ends are complementary to each other. If an insert is attempted to be ligated into this vector, it is highly probable that the vector religates under the influence of the ligase without taking up any insert. In order to inhibit a religation of single enzyme digested vectors, a phosphatase was used to hydrolyse the 5' phosphate groups of the vector´s ends. Without these groups, it is not possible for the ligase to catalyse the connection of two complementary DNA ends. Only if an insert with an intact 5' phosphate group is inserted, it is possible to ligate the vector and the fragment together. During this work, the NEB antarctic phosphatase from *Pandalus borealis* was used. The samples were incubated for 15 min at 37 °C for 5' extensions or blunt ends and 60 min at 37 °C for 3' extensions. The reaction batches were prepared following the manufacturer´s protocol.

2.2.1.9 Attachment of Terminal Phosphate Groups

Since unphosphorylated primers were used during this work, it was necessary to phosphorylate PCR products if they were supposed to be cloned blunt into a dephosphorylated vector. For this purpose, the NEB T4 polynucleotide kinase was used, which attaches terminal phosphate groups to DNA ends under ATP usage. Instead of the original T4 polynucleotide kinase buffer, which does not include ATP, the NEB T4 Ligase buffer was used during this reaction. This buffer already contains ATP, which makes an addition of this ligand unnecessary. The reaction was performed for 1 h at 37 °C. The reaction batches were prepared following the manufacturer´s protocol.

2.2.2 Amplification and Analysis of Nucleic Acids

2.2.2.1 Primer Design

The primers used during this work were designed with Primer3Plus, an online primer design tool, which is available at http://www.primer3plus.com. If one or two restriction sites were added to the complementary primer sequence, an additional stuffer sequence of 4 bp to 6 bp was added to one end of each primer, which provides enough surrounding DNA sequence for an efficient binding and cutting of the particular restriction enzyme. All primers were purchased from Eurofins MWG Operon GmbH, Ebersberg and were diluted with ddH_2O to a final stock concentration of 100 µM.

2.2.2.2 Polymerase Chain Reaction

The Polymerase Chain Reaction (PCR) allows a quick and specific amplification of DNA fragments *in vitro* from nearly every DNA template. For a PCR, desoxynucleotides, primers (oligonucleotides with a length of 15 bp to 30 bp), a DNA polymerase and a DNA template are needed. It is performed in several cycles which can be subdivided into three distinct reaction steps. The first one is the denaturation step, at which the two DNA strands are separated by incubating the samples at 95 °C for 30 sec. This allows the primers to access and bind the DNA strands, which is performed in the second step, the annealing phase. Here, the samples are incubated at a primer specific temperature which allows the primers to bind the template strands efficiently. The annealing temperature depends on the length of the primers as well as on the number of G and C nucleotides present. The primers are necessary as a

starting point for the polymerase from which it subsequently synthesizes a new complementary DNA strand during the elongation step. The duration and the temperature of the elongation phase depend on the polymerase used. For the amplification of DNA fragments used for further cloning steps, the Thermo Fisher Scientific Phusion™ High-Fidelity DNA Polymerase was used, which has an activity optimum at 72 °C and which synthesizes a strand of approximately 1 kb per 30 sec. In addition, this polymerase provides a proof reading function, which reduces failures during elongation steps. All reaction steps are repeated every cycle, and an average of 35 cycles was performed in each PCR. In addition, there is a first denaturation step at the beginning of each PCR at which the samples are incubated for 2 min at 95 °C and a last elongation step at the end at which the samples are incubated for 5 min at 72 °C. The permanent repeat of denaturation, annealing and elongation leads to a virtually exponential amplification of a specific DNA fragment present within the sample. In this work, the thermo cyclers Eppendorf Mastercycler, Applied Biosystems GeneAmp® PCR System 9700 and MWG Biotech Primus 96 Plus were used. The reaction batches were prepared following the manufacturer´s protocol.

2.2.2.3 Reverse Transcriptase Polymerase Chain Reaction

For analysis of the expression level of genes of interest, the isolated total RNA had to be transcribed into complementary DNA (cDNA). DNA is much more stable than RNA and is both easier to maintain and to use. In addition, the cDNA can be used as a working solution in order to keep the RNA from being contaminated with RNases. Therefore, a reverse transcriptase PCR (RT-PCR) was performed to synthesize cDNA. The reverse transcriptase catalyses the binding of free desoxynucleotide triphosphates (dNTPs) to the template RNA and subsequently elongates the cDNA strand. Here, Promega oligo dT primers were used, which only bind to the poly adenosine tail of any mRNA present. Before starting the reverse transcription, the concentrations of the RNA samples were measured and the RNA was subsequently diluted with ddH_2O to provide an equal concentration of RNA within all samples. An equal amount of RNA was then used for each RT-PCR reaction. The RNA samples themselves were first of all incubated for 5 min at 65 °C in order to denature loops which lead to double strand formation. The Invitrogen SuperScript® II Reverse Transcriptase was used for the following reverse transcription. This reaction can be divided into three phases: annealing, reverse transcription and enzyme inactivation. During the annealing phase, the oligo dT primers bind to the template RNA, which was performed for 5 min at 42 °C. The

transcription of RNA to cDNA was performed for 50 min at 42 °C and the reverse transcriptase was finally inactivated by incubating the samples for 10 min at 70 °C. The cDNA was subsequently used for a following PCR or was stored at - 20 °C.

2.2.2.4 Quantitative Real-Time Polymerase Chain Reaction

The quantitative real-time PCR (qPCR) is based on a regular PCR, but in addition, it is possible to directly track the amount of products produced during the reaction in real-time. This is achieved by using a fluorescent dye, which intercalates into the synthesised products. The more specific template DNA is present within the sample, the more products are produced and the stronger becomes the fluorescence of the sample, which is permanently detected by a laser beam. By using cDNA as a template, it is therefore possible to quantify the expression level of a gene of interest within the tissues used. For this purpose, the crossing point values (CP) of both the gene of interest and a housekeeping gene were analysed. The CP value indicates the exact number of cycles which were necessary for the product fluorescence to rise above the background fluorescence. The more specific template DNA is present within the sample, the fewer cycles are needed for crossing this point. The results were subsequently analysed using the ΔΔCP method. First, the ΔCP values were determined by subtracting the CP value of the housekeeping gene from the CP value of the gene of interest for each sample. The average ΔCP value of all wild type or untreated samples was subsequently subtracted from each sample in order to calculate the ΔΔCP values. Fold change values were received by further calculating $2^{-\Delta\Delta CP}$. The fold change values were subsequently blotted.
In addition, a melting curve was generated at the end of each qPCR by slowly increasing the temperature from 60 °C to 99 °C in 0.5 °C steps. The resulting graph shows distinct peaks for each product, which depends on its specific G/C content as well as its length. In this work, the Roche LightCycler® 480 in combination with the Roche LightCycler® 480 SYBR Green I Master kit was used for cycling and quantification. The included LightCycler® 480 1.5.0 software was used for evaluation. All qPCRs were carried out using an annealing temperature of 60 °C.

2.2.2.5 Genotyping

The mice used during this work were genotyped at an age of 3 weeks. For this purpose, the tail tip of the particular mouse was cut and the genomic DNA was isolated. This DNA served

as a template in a set of PCRs, each specific for one of the genetic mutations present within the mouse strain. If separated via agarose gel electrophoresis, the specific sizes of the PCR products indicate if and how many mutated alleles the genome of the mouse holds. The PCRs were carried out using the KAPA Biosystems KAPA2G Fast HS Genotyping Mix or the Sigma-Aldrich RedTaq® Ready Mix™ PCR Reaction Mix as described in the manufacturer´s protocol. All genotyping PCRs performed during this work, the particular primers used, their annealing temperatures as well as their product sizes are specified below.

Gene	Primers	T_m	Product Wild type	Product Mutated
Cre	Cre001, Cre002, Cre003, Cre004	58 °C	324 bp	199 bp
Cre (Ptf1a)	p48-Cre487 F, p48-as1642 R	58 °C	-	1155 bp
$Egfr^{\Delta Panc}$	ms_Egfr_Fw2, ms_Egfr_Rv1	58 °C	180 bp	320 bp
$Egr1^{KO}$	mG_Egr1_wt, mG_Egf1_mut, mG_Egr1_common	58 °C	416 bp	420 bp
$Kras^{G12D}$	mG_Kras_wt_UP1, mG_Kras_mut_UP, mG_Kras_URP_Lp1	58 °C	280 bp	180 bp
Mek1DD	mG_Mek1DD_wt, mG_Mek1DD_mut, mG_Mek1DD_comm	58 °C	297 bp	347 bp
$P53^{R172H}$	$p53^{R172H}$-wt-for, $p53^{R172H}$-mut-for, $p53^{R172H}$-uni-rev	58 °C	565 bp	270 bp
$P110\alpha^{H1047R}$	mG_p110a_UP, mG_p110a_MUT, mG_p110a_WT	58 °C	600 bp	410 bp
Tgfα	TGFα for, TGFα rev	58 °C	-	550 bp

Table 2.4: Genotyping primers and their expected PCR products.

2.2.2.6 Agarose Gel Electrophoresis

In order to separate DNA fragments by their size, an agarose gel electrophoresis was performed as described previously (Sambrook and Russell, 1989). The gels used had an agarose concentration of 1 % to 2 %, depending on the size of fragments being separated. Per 100 ml gel, 5 µl of 1 mg/ml ethidium bromide were added which intercalates into the DNA during electrophoresis. To provide an improved sink down into the gel slots and the possibility to track the samples within the gel, a DNA loading buffer was added at a ratio of 1:6 to each sample. In addition to the samples, a size marker was loaded onto the gel to allow an estimation of the DNA fragment sizes. During this work, the Peqlab peqGOLD DNA Ladder Mix as well as the Peqlab Blue Loading Buffer were used. The separation was performed with 1 x TAE buffer at a voltage of 120 V to 160 V using the Bio-Rad Sub-Cell® GT electrophoresis chamber. Subsequently, the DNA was made visible under UV light which induces a fluorescence of the intercalated ethidium bromide. The fluorescenting bands were documented by photography using the Bio-Rad Gel Documentation System as well as the Bio-Rad Quantity One 4.5.2 software.

2.2.2.7 Spectrophotometry

The concentration of DNA within a sample was measured photometrical by sending a ray of light of a specific wave length through the sample. The Thermo Fisher NanoDrop 2000 spectrophotometer and the NanoDrop 2000 1.4.1 software were used for this purpose, which emits the wave lengths 260 nm and 280 nm. It detects the amounts of light which passes the mixture and calculates the rate of its absorbance. A light absorbance of 1.0 at 260 nm approximately equals 50 µg/ml of DNA. In addition, the quotient of the absorbance rate at 260 nm and the absorbance rate at 280 nm provides information about the purity of the sample. A ratio of 1.8 equals a pure sample, while a ratio above this value indicates a protein contamination.

2.2.2.8 Sequencing

All sequences which were amplified via PCR and subsequently cloned into vectors were verified via sequencing. The vector containing the sequence of interest was isolated from *E. coli*, diluted to a final concentration of 100 ng/µl of DNA and sequenced at Eurofins MWG Operon GmbH, Ebersberg.

2.2.3 Isolation and Analysis of Proteins

2.2.3.1 Isolation of Proteins from Mammalian Cells and Tissues

Protein isolation was performed using radio immunoprecipitation assay (RIPA) buffer or non-denaturing lysis buffer (NDLB). RIPA buffer is a strong denaturing buffer capable of disrupting nuclear membranes, which is helpful for isolation of proteins present in the nucleus. However, the usage of RIPA buffer can also lead to denaturing of some proteins. NDLB buffer is a mild lysis buffer which does not denature most proteins. To isolate proteins from mammalian cells grown in monolayers, the cells were washed twice with PBS and an appropriate amount of lysis buffer was added. Cells grown in suspension cultures were sedimented via spinning at 430 x g. The cell pellet was washed twice with PBS and resuspended in an appropriate amount of lysis buffer. For isolation of proteins from mammalian tissue, three small pieces of different areas were cut out of a fresh organ and frozen at - 80 °C or directly lysed. The tissue pieces were lysed by adding 300 µl of lysis buffer and shredded using the Heidolph Silentcrusher M shredder. In all cases, the lysed

samples were incubated on ice for 20 min and subsequently sonicated for 10 sec using the Bandelin Electronic Sonopuls UW2070 sonicater. This sonicater sends out an ultrasound which disrupts cell and also nuclear membranes and therefore facilitates the lysis of the sample. Subsequently, remaining cell and tissue debris was sedimented via spinning for 20 min at 14.000 x g and 4 °C and the protein containing supernatant was frozen at - 80 °C or directly used for downstream applications.

2.2.3.2 Bicinchoninic Acid Assay

The bicinchoninic acid (BCA) assay was used for determination of the protein concentration of a sample and is based on the measurement of a colour change proportional to the amount of protein present. The peptide bonds of the proteins reduce Cu^{2+} ions to Cu^{+} ions, leading to a Cu^{+} concentration proportional to the concentration of protein present. The Cu^{+} ions further react with BCA and form a purple coloured product which is capable of absorbing light of a wavelength of 562 nm. The absorbance rate of the samples can be measured with a photometer. If standards are analysed simultaneously, a standard curve can be drawn and the protein concentration of the samples can be calculated. During this work, the Thermo Scientific Pierce® BCA Protein Assay kit was used and the assay was performed as described in the technical manual. The absorbance of samples was subsequently measured using the Thermo Scientific Multiskan FC photometer.

2.2.3.3 Western Blot

Western Blots were performed in order to analyse the expression levels of specific proteins of a sample. This method is based on the separation of the proteins via SDS page, a subsequent transfer to a nitrocellulose membrane and the detection of the desired protein using a specific antibody. The samples were diluted with the particular lysis buffer to an equal volume and concentration. Depending on the concentration of the samples, an average of 10 µg to 40 µg of protein was used for Western Blotting. Laemmli loading buffer was added to the samples at a ratio of 1:6 and they were subsequently incubated for 10 min at 95 °C. An SDS page gel was prepared, consisting of an upper stacking gel and a lower separation gel. An acryl amide concentration of 3 % was used for the stacking gel; the concentration of the separation gel was chosen depending on the size of proteins to be analysed. For most proteins blotted during this work, a concentration of 8 % was used. The samples and the Bio-Rad Precision Plus

Protein™ All Blue Standard were loaded onto the gel and separated via electrophoresis at 120 V using the Bio-Rad Power Pac™ Basic power supply and the Bio-Rad Mini Protean Gel System chambers containing SDS running buffer until the desired level of separation was achieved. After separation, the proteins were transferred to a methanol activated nitrocellulose membrane via electrophoresis for 2 h at 100 V in transfer buffer. Here, the gel and the membrane were flanked by two filter papers and a sponge on each side. During transfer, the blotting chamber was cooled on ice to avoid an overheating of both the buffer and the gel. The membrane was subsequently washed twice for 5 min at RT in TBS-T and was incubated for 1 h at RT in TBS-T containing 5 % of skim milk powder in order to block unspecific binding sites. The primary antibody against the protein of interest was diluted at a suitable ratio in TBS-T and 5 % skim milk powder and was added to the membrane. The membrane was incubated 1 h at RT or o/n at 4 °C. Subsequently, the membrane was washed three times for 10 min at RT in TBS-T and incubated for 1 h at RT in TBS-T and 5 % skim milk powder containing the specific horseradish peroxidase (HRP) linked secondary antibody at a ratio of 1:10,000. The membrane was washed three times for 5 min at RT in TBS-T and incubated for 5 min in GE Healthcare Amersham™ ECL™ Western Blotting Detection Reagents or in Thermo Scientific SuperSignal® West Fempto Maximum Sensitivity Substrate. These reagents emit light under the influence of the HRP. The chemoluminescence was subsequently detected using GE Healthcare Amersham Hyperfilm™ ECL films and the Amersham Biosciences Hyper Processor developing system.

2.2.3.4 Chromatin Immunoprecipitation Assay

A chromatin immunoprecipitation was performed in order to investigate if a transcription factor binds to a certain gene of interest, which indicates direct regulation. Tissue pieces of a size of approx. 2 mm were cut out of the pancreas and incubated in 10 ml of PBS and 1 % of PFA for 12 min at RT; at this step, the genomic DNA bound is cross-linked to the transcription factor. Subsequently, 1140 µl of glycine (1.25 M) were added, the sample was mixed briefly via vortexing and incubated for 5 min at RT. After washing in PBS and protease inhibitors at 4 °C, the tissue pieces were transferred into 600 µl of lysis buffer L2 at 4 °C. In order to achieve DNA fragments of a size of approx. 500 bp, the sample was sonicated twice for 15 sec at 30 % power using the Bandelin Electronic Sonopuls UW2070 sonicater. Subsequently, cell debris was sedimented via spinning for 10 min at 13,000 rpm and 4 °C. The supernatant was transferred into a new reaction tube, the DNA concentration was

measured via spectrophotometry and an appropriate volume of DNA was separated via agarose gel electrophoresis in order to verify the correct size of the DNA fragments. Subsequently, 80 µl of Protein A Agarose / Salmon Sperm DNA were added to the sample and incubated for 2 h at 4 °C with agitation. The beads were sedimented via spinning for 1 min at 2,000 rpm and 4 °C and the supernatant was transferred to a new reaction tube. After splitting the sample into three equal volumes, a primary antibody against the transcription factor of interest was added to the first part of the sample. An antibody against acetyl-Histone H4 was added to the second part and served as a positive control; serum of the species the first antibody was made in was added in an equal dilution to the third sample and served as a negative control. All samples were incubated o/n at 4 °C with agitation. Subsequently, 80 µl of Protein A Agarose / Salmon Sperm DNA were added to each sample and they were incubated for 2 h at 4 °C with agitation. The beads were sedimented via spinning for 1 min at 800 rpm and 4 °C, the supernatant was stored at - 20 °C and the pellet was washed four times with 1 ml of low salt buffer. After transferring the beads into a new reaction tube, they were washed four times with 1 ml of LiCl buffer and again transferred into a new reaction tube. Subsequently, the beads were washed four times with 1 ml of high salt buffer and transferred into a new reaction tube. In order to elute the protein – DNA complexes from the Protein A Agarose / Salmon Sperm DNA, 300 µl of elution buffer were added to each sample and they were incubated for 15 min at 800 rpm and 65 °C. The beads were sedimented via spinning for 1 min at 800 rpm and RT, 250 µl of supernatant were collected and the elution was repeated with another 300 µl of elution buffer. The beads were sedimented via spinning for 1 min at 800 rpm and RT, the supernatant was collected and combined with the first supernatant. Subsequently, 30 µl of NaCl (5 M) were added to the samples and they were incubated for 5 h at 800 rpm and 65 °C in order to reverse the cross-linking of the transcription factor and the bound genomic DNA. Subsequently, the proteins present within the samples were digested by adding 2 µl of Proteinase K and incubating for 2 h at 400 rpm and 55 °C. The remaining DNA was precipitated via a phenol - chloroform extraction. Here, 532 µl of phenol / chloroform were added to the samples, they were mixed briefly via vortexing and phases were separated via spinning for 5 min at 14,000 rpm and RT. The upper phase was collected and transferred into a new reaction tube. Subsequently, 515 µl of chloroform were added, the samples were mixed briefly via vortexing and the phases were separated via spinning for 5 min at 14,000 rpm and RT. The supernatant was transferred into a new reaction tube and 50 µl of NaCl (3 M, pH 5.2) were added. After mixing briefly via vortexing, 1,100 µl of 100 % EtOH were added, the samples were mixed briefly via vortexing again and subsequently incubated for 1 h

at - 20 °C. The precipitated DNA was sedimented via spinning at 14,000 rpm and 4 °C, the supernatant was discarded and the pellet was washed with 300 µl of 70 % EtOH. The supernatant was discarded, the pellet was dried at RT and resuspended in 40 µl of ddH_2O. Subsequently, the samples were analysed via PCR and stored at - 20 °C. Primers used for PCR analysis are listed below.

Gene	Primers	T_m	Product Size
Ck19	ChIP CK19 for 1, ChIP CK19 rev 1	62 °C	140 bp
	ChIP CK19 for 2, ChIP CK19 rev 2	62 °C	150 bp
	ChIP CK19 for 3, ChIP CK19 rev 3	62 °C	142 bp
Egfr	ChIP EGFR for 1, ChIP EGFR rev 1	62 °C	102 bp
	ChIP EGFR for 2, ChIP EGFR rev 2	62 °C	96 bp

Table 2.5: ChIP Assay primers and their expected PCR products.

2.2.4 Cell Culture Methods

2.2.4.1 Culturing of *E. coli*

E. coli cells were cultured in solid or fluid LB media at 37 °C. In order to separate single colonies, *E. coli* cells were spread and cultured o/n on LB_{solid} media at 37 °C. For vector DNA isolation purposes, where high bacterial cell densities were needed, *E. coli* were cultured in an appropriate volume of LB_{fluid} medium at 230 rpm and 37 °C. Antibiotics were added to the media depending on the antibiotic resistance gene present within the vector the cells were transformed with. In case of Ampicillin, a final concentration of 100 µg/ml was used. For short-term storage of approx. 1 to 7 days, *E. coli* cells were stored at 4 °C. For long-term storage, the cells were stored via cryoconservation at - 80 °C.

2.2.4.2 Cryoconservation of *E. coli*

E. coli cells were stored long-term by inoculating glycerine cultures. Here, 1 ml of the particular *E. coli* LB_{fluid} culture was added to 1 ml of 99.8 % glycerine, which prevents the bacterial cells from being damaged by ice crystals. The samples were mixed well and subsequently stored at - 80 °C. If a new culture was to be inoculated for preparation of DNA, the cells were defrosted on ice until the glycerine culture became fluid, the new culture was inoculated and the glycerine culture was subsequently stored again at - 80 °C.

2.2.4.3 Culturing of Mammalian Cells

Mammalian cell lines were cultured in 25 cm², 75 cm² or 150 cm² cell culture flasks in the Heraeus Hera Cell 240 incubator at 37 °C with a CO_2 concentration of 5 % and 100 % humidity. Pancreatic tumour derived mouse cell lines were provided with $DMEM_{FCS+NEAA+P/S}$ medium. For culturing of 266-6 cells, 5 to 10 ml of 1 % gelatine were added to culture flasks and subsequently aspirated. The flasks were incubated for 1 h at 37 °C and the 266-6 cells were added afterwards, provided with $DMEM_{FCS+NEAA+P/S}$ medium containing 1 % of FCS. In order to establish primary cell lines from mouse tumours, fresh pancreatic tumour tissue was cut into small pieces, provided with $DMEM_{FCS+NEAA+P/S}$ medium and cultured at 37 °C. After 24 to 48 h, the remaining tissue pieces were removed and the medium was renewed. The cells were cultured for 2 to 3 passages and subsequently cryoconserved or directly transferred into secondary culture.

Cell proliferation was controlled via bright field microscopy using the Zeiss Axiovert 40 CFL microscope. In order to provide optimal growth and proliferation conditions, the growth medium was renewed every 2 to 3 days, and the culture batches were splitted every 3 to 5 days, depending on the cell line cultured as well as on their specific proliferation rate. For culture batch splitting the medium was removed, the cells were washed once with PBS and subsequently detached by incubating in 3 ml of Trypsin for 5 min at 37 °C. After resuspending, 0.3 ml to 1 ml of the cell suspension was recultured by adding 15 ml of the appropriate growth medium; the remaining suspension was discarded. All cell culture experiments were performed sterile using the Heraeus Hera Safe working bench.

2.2.4.4 Cryoconservation of Mammalian Cells

For long-term storage of mammalian cells, the culture medium was removed and the cells were detached by adding 3 ml of Trypsin for 5 min. Subsequently, the cells were sedimented via spinning using the Eppendorf Centrifuge 5702 R for 5 min at 430 x g. The supernatant was removed, an appropriate volume of $DMEM_{Cryo}$ medium was added and the cells were resuspended and allocated into cryotubes with 1 ml each. The samples were transferred into a freezing container and frozen for 4 h at - 80 °C. Subsequently, the samples were stored in liquid nitrogen.

2.2.4.5 Selection of Mammalian Cells with Neomycin

Transfected cells were selected with neomycin to make sure that only transgenic cells which carried the neomycin resistance gene were cultured. For this purpose, 2 days after transfection the medium was removed and the cells were detached with Trypsin. Subsequently, medium with 500 µg/ml of G418 was added, which was changed every 1 to 2 days. The selection was carried out for approx. 10 days; if necessary the cells were occasionally detached and re-cultured to accelerate the selection.

2.2.4.6 Determination of the Cell Count

If a specific cell count was needed for transfection, the cells were detached with Trypsin and counted in a Neubauer improved counting chamber. The cell count was calculated using the following formula:

$$\text{cell count / ml} = \frac{\text{cells in 4 big squares}}{4} \cdot 10^4 \cdot \text{dilution factor}$$

2.2.4.7 *Ex Vivo* Acinar Explants

In order to perform *in vitro* studies with fresh, non-transformed pancreatic acinar cells, *ex vivo* acinar explants were used. The pancreas of a 4 to 5 weeks old mouse was freshly prepared, washed twice with sterile PBS in a culture dish and 5 ml of acinar explant solution II was added in order to digest the extracellular matrix of the acinar cells. The tissue was cut into small pieces with a scalpel and incubated for 10 min at 37 °C in the Hera Cell 240 incubator. The sample was shaken from time to time. Subsequently, the sample was transferred into a 50 ml falcon tube; the culture dish was washed with 10 ml of acinar explant solution I to remove residual cells and also transferred into the 50 ml falcon tube. The sample was sedimented by spinning for 5 min at 300 rpm and RT and the supernatant was discarded. The cell pellet was resuspended in 5 ml of acinar explant solution II and incubated for 10 min at 37 °C. A 100 µm nylon mesh was positioned on a 50 ml falcon tube, the sample was filtered through the mesh and residual tissue pieces were pressed through the mesh using a syringe plunger. Both the tissue dish and the nylon mesh were washed with 10 ml of acinar explant solution I and the sample was sedimented via spinning for 5 min at 300 rpm and RT. The supernatant was removed and the pellet was washed with 20 ml of acinar explant solution I.

The cell pellet was resuspended in 5 ml of acinar explant medium containing 30 % of FCS and incubated for 60 min at 37 °C. A 48-well culture plate was coated with 100 µl of collagen solution and incubated for 30 min at 37 °C. The sample was sedimented via spinning for 5 min at 300 rpm and RT, resuspended in an appropriate amount of acinar explant medium containing 0.1 % of FCS and mixed 1:1 with collagen solution. The cells were plated in 48-wells with 100 µl each and incubated for 30 min at 37 °C. Another 100 µl of collagen solution was added to each well and the plate was incubated for 30 min at 37 °C. Acinar explant medium was added carefully to the collagen embedded cells and they were subsequently cultured at 37 °C.

2.2.4.8 Lactate Dehydrogenase Assay

The viability of *ex vivo* acinar explants was verified by performing a lactate dehydrogenase (LDH) assay. LDH is a cytosolic enzyme which is released into surrounding culture medium by damaged cells. Therefore, the amount of enzyme present allows a conclusion about the amount of dead cells in a sample. The LDH assay is based on an enzymatic reaction which leads to a red product. The more lactate dehydrogenase is present in the medium, the more red dye is produced, which can be subsequently quantified via photometry. In this work, the Thermo Scientific Pierce® LDH Cytotoxicity Assay kit was used and performed as described in the technical manual. The samples were subsequently analysed using the Thermo Scientific Multiskan FC photometer.

2.2.4.9 Immunocytochemistry

Immunocytochemistry allows the staining of one or more proteins of interest within cells using a fluorophore bound antibody. Therefore, it is possible to determine where a protein is expressed and if it is possibly co-localised with others. For this purpose, cells were seeded on a chamber slide and cultured at 37 °C until they reached a confluency of about 50 %. The culture medium was removed and the cells were washed twice with PBS at RT. Subsequently, the cells were fixated with either 2 % of paraformaldehyde (PFA) for 20 min at RT or with 50 % Methanol, 50 % Acetone for 5 min at - 20 °C. The cells were washed three times with PBS-T at RT for 5 min and unspecific binding sites were blocked via incubating the slides with PBS-T containing 10 % of goat serum for 1 h at RT. A specific antibody against the protein of interest was diluted at an appropriate ratio in PBS-T containing 10 % of goat serum,

added to the cells and incubated o/n at 4 °C. The slides were washed three times with PBS-T for 5 min at RT and a fluorophore bound secondary antibody was added, diluted 1:500 in PBS-T containing 10 % of goat serum. After incubating for 60 min at RT, the slides were washed twice with PBS-T for 5 min at RT and nuclei were stained using the Vector Labs VECTASHIELD® mounting medium with diamidinophenylindole (DAPI). Subsequently, the slides were covered with a coverslip and analysed via fluorescence microscopy.

2.2.5 Transformation and Transfection Methods

2.2.5.1 Transformation of *E. coli*

The bacteria used for transformation were Invitrogen *E. coli* OneShot®TOP10 cells which were artificially made competent via the rubidium chloride method (Hanahan, 1983). The plasmid to be cloned was added to the bacteria, incubated on ice for 30 min and heat-shocked for 30 sec at 42 °C. Subsequently, the sample was incubated on ice for 5 min, 500 µl of LB_{fluid} medium were added to the transformed cells and they were incubated on a shaker for 30 min at 37°C and 230 rpm. The bacteria were plated on LB_{Amp} media and were cultured o/n at 37 °C.

2.2.5.2 Transfection of Mammalian Cells

During this work, cell lines were transfected using the Invitrogen Lipofectamine 2000 kit, which is based on the transfection of cells via lipovesicles. Here, lipids enclose the DNA and built up a vesicle which is able to fuse with the cell membrane of target cells. During this process, the DNA is released into the cytosol and is able to integrate into the host genome. For an efficient integration, the host cell has to undergo mitosis at the point of transfection so that the nucleus is degraded and the genomic DNA is set free. Transfections were performed as described in the technical manual.

2.2.6 Histology

2.2.6.1 Preparation of Paraffin Sections

Mice of an appropriate age and genotype were sacrificed and the pancreas as well as tissue pieces of the duodenum, liver and lung were incubated in a tissue cassette for 24 h at 4 °C in

4 % of PFA. Subsequently, the sample was dehydrated o/n using the Leica ASP300S dehydrator and embedded in paraffin using the Leica EG 1150 H. Sections of a thickness of 1 to 2 µm were prepared using the Thermo Scientific Microm HM 355S microtome and were dried at RT for 2 h. Subsequently, the slides were directly used for downstream techniques or stored at RT.

2.2.6.2 Hämalaun & Eosin Staining

Basic phenotypic characterization of pancreatic tissue was performed with Hämalaun & Eosin (H & E) stained paraffin sections. Here, Hämalaun stains cell structures such as nuclei and collagen filaments, while Eosin is used for counterstaining of the cytoplasm. Dry paraffin sections were deparaffinised by incubating them twice in Carl Roth Roti®-Histol for 5 min. Subsequently, the slides were hydrated by passing through a descending ethanol series consisting of two 100 % EtOH, 96 % EtOH, 70 % EtOH and ddH_2O baths. The slides were incubated for 3 min in each bath and stained with Hämalaun for 5 min. The samples were rinsed three times with ddH_2O, incubated for 5 sec in ammoniac water and rinsed twice in ddH_2O. Subsequently, the slides were incubated for 2 sec in HCl water, rinsed twice in ddH_2O and incubated for 5 sec in ammoniac water. After rinsing twice in ddH_2O, the slides were incubated for 3 min in 70 % EtOH, counterstained in Eosin for 2 min and incubated three times in 100 % EtOH for 3 min each. Subsequently, the slides were incubated twice for 5 min each in Roti®-Histol and covered with a coverslip. All steps were performed at RT.

2.2.6.3 Immunohistochemistry

Immunohistochemistry allows the staining of proteins within tissues and cells and grants an insight into where a protein of interest is expressed. Paraffin sections to be stained were deparaffinised by incubating twice for 5 min at RT in Roti®-Histol and hydrated by passing through a descending ethanol series as described above. Antigens within the tissue were revealed by cooking the slides for 15 min in Vector Labs Antigen Unmasking Solution. The slides were cooled down to RT and incubated for 10 min in 3 % H_2O_2. Subsequently, the samples were washed three times for 5 min at RT in PBS-T and incubated for 60 min in PBS-T containing 10 % goat serum in order to block unspecific binding sites. A specific antibody against the protein of interest was diluted at an appropriate ratio in PBS-T containing 10 % goat serum. The slides were incubated with the diluted antibody o/n at 4 °C.

Subsequently, the samples were washed three times for 5 min at RT in PBS-T and incubated with a biotinylated secondary antibody diluted 1:1000 in PBS-T containing 10 % goat serum for 60 min at RT. The slides were washed three times for 5 min at RT in PBS-T and incubated in Thermo Scientific Pierce® Avidin-Biotin Complex (ABC) Solution for 60 min at RT. After washing three times for 5 min at RT in PBS-T, the slides were stained using the Vector Labs diaminobenzidine (DAB) staining kit for up to 10 min at RT depending on the desired staining intensity. The reaction was stopped by rinsing the slides in ddH_2O and they were counterstained with Hämalaun for 2 min at RT. The samples were rinsed three times with ddH_2O, passed through a rising ethanol series as described above, incubated twice for 5 min each at RT in Roti®-Histol and covered with a coverslip.

2.2.6.4 Immunofluorescence

As an alternative to staining proteins of interest via immunohistochemistry, they were also made visible using a fluorescent secondary antibody, which provides the possibility to stain two or more different proteins on one tissue slide in a row. Analogue to the procedure described above, the slides were prepared and incubated with the primary antibody. Instead of a biotinylated secondary antibody, a fluorophore bound secondary antibody was incubated with the slides, diluted at a ratio of 1:500 in PBS-T containing 10 % goat serum. The samples were washed twice for 5 min at RT in PBS-T and nuclei were stained using the Vector Labs VECTASHIELD® mounting medium with DAPI. The slides were covered with a coverslip and analysed via fluorescence microscopy.

2.2.7 Microscopy

2.2.7.1 Bright Field Microscopy

Paraffin embedded tissue slides were analysed via bright field microscopy. Here, the Zeiss Axio Imager.A1 microscope with the EC Plan-Neofluar 10x 0.3 and EC Plan-Neofluar 20x 0.5 objectives were used. Photos were taken using the Zeiss AxioCam HRc camera and the AxioVision 3.1.2.1 software.

2.2.7.2 Fluorescence Microscopy

Fluorophore conjugated antibodies as well as the expression of fluorescent reporter proteins were detected via fluorescence microscopy. For this purpose, the Zeiss Axiovert 200M microscope was used. Blue or green light was emitted by a fluorescence lamp and light with a wavelength of 509 nm or 610 nm, emitted by the fluorescing marker proteins, was detected. For microscopy, the appropriate fluorescence light filters as well as the Zeiss EC Plan-Neofluar 20x 0.4 Ph2 and EC Plan-Neofluar 40x 1.3 Oil Ph3 objectives were used. Pictures were taken with the Zeiss AxioCam MRm camera and the AxioVision 3.1.2.1 software.

2.2.7.3 Confocal Microscopy

Confocal microscopy was performed using the Leica TCS SP5 microscope. Pictures were taken using the Leica Application Suite Advanced Fluorescence.

2.2.8 Induction of Acute Pancreatitis

Acute pancreatitis was induced in 6 – 8 weeks old mice via cerulein treatment following the "consecutive" protocol (Jensen *et al.,* 2005). Prior to the first injection, the mice were starved at least 12 h and subsequently weighed. Cerulein was injected intraperitoneal (i.p.), using 50 ng of cerulein per g of mouse weight. Injections were administrated hourly with a maximum of 8 injections in total. The mice were sacrificed and samples were obtained 1 h, 4 h, 8 h, 24 h and 72 h after the first injection. Untreated mice of the same genotype served as a control group.

3 RESULTS

3.1 MEK1DD IN ADM AND PANIN DEVELOPMENT

3.1.1 MEK1DD is sufficient for ADM and PanIN development

The impact of MEK on ADM and PanIN development was investigated via analysis of *Mek1DD* mice. These mice hold a mutated *Mek1* gene within the *ROSA26* locus, which leads to an ectopic expression of a constitutively active MEK1 protein. The sustained activity of this protein is achieved via two serine-to-aspartic-acid mutations, located at the amino acids 218 and 222 (S218D and S222D). A polyA stop signal flanked by two *loxP* sites is situated upstream of the *Mek1DD* gene, allowing a pancreas specific expression if crossed with $Ptf1a^{+/Cre}$ mice. The construct further holds an *Egfp* gene, which is situated downstream of *Mek1DD*, separated by an IRES sequence (figure 3.1). *Mek1DD* mice were purchased from The Jackson Laboratories and bred at the Klinikum rechts der Isar.

A histological analysis was performed in order to elucidate if and what kind of lesions are developed in *Mek1DD* mice at different stages of life. Commonalities and differences in lesion development compared to the well-established $Kras^{G12D}$ mouse model were evaluated. *Mek1DD* samples were further compared to the recently published $P110\alpha^{H1047R}$ mouse model, which expresses a dominant active PI3K protein, leading to sustained AKT signalling (Eser *et al.,* 2013). For this purpose, mice were sacrificed at an age of 4 weeks, 12 weeks and 6 months and tissue slides were stained with H & E. At an age of 4 weeks, $Kras^{G12D}$, *Mek1DD* and $P110\alpha^{H1047R}$ mice exhibited ADM, while $Kras^{G12D}$ and *Mek1DD* samples also showed PanIN lesions. However, most parts of the pancreas of both genotypes exhibited a wild type phenotype (figure 3.2 A – D). 12 weeks old $Kras^{G12D}$ and $P110\alpha^{H1047R}$ mice showed an elevated number of ADM and PanIN lesions; most areas of the pancreas still exhibited normal acinar tissue, though. *Mek1DD* mice of the same age exhibited ADM, but predominantly

Figure 3.1: The *Mek1DD* construct, schematic. A mutated *Mek1* gene, leading to a constitutively active protein, was inserted into the *ROSA26* locus. A *loxP*-polyA-*loxP* site upstream of the *Mek1DD* gene grants a tissue specific expression, depending on the Cre recombinase coexpressed. The downstream *Egfp* gene provides the possibility to track the expression *in vivo* via fluorescence microscopy. An IRES sequence between the *Mek1DD* and the *Egfp* gene prevents the expression of fusion proteins.

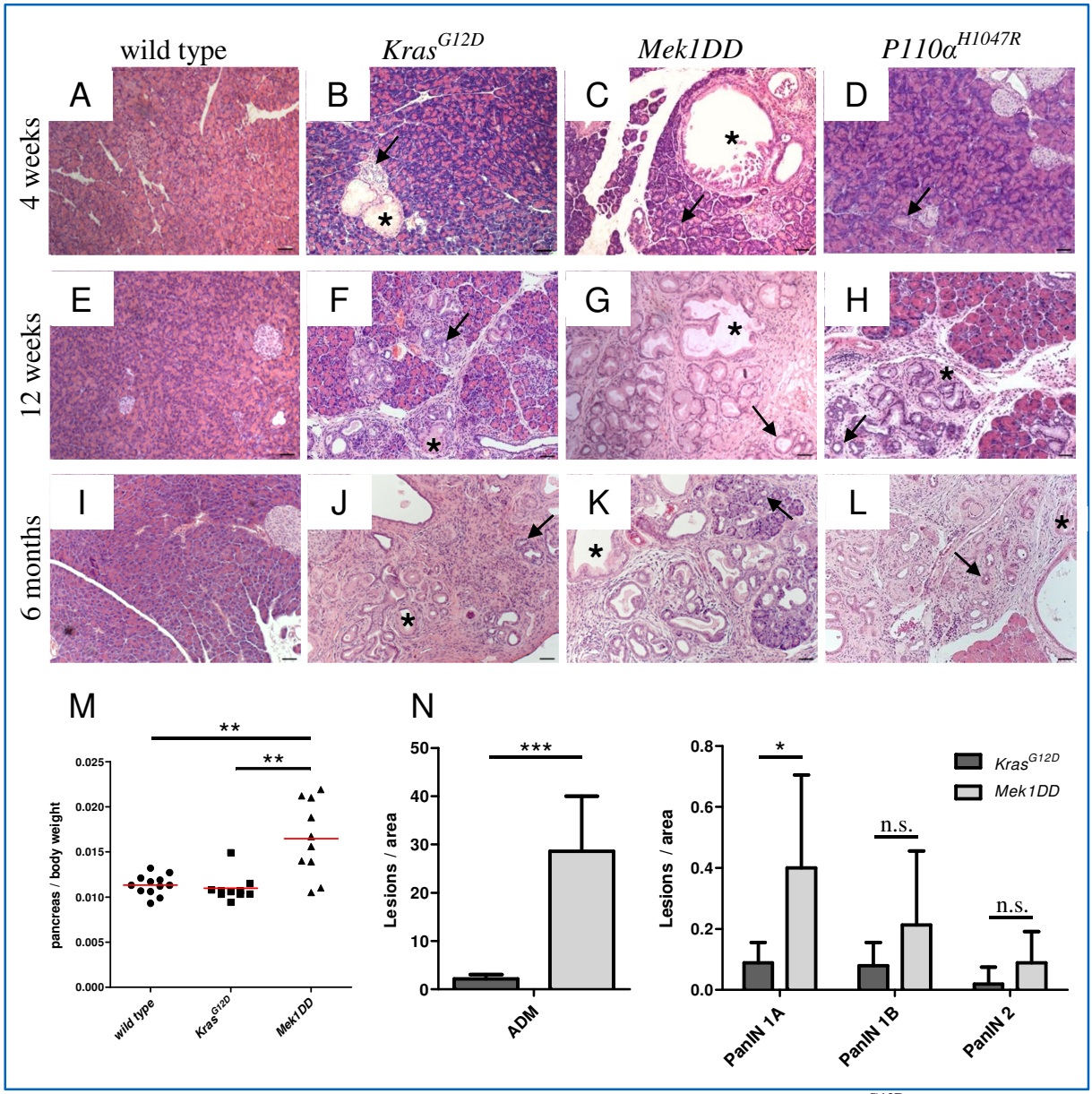

Figure 3.2: MEK1DD leads to accelerated lesion development compared to KRAS^{G12D}. **(A) – (L)** H & E staining of tissue slides of wild type, *Kras*^{G12D}, *Mek1DD* and *P110α*^{H1047R} mice (n = 3 – 11; scale bar represents 50 µm). Mice were analysed at an age of **(A) – (D)** 4 weeks, **(E) – (H)** 12 weeks and **(I) – (L)** 6 months. *Kras*^{G12D} and *Mek1DD* samples exhibit ADM (arrows) and PanIN lesions (asterisks) at all timepoints. *P110α*^{H1047R} mice at an age of 4 weeks show only ADM. Later timepoints also show PanIN lesions. **(M)** Ratio of pancreas to body weight of 4 weeks old wild type, *Kras*^{G12D} and *Mek1DD* mice. Pancreata of *Mek1DD* mice exhibit a significantly elevated ratio compared to wild type and *Kras*^{G12D} pancreata (n = 9 – 11; ** ≙ $p < 0.01$). **(N)** Quantification of ADM and PanIN lesions of 4 weeks old *Kras*^{G12D} and *Mek1DD* mice. *Mek1DD* samples exhibit a significantly elevated number of ADM and PanIN1A lesions compared to *Kras*^{G12D} samples. No significant differences can be observed for PanIN1B and PanIN2 lesions. Data shown are average values with standard deviation of all counted areas, with 8 randomly chosen, counted fields per area and 1 - 3 counted areas per mouse, spaced by 100 µm each (n = 3 - 9; * ≙ $p < 0.05$; *** ≙ $p < 0.001$; n.s. ≙ not significant).

PanIN lesions in most parts of the pancreas. Only small areas with normal acinar tissue remained (figure 3.2 E – H). At an age of 6 months, both *Kras*^{G12D} and *Mek1DD* mice exhibited predominantly ADM and PanIN lesions with only small parts of remaining acinar tissue. However, *Mek1DD* pancreata showed less PanIN lesions than at an age of 12 weeks,

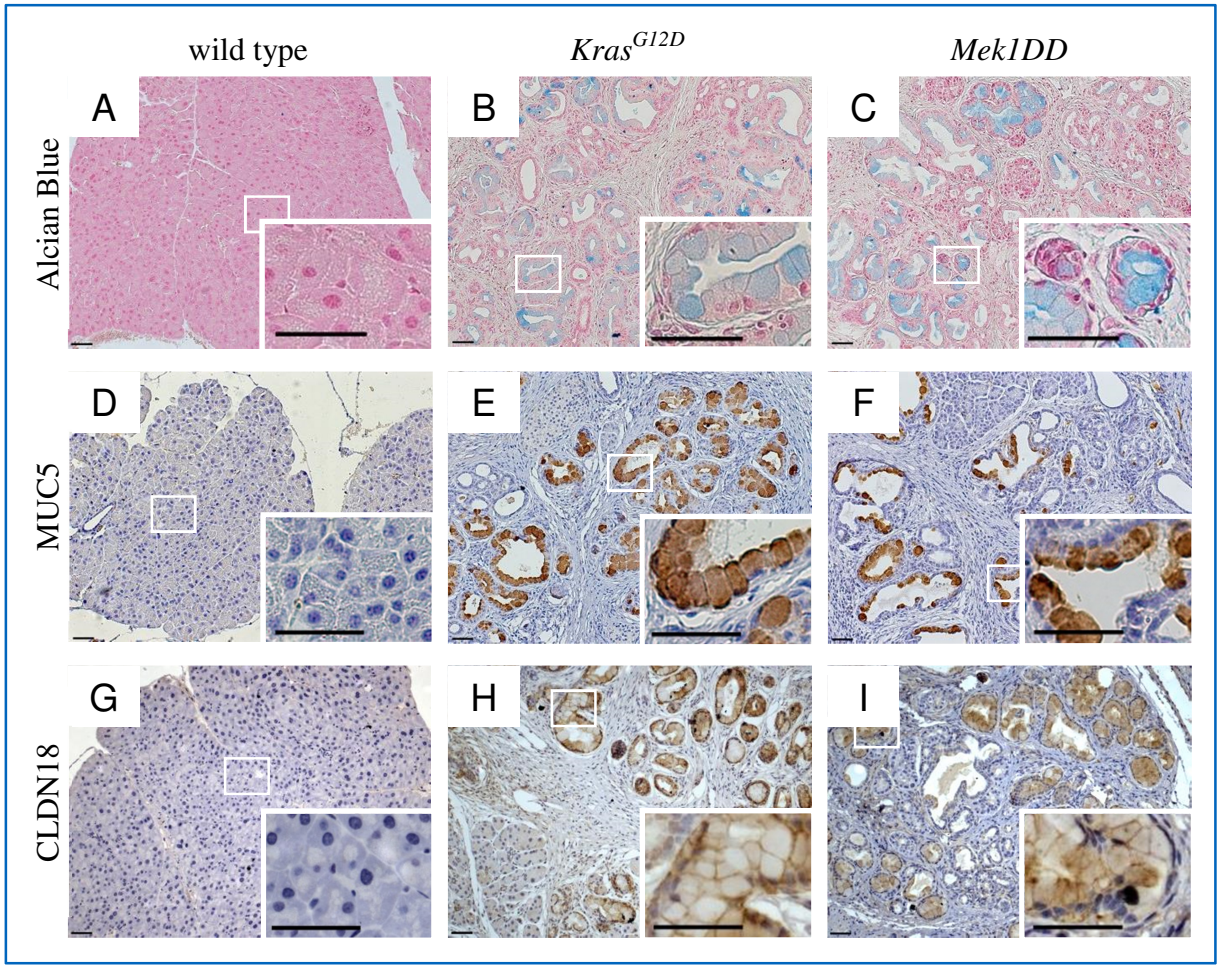

Figure 3.3: Lesions of *Kras*^{G12D} and *Mek1DD* pancreata are positive for PanIN markers. Tissue slides of 6 months old wild type, *Kras*^{G12D} and *Mek1DD* mice were stained for the PanIN markers **(A) – (C)** Alcian Blue, **(D) – (F)** Mucin 5 and **(G) – (I)** Claudin 18. Lesions of both *Kras*^{G12D} and *Mek1DD* samples were positive for all three markers (n = 3 - 4; scale bar represents 50 µm).

but a rising number of ADM. *P110α*^{H1047R} mice exhibited an elevated number of both ADM and PanIN lesions compared to 12 weeks old pancreata, though large areas of normal acinar tissue still remained (figure 3.2 I – L). Wild type controls showed no abnormalities at all stages of life.

The influence of MEK1DD on pancreas mass was measured by calculating the ratio of pancreas to body weight of each mouse. At an age of 4 weeks, this ratio was significantly elevated for *Mek1DD* pancreata compared to both wild type and *Kras*^{G12D} samples. Wild type and *Kras*^{G12D} mice showed no significant differences to each other (figure 3.2 M). Furthermore, ADM and PanIN lesions of 4 weeks old *Kras*^{G12D} and *Mek1DD* pancreata were quantified. *Mek1DD* samples exhibited significantly more ADM and PanIN1A lesions than *Kras*^{G12D} samples of the same age. The observed number of PanIN grade 1B and 2 was not significantly different (figure 3.2 N).

In order to confirm the investigated lesions as PanIN lesions, tissue slides of 6 months old *Kras*^{G12D} and *Mek1DD* mice were stained for the PanIN markers Alcian Blue, Mucin 5 and Claudin 18. The cytosol of lesions of both *Kras*^{G12D} and *Mek1DD* pancreata were positive for Alcian Blue (figure 3.3 A – C) and Mucin 5 (figure 3.3 D – F). The membrane protein Claudin 18 was detected in the lesions` cell membranes of these genotypes as well (figure 3.3 G – I). Wild type controls were negative for all three PanIN markers.

3.1.2 MEK1DD is incapable of inducing PDAC

Long-term analysis of *Mek1DD* animals was performed by keeping the mice to their natural death. Here, it was of particular interest if these mice develop PDAC during their span of life. Although this analysis was still ongoing at the time of this thesis, preliminary data indicated that *Mek1DD* mice exhibit a mean survival time of approx. 498 days. The mice analysed were healthy for more than one year without showing any obvious physical interference, but exhibited a highly enlarged abdomen at the time of their natural death. Macroscopic analysis revealed that this enlargement was caused by cysts which had formed within the pancreas, filled with high amounts of fluid (figure 3.4 A). These were also detectable on H & E stained tissue slides. Here, a high number of cysts were visible throughout the pancreas (figure 3.4 B). Alongside small remaining areas of normal acinar tissue, PanIN lesions of grade 1 – 3 were the predominant types of lesions within the pancreas (figure 3.4 C), but also ADM were detected (figure 3.4 D). In addition, intraductal papillary mucinous neoplasms (IPMN) were also observed, though these were rarely present (figure 3.4 E). PDAC was not observed in any samples investigated.

Mek1DD mice were further crossed with *P53*^{R172H} mice which were descried previously (Hingorani *et al.,* 2005). These mice express an activated form of the tumour suppressor P53, P53^{R172H}. *Mek1DD;P53*^{R172H} mice were kept to their natural death and exhibited a mean survival of approx. 314 days. At the time of their death, these mice exhibited not only numerous cysts and PanIN lesions, but also large tumours (figure 3.4 F – H). Survival data for *Kras*^{G12D} and *P110α*^{H1047R} mice were already available prior to this work. Here, *Kras*^{G12D} mice exhibited a mean survival of approx. 384 days, *P110α*^{H1047R} mice approx. 414 days (figure 3.4 I). All observations described were confirmed by the pathologist Prof. Dr. Irene Esposito, Institute of Pathology, Technische Universität München.

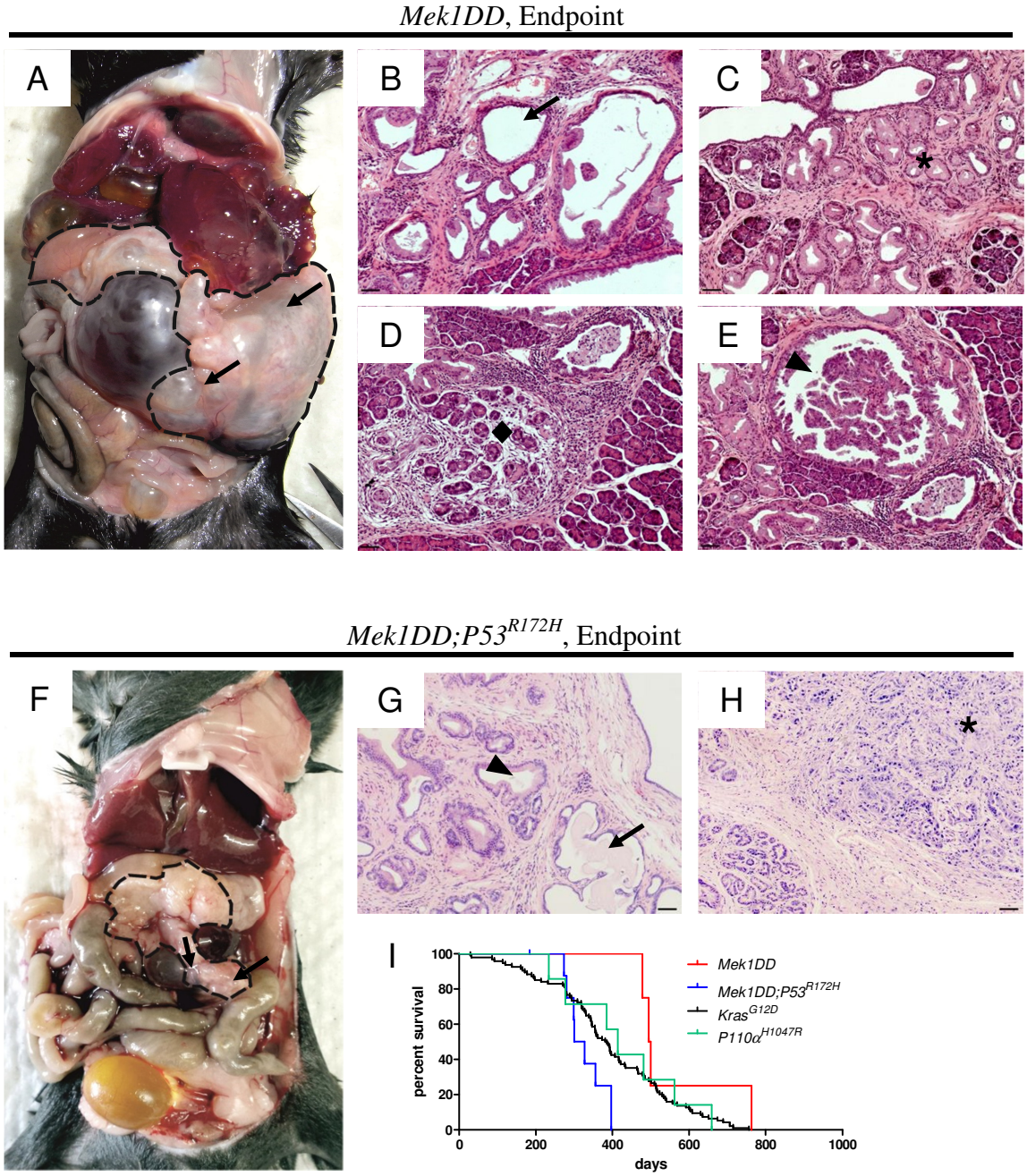

Figure 3.4: MEK1DD is incapable of inducing PDAC. (A) Macroscopic view of the pancreas (dashed line) and other organs of the gastrointestinal tract of a *Mek1DD* mouse at the time of its natural death (n = 4). Cysts can be observed in the pancreas (arrows). **(B) – (E)** H & E staining of tissue slides (n = 4; scale bar represents 50 µm). **(B)** Numerous cysts (arrow) are present within the pancreas. **(C)** Predominantly, high- and low-grade PanIN lesions can be observed (asterisk), but also **(D)** ADM (diamond). **(E)** Sporadic IPMN lesions (arrowhead) can also be seen. **(F)** Macroscopic view of the pancreas (dashed line) and other organs of the gastrointestinal tract of a *Mek1DD;P53*^{R172H} mouse at the time of its natural death (n = 4). Cysts can be observed in the pancreas (arrows). **(G) – (H)** H & E staining of tissue slides (n = 4; scale bar represents 50 µm). **(G)** Cysts (arrow) and numerous PanIN lesions (arrowhead) are present within the pancreas. **(H)** Large areas of PDAC can also be observed (asterisk). **(I)** Survival analysis of *Kras*^{G12D} (n = 94; mean survival = 384 days), *Mek1DD* (n = 4; mean survival = 498 days), *Mek1DD;P53*^{R172H} (n = 7; mean survival = 314 days) and *P110α*^{H1047R} (n = 7; mean survival = 414 days) mice.

3.1.3 MEK1DD activates ERK and AKT

The incapability of *Mek1DD* mice to develop PDAC was further investigated by analysing ERK and AKT activation in 6 months old wild type, $Kras^{G12D}$, *Mek1DD* and $P110\alpha^{H1047R}$ pancreata. Immunohistochemistry staining showed a strong nuclear staining for pERK in pancreatic lesions of $Kras^{G12D}$, *Mek1DD* and $P110\alpha^{H1047R}$ mice; wild type controls were negative (figure 3.5 A - D). Western Blot analysis showed a weak pERK signal in wild type controls. However, $Kras^{G12D}$, *Mek1DD* and $P110\alpha^{H1047R}$ samples exhibited elevated pERK levels compared to wild type pancreata (figure 3.5 I). Immunohistochemistry staining for pAKT showed a strong nuclear staining in pancreatic lesions of $Kras^{G12D}$, *Mek1DD* and $P110\alpha^{H1047R}$ mice; nuclei of normal acinar tissue were also positive in these genotypes, though less strong. Wild type controls were negative (figure 3.5 E - H).

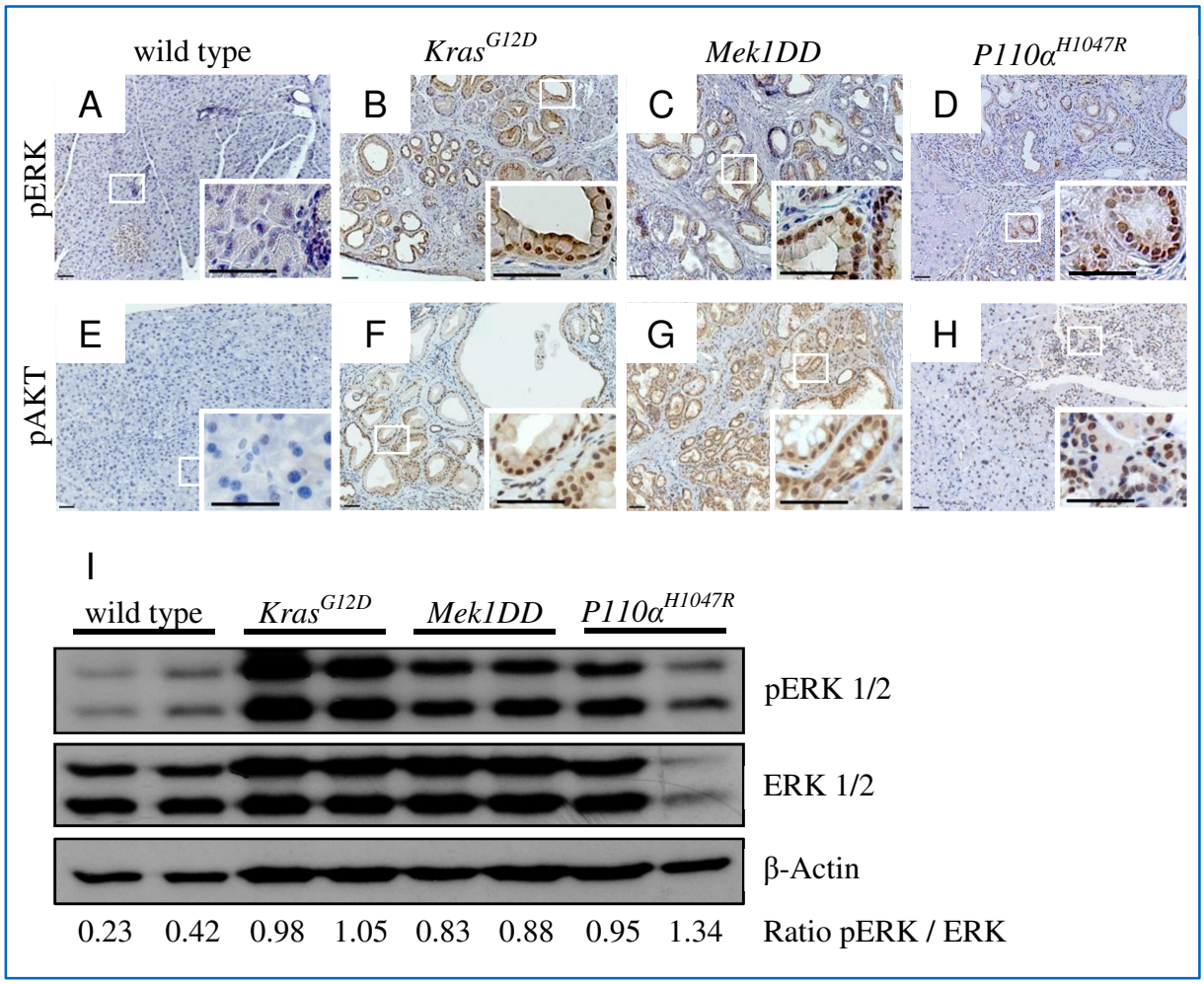

Figure 3.5: MEK1DD activates ERK and AKT. Expression analysis of pERK **(A) – (D), (I)** in pancreata of 6 months old mice, showing elevated levels of pERK in $Kras^{G12D}$, *Mek1DD* and $P110\alpha^{H1047R}$ samples compared to wild type controls via **(A) – (D)** immunohistochemistry staining (n = 3 - 4; scale bar represents 50 µm) and **(I)** Western Blot analysis. **(E) – (H)** Expression analysis of pAKT via immunohistochemistry staining (n = 3 - 4; scale bar represents 50 µm) showed high pAKT levels in lesions of $Kras^{G12D}$, *Mek1DD* and $P110\alpha^{H1047R}$ samples.

3.2 EGR1 IN PDAC INITIATION AND PROGRESSION

3.2.1 EGR1 is regulated via the EGFR - KRAS - MEK pathway

Being a prominent cancer related downstream target of the MEK – ERK pathway in various reports (Midgley and Khachigian, 2004; Khachigian, 2006; Hasan and Schafer, 2008), the transcription factor EGR1 was investigated as a potential mediator between MEK – ERK signalling and the observed phenotype of *Kras*^{G12D} and *Mek1DD* mouse models. Since it has been shown that MEK1DD leads to PDAC precursor lesions at early stages of life, the expression of EGR1 during these early events was of particular interest. At first, the expression pattern of EGR1 was analysed via immunohistochemistry staining of tissue slides of 4 weeks old mice. Here, in addition to *Mek1DD* samples, *Mek1DD*;*Egfr*$^{\Delta Panc}$ mice were bred and analysed in order to clarify the relation between EGFR, MEK and EGR1. While EGR1 was undetectable in wild type controls, *Mek1DD* as well as *Mek1DD;Egfr*$^{\Delta Panc}$ samples showed a strong nuclear staining in many, but not all, metaplastic cells of ADM. Some ADM were completely negative, but most exhibited a few positive cells, with two or three of these arranged in clusters, surrounded by adjacent negative cells. The same was observed for larger normal ducts in these mice. Acinar tissue of *Mek1DD* and *Mek1DD;Egfr*$^{\Delta Panc}$ pancreata was mostly negative, only exhibiting scattered positive cells. These positive cells, however, were also often arranged in clusters (figure 3.6 A – C).

The expression of EGR1 was further investigated in the well-established *Kras*^{G12D} and *Kras*^{G12D}*;Egfr*$^{\Delta Panc}$ mouse models. Immunohistochemistry staining of *Kras*^{G12D} tissue slides showed a strong nuclear staining in some metaplastic cells within ADM as well as larger ducts, which were again arranged in clusters of two to three cells. Normal acinar tissue was almost completely negative in these mice, with only rare single cells being positive. Wild type

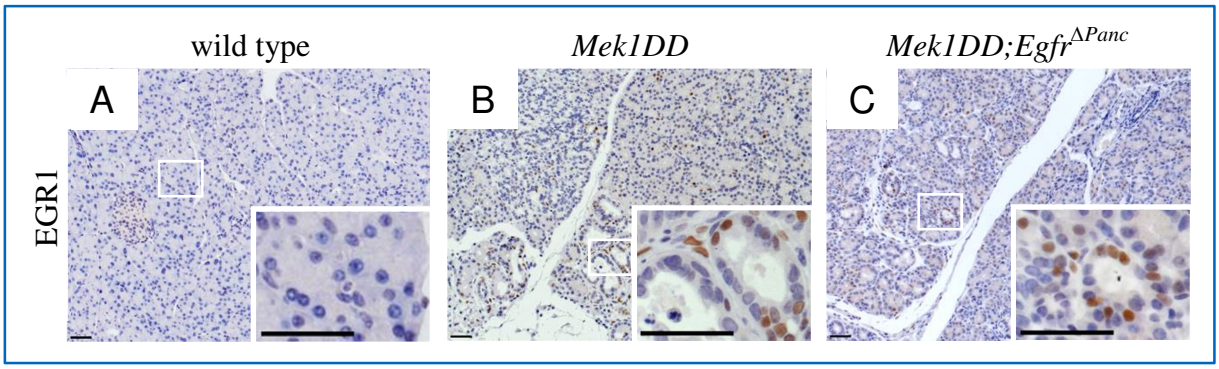

Figure 3.6: EGR1 is upregulated in pancreata of *Mek1DD* and *Mek1DD;Egfr*$^{\Delta Panc}$ mice. (A) – (C) Immunohistochemistry staining of EGR1 in 4 weeks old wild type, *Mek1DD* and *Mek1DD;Egfr*$^{\Delta Panc}$ samples, revealing that EGR1 is absent in wild type pancreata but strongly expressed in nuclei of both acinar and metaplastic cells of *Mek1DD* and *Mek1DD;Egfr*$^{\Delta Panc}$ mice in a scattered manner (n = 6 – 8; scale bar represents 50 µm).

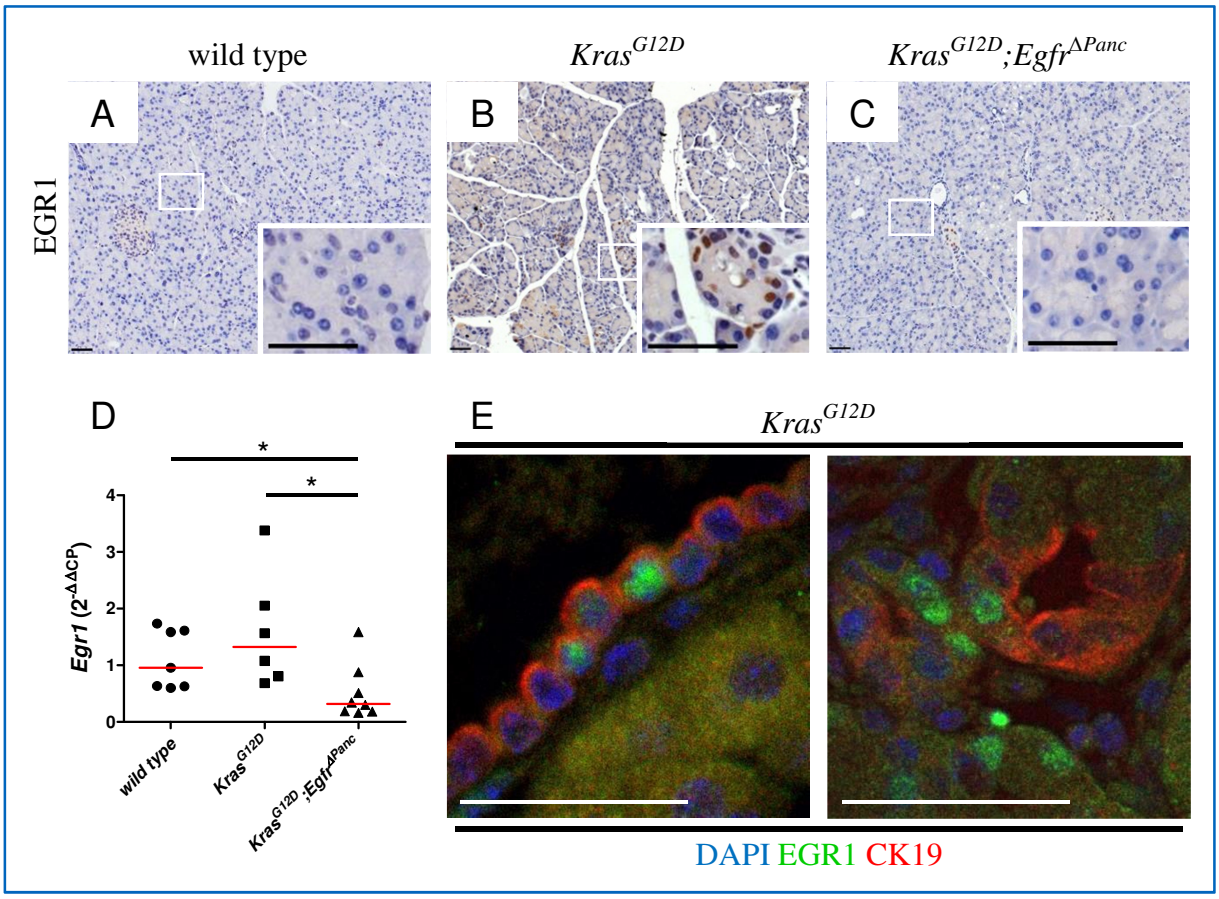

Figure 3.7: EGR1 is upregulated in pancreata of *Kras*^{G12D} but not *Kras*^{G12D};*Egfr*$^{\Delta Panc}$ mice. (A) – (C) Immunohistochemistry staining of tissue slides of 4 weeks old mice, exhibiting a strong nuclear staining for EGR1 in scattered metaplastic cells, but not in normal acinar tissue of *Kras*^{G12D} pancreata; *Kras*^{G12D};*Egfr*$^{\Delta Panc}$ samples as well as wild type controls are EGR1 negative (n = 3 – 5; scale bar represents 50 µm). **(D)** qPCR analysis of *Egr1* mRNA levels showing a significant downregulation of *Egr1* expression in *Kras*^{G12D};*Egfr*$^{\Delta Panc}$ pancreata compared to both *Kras*^{G12D} and wild type samples (n = 6 – 8; * ≙ $p < 0.05$). **(E)** Confocal microscopy of immunofluorescence co-staining for EGR1 and CK19 on tissue slides of 4 weeks old *Kras*^{G12D} mice.

controls as well as *Kras*^{G12D};*Egfr*$^{\Delta Panc}$ pancreata were completely negative (figure 3.7 A – C). qPCR analysis showed a significant decrease of *Egr1* mRNA levels in *Kras*^{G12D};*Egfr*$^{\Delta Panc}$ samples compared to both *Kras*^{G12D} and wild type samples. No significant difference could be observed between *Kras*^{G12D} and wild type mice (figure 3.7 D). Immunofluorescence co-staining of EGR1 and the ductal marker CK19 on tissue slides of 4 weeks old *Kras*^{G12D} mice showed a co-localisation in some, but not all, ductal (left) and metaplastic (right) cells. Most of the EGR1 positive cells co-expressed CK19 or were situated adjacent to CK19 positive cells. However, only a few CK19 positive cells co-expressed EGR1 (figure 3.7 E).

Another well-studied ADM mouse model is *Tgfα*, which ectopically overexpresses the EGFR ligand TGFα, leading to a permanently active EGFR signalling (Wagner *et al.,* 2001). Since ADM can be observed very early during development in this model, 7 days old mice were used for EGR1 expression analysis. Immunohistochemistry staining for EGR1 showed a strong signal in most nuclei of both metaplastic and acinar cells of *Tgfα* mice; ducts exhibited

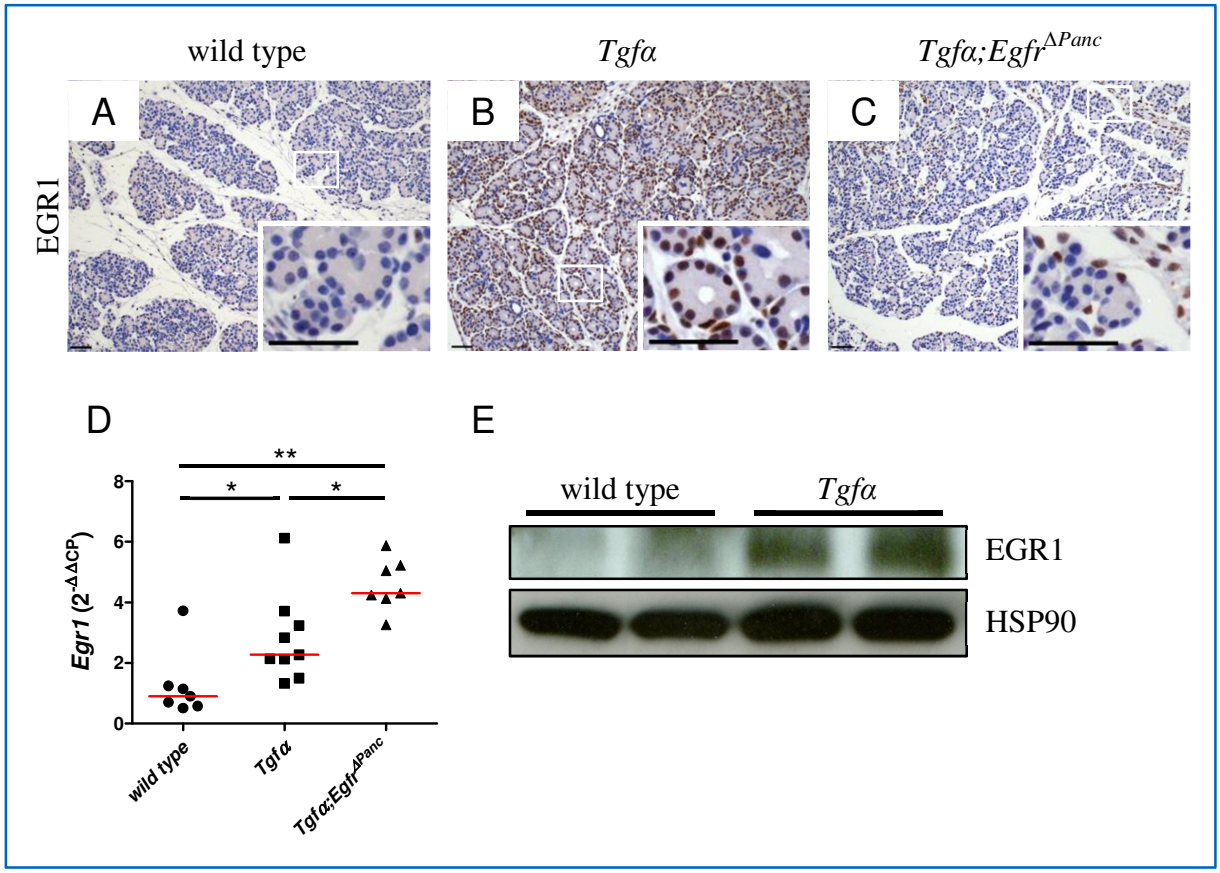

Figure 3.8: EGR1 is upregulated in pancreata of *Tgfα* but not *Tgfα;Egfr*$^{\Delta Panc}$ mice. (A) – (C) Immunohistochemistry staining of tissue slides of 7 days old mice exhibiting a strong nuclear staining for EGR1 in most acinar and metaplastic cells of *Tgfα* pancreata. Wild type controls as well as acinar cells of *Tgfα;Egfr*$^{\Delta Panc}$ mice are EGR1 negative, but infiltrating fibroblasts in both *Tgfα* and *Tgfα;Egfr*$^{\Delta Panc}$ samples are highly EGR1 positive (n = 4; scale bar represents 50 µm). **(D)** qPCR analysis of *Egr1* mRNA levels showing a significant upregulation of *Egr1* expression in both *Tgfα* and *Tgfα;Egfr*$^{\Delta Panc}$ pancreata compared to wild type samples. *Tgfα;Egfr*$^{\Delta Panc}$ pancreata further exhibit a significantly higher *Egr1* expression than *Tgfα* samples (n = 4 – 9; * ≙ $p < 0.05$; ** ≙ $p < 0.01$). **(E)** Western Blot analysis revealing an elevated EGR1 protein expression in *Tgfα* samples compared to wild type tissue.

only single positive cells. *Tgfα;Egfr*$^{\Delta Panc}$ samples were completely negative for EGR1, except for invading fibroblasts which were strongly EGR1 positive and also detectable in *Tgfα* mice (figure 3.8 A – C). qPCR analysis showed a significant upregulation of *Egr1* mRNA levels in both *Tgfα* and *Tgfα;Egfr*$^{\Delta Panc}$ pancreata compared to wild type samples; *Tgfα;Egfr*$^{\Delta Panc}$ pancreata further exhibited a significantly higher *Egr1* expression than Tgfα pancreata (figure 3.8 D). Increased EGR1 protein levels were also detectable via Western Blot analysis in *Tgfα* mice (figure 3.8 E).

3.2.2 EGR1 is elevated during induced acute pancreatitis

Cerulein induced acute pancreatitis leads to a variety of inflammatory responses which promote metaplastic transition of acinar cells. Hence, it is an adequate model for investigating

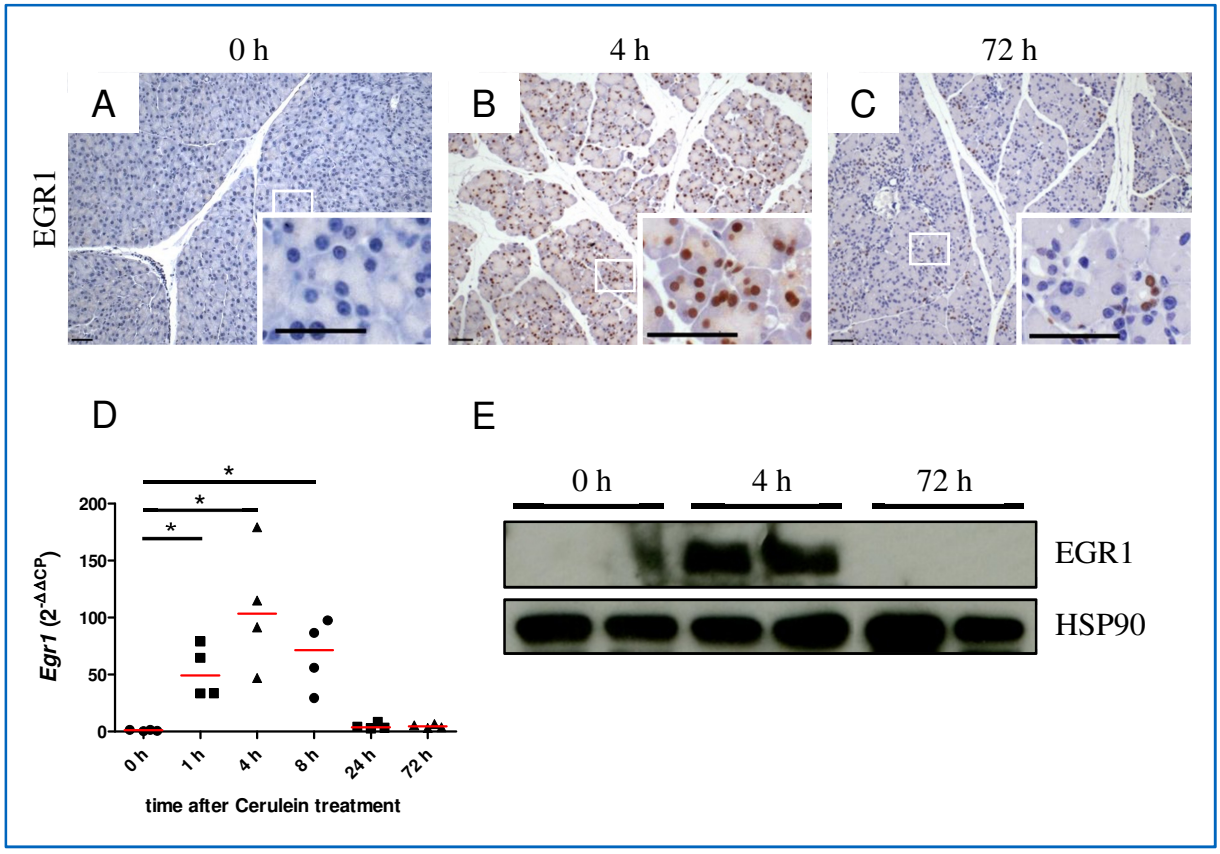

Figure 3.9: EGR1 is upregulated during cerulein induced acute pancreatitis. (A) – (C) Immunohistochemistry staining of induced acute pancreatitis samples showing a strong nuclear staining for EGR1 in all acinar cells 4 h after the first cerulein injection. EGR1 expression is downregulated again 72 h after the first treatment, showing only scattered remaining positive cells (n = 4; scale bar represents 50 µm). **(D)** qPCR analysis of *Egr1* mRNA levels showing a significant upregulation of *Egr1* expression 1 h, 4 h and 8 h after the first injection compared to wild type levels (n = 4; * ≙ $p < 0.05$). **(E)** Western Blot analysis showing a strong upregulation of EGR1 4 h after the first cerulein treatment. After 72 h, EGR1 is undetectable again. Induced pancreatitis samples used here were obtained by Roxanne Brodylo and available prior to this work.

early events during ADM development in a non-oncogenic context. Immunohistochemistry staining for EGR1 showed a strong nuclear signal in every acinar cell 4 h after the first cerulein injection. Untreated controls (denoted as 0 h) were EGR1 negative. 72 h after the first injection, EGR1 was undetectable again in most pancreatic cells, with only scattered positive clusters remaining. These clusters were observed in ADM that had formed, but also in acinar tissue, where they consisted of two to three adjacent cells (figure 3.9 A – C). qPCR analysis revealed that *Egr1* mRNA levels were already significantly upregulated 1 h after the first cerulein injection, with a maximum 4 h after the first treatment. After 24 h, the expression was back to wild type levels again (figure 3.9 D). These results were confirmed via Western Blot analysis, which showed a strong EGR1 signal 4 h after the first injection. The protein was undetectable in untreated controls as well as 72 h after the first cerulein treatment (figure 3.9 E).

3.2.3 EGR1 is elevated in human ADM and PDAC

EGR1 was subsequently analysed in human pancreatic samples. For this purpose, slides of healthy pancreatic tissue as well as of tissue exhibiting ADM and PDAC were stained. ADM samples exhibited a strong nuclear staining in most of the metaplastic cells, while adjacent normal acinar tissue was EGR1 negative; PDAC samples showed a strong nuclear signal in most cells. In healthy pancreatic tissue, EGR1 was undetectable (figure 3.10 A – C).

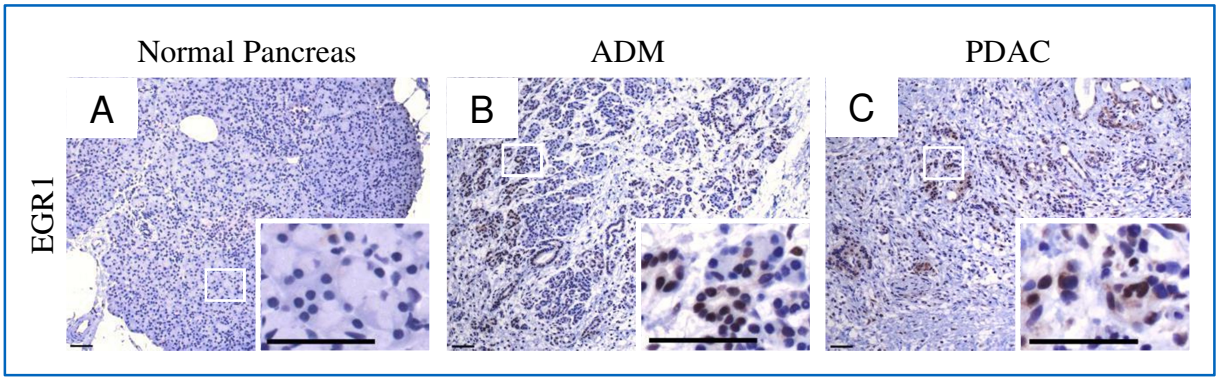

Figure 3.10: EGR1 is elevated in human ADM and PDAC. (A) – (C) Immunohistochemistry staining of human ADM and PDAC samples compared to healthy acinar tissue. EGR1 was strongly expressed in nuclei of both ADM and PDAC samples, but undetectable in healthy tissue (n = 4; scale bar represents 50 µm).

3.2.4 *Egr1*^{KO} does not alter normal pancreatic development

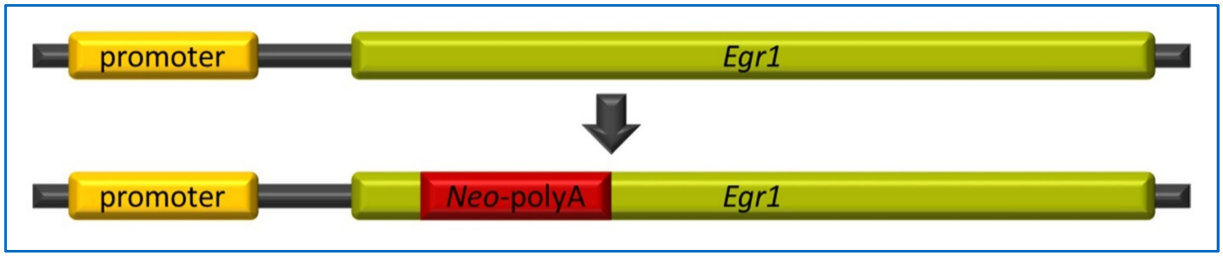

Figure 3.11: The *Egr1*^{KO} construct, schematic. A neomycine resistance cassette, followed by a polyA stop signal, was inserted into the endogenous *Egr1* gene via homologous recombination. This leads to the expression of a truncated and therefore non-functional EGR1 protein, which is not tissue restricted.

In order to further elucidate the role of EGR1 during PDAC initiation and progression, *Egr1*^{KO} mice were purchased from The Jackson Labs and bred at the Klinikum rechts der Isar. The knockout within these mice was achieved by inserting a neomycine resistance gene, followed by a polyA stop signal, into the endogenous *Egr1* gene via homologous recombination. This procedure led to a disruption of the *Egr1* sequence and consequently to the expression of a truncated, non-functional protein (figure 3.11). Since this modification is not tissue specific, *Egr1*^{KO} mice exhibit a whole body knockout of the *Egr1* gene. The impact of this knockout on pancreatic development was investigated by comparing H & E stained tissue slides of 6 months old wild type and *Egr1*^{KO} mice. The pancreata of *Egr1*^{KO} samples had a normal appearance and showed no obvious abnormalities throughout life span. Acinar tissue, ducts as well as islets of Langerhans were fully developed (figure 3.12 A – B).

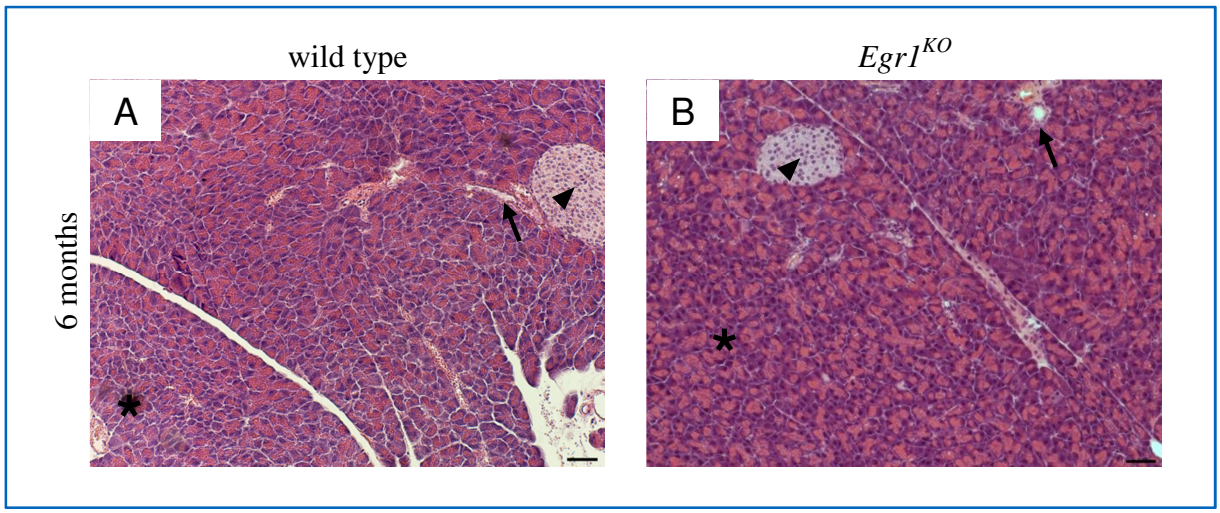

Figure 3.12: *Egr1*^{KO} does not alter normal pancreatic development. H & E staining of tissue slides of 6 months old **(A)** wild type and **(B)** *Egr1*^{KO} mice, showing no obvious abnormalities in pancreata of *Egr1*^{KO} samples. Acinar tissue (asterisk), ducts (arrow) as well as islets of Langerhans (arrowhead) were fully developed (n = 2 – 4; scale bar represents 50 µm).

3.2.5 *Egr1*^{KO} blocks acinar cell transdifferentiation *ex vivo*

Wild type *ex vivo* acinar explants spontaneously transdifferentiate to duct-like structures under the influence of growth factors within the culture medium (Heid *et al.,* 2011). This process can be enhanced by adding additional EGF, an EGFR ligand, to the medium, and is impaired in explants of *Egfr*$^{\Delta Panc}$ mice. The impact of EGR1 on transdifferentiation was investigated by comparing *ex vivo* acinar explants of *Egr1*^{KO} pancreata to those of wild type mice. Directly after isolation, acinar cell clusters of both genotypes exhibited the same appearance (figure 3.13 A). Western Blot analysis of these cells showed that wild type as well as *Egr1*^{KO} explants expressed high amounts of the acinar marker-protein Amylase, though the expression level was lower in *Egr1*^{KO} cells. The ductal marker-protein Cytokeratin 19 was undetectable in explants of both genotypes (figure 3.13 B). After 5 days of culturing, the overall transdifferentiation percentage was calculated. Wild type explants without EGF treatment showed a mean transdifferentiation rate of approx. 20 %, those with EGF addition approx. 40 %. Explants of *Egr1*^{KO} mice exhibited less than 5 % of duct-like structures, independently of EGF treatment, which was highly significantly lower compared to wild type samples (figure 3.13 C / D). This impaired transdifferentiation was not a result of higher cell mortality (figure 3.13 E). Western Blot analysis of these cells revealed that *Egr1*^{KO} explants exhibited a higher Amylase expression than wild type cells, which was true for both untreated and EGF treated samples. Cytokeratin 19 expression was higher in *Egr1*^{KO} explants, though, independently of EGF treatment (figure 3.13 F).

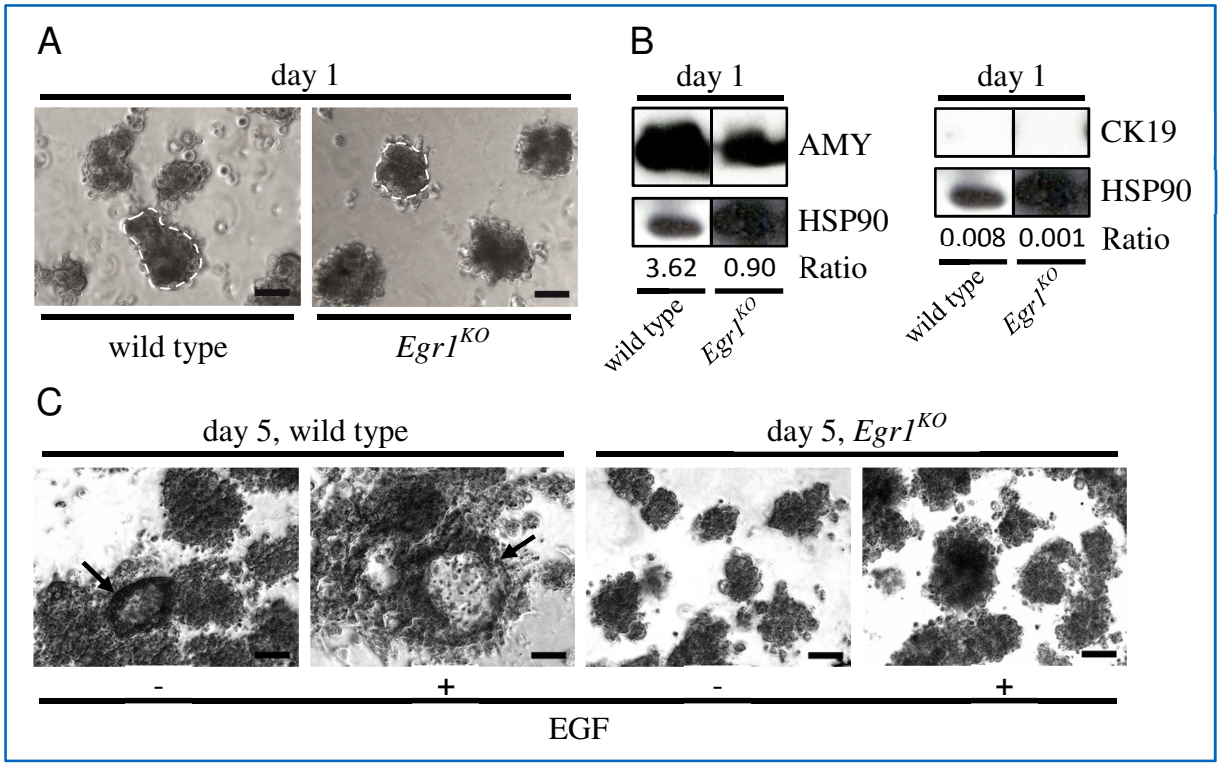

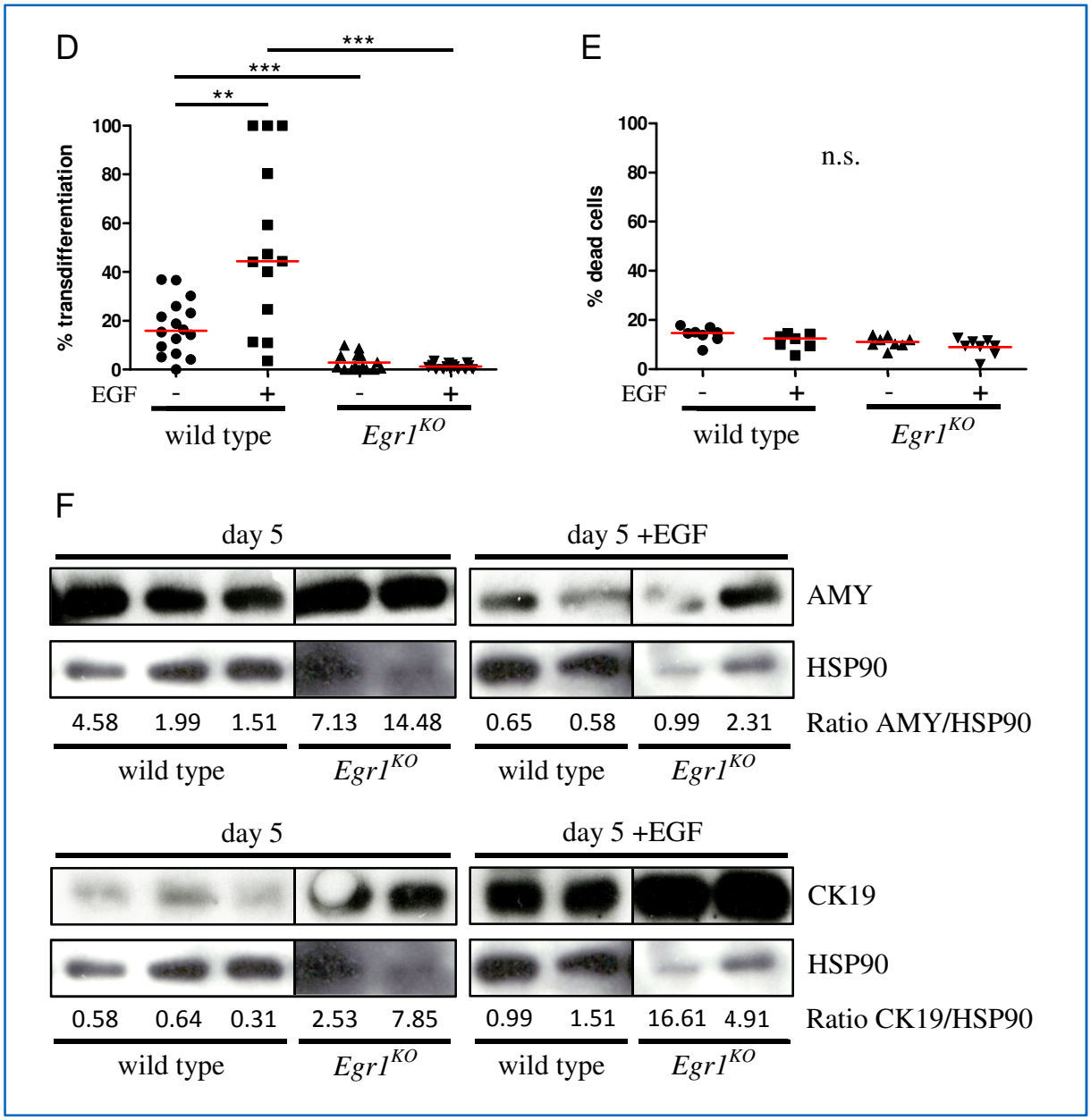

Figure 3.13: *Egr1*^{KO} blocks acinar cell transdifferentiation *ex vivo*. **(A)** Bright field microscopy of wild type and *Egr1*^{KO} *ex vivo* acinar explants at day 1, showing the same appearance for cell clusters (dashed line) of both genotypes (n = 4; scale bar represents 50 µm). **(B)** Western Blot analysis showing high Amylase expression for both genotypes at day 1; Cytokeratin 19 was undetectable. **(C)** Bright field microscopy of wild type and *Egr1*^{KO} explants at day 5. Wild type samples exhibit transdifferentiated cell clusters (arrow; n = 4). **(D)** Percentage of transdifferentiated cell clusters at day 5. *Egr1*^{KO} samples exhibited highly significantly less duct-like structures than wild type explants. Each data point represents one well, with 3 counted, randomly chosen fields per well and 3 – 5 wells per mouse. (n = 4; ** ≙ $p < 0.01$; *** ≙ $p < 0.001$). **(E)** LDH assay at day 5, exhibiting no significant differences in cell mortality. **(F)** Western Blot analysis showing both higher Amylase and Cytokeratin 19 expression in *Egr1*^{KO} samples compared to wild type explants at day 5.

3.2.6 *Egr1*^{KO} enhances PDAC initiation in the *Kras*^{G12D} model

In order to investigate the functional role of *Egr1* during preneoplastic lesion development *in vivo*, *Kras*^{G12D};*Egr1*^{KO} mice were bred and analysed. H & E staining of tissue slides of *Kras*^{G12D} and *Kras*^{G12D};*Egr1*^{KO} samples revealed that both genotypes exhibited ADM and scattered PanIN lesions at an age of 4 weeks; most of the pancreata exhibited normal acinar tissue, though (figure 3.14 A - C). At an age of 12 weeks, pancreata of *Kras*^{G12D} mice

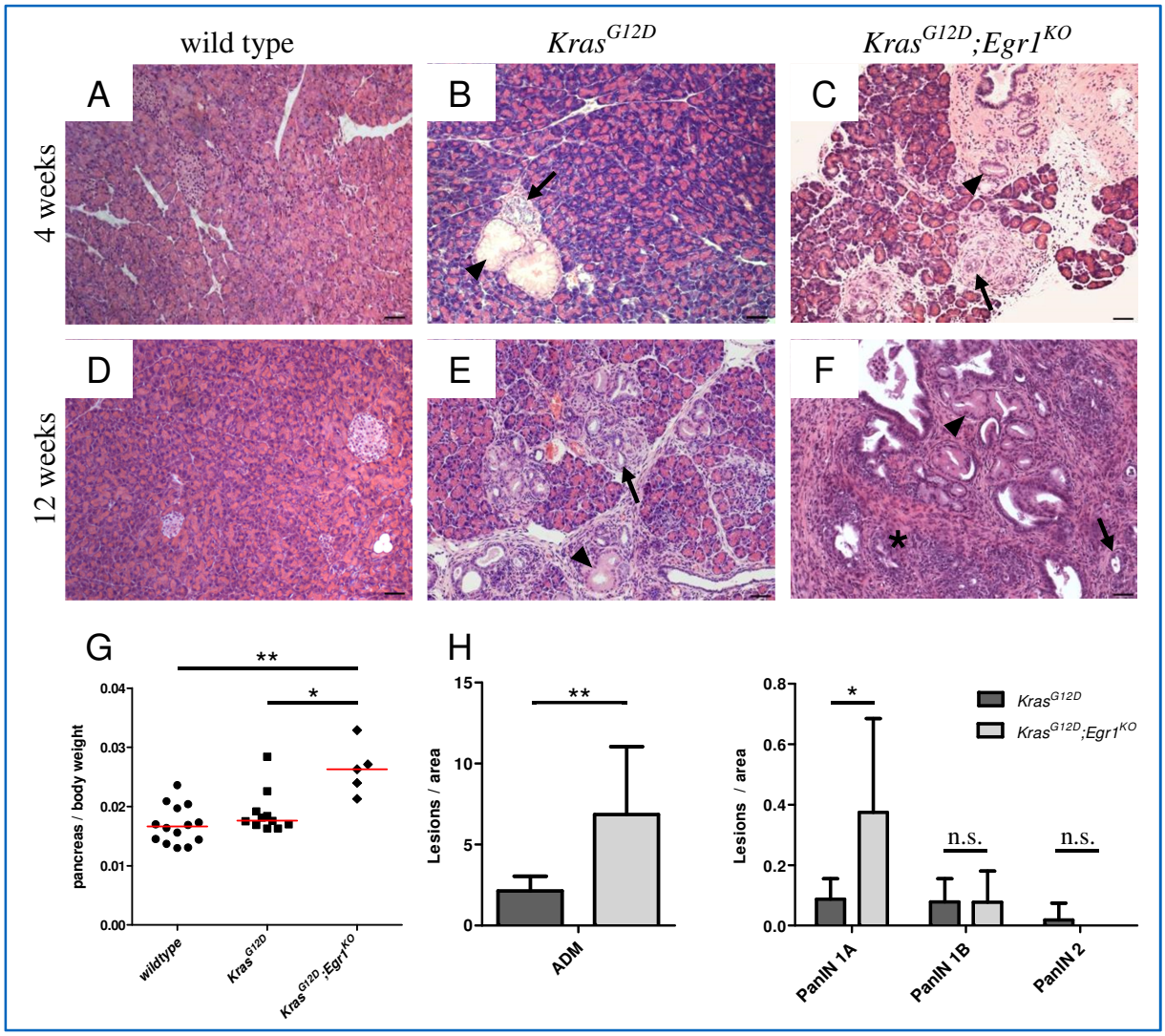

Figure 3.14: *Egr1*^{KO} enhances PDAC initiation in the *Kras*^{G12D} model. (A) – (C) H & E staining of tissue slides of 4 weeks old wild type, *Kras*^{G12D} and *Kras*^{G12D};*Egr1*^{KO} mice. *Kras*^{G12D} pancreata exhibit scattered ADM (arrow) and PanIN lesions (arrowhead), *Kras*^{G12D};*Egr1*^{KO} samples show several areas with multiple ADM and scattered PanIN lesions (n = 3 – 6; scale bar represents 50 µm). **(D) – (F)** H & E staining of tissue slides of 12 weeks old mice, exhibiting multiple ADM (arrow) and PanIN lesions (arrowhead) in *Kras*^{G12D} mice, while *Kras*^{G12D};*Egr1*^{KO} samples show predominantly PanIN lesions as well as foci of malignant transformation (asterisk; n = 5 – 6; scale bar represents 50 µm). **(G)** Pancreata of 12 weeks old *Kras*^{G12D};*Egr1*^{KO} mice exhibit a significantly elevated ratio of pancreas to body weight compared to wild type and *Kras*^{G12D} pancreata (n = 5 – 14; * ≙ $p < 0.05$; ** ≙ $p < 0.01$). **(H)** Quantification of ADM and PanIN lesions in 4 weeks old *Kras*^{G12D} and *Kras*^{G12D};*Egr1*^{KO} pancreata. *Kras*^{G12D};*Egr1*^{KO} mice show a significantly elevated number of ADM and PanIN 1A lesions compared to *Kras*^{G12D} mice. No significant differences can be detected for PanIN 1B and 2 quantity. Data shown are average values with standard deviation of all counted areas, with 6 - 8 randomly chosen, counted fields per area and 1 - 3 counted areas per mouse, spaced by 100 µm each (n = 3; * ≙ $p < 0.05$; ** ≙ $p < 0.01$).

exhibited an increased number of ADM and PanIN lesions, still with large areas of normal acinar tissue remaining. $Kras^{G12D};Egr1^{KO}$ mice showed predominantly PanIN lesions with almost no remaining acinar tissue and also exhibited foci of malignant transformation (figure 3.14 D - F). Moreover, the ratio of pancreas to body weight was significantly elevated in these mice compared to both $Kras^{G12D}$ and wild type samples (figure 3.14 G). Quantification of ADM and PanIN lesions of 4 weeks old mice revealed that $Kras^{G12D};Egr1^{KO}$ pancreata exhibited a significantly increased number of ADM and PanIN1A lesions compared to $Kras^{G12D}$ samples. However, no significant differences were detected for PanIN grade 1B and 2 lesion quantity between these genotypes (figure 3.14 H).

In order to investigate which factors might contribute to the enhanced development of pancreatic lesions as well as early tumour formation in $Kras^{G12D};Egr1^{KO}$ mice, the expression of the ductal marker Cytokeratin 19 and the acinar marker Amylase were analysed. Immunohistochemistry staining revealed an elevated Cytokeratin 19 expression in normal acinar tissue of 4 weeks old $Kras^{G12D};Egr1^{KO}$ samples. No Cytokeratin 19 expression was found in acinar-like cells of both wild type and $Kras^{G12D}$ mice (figure 3.15 A – C). Amylase expression was detected in acinar tissue of all genotypes; no obvious differences were observed between these samples (figure 3.15 D – F).

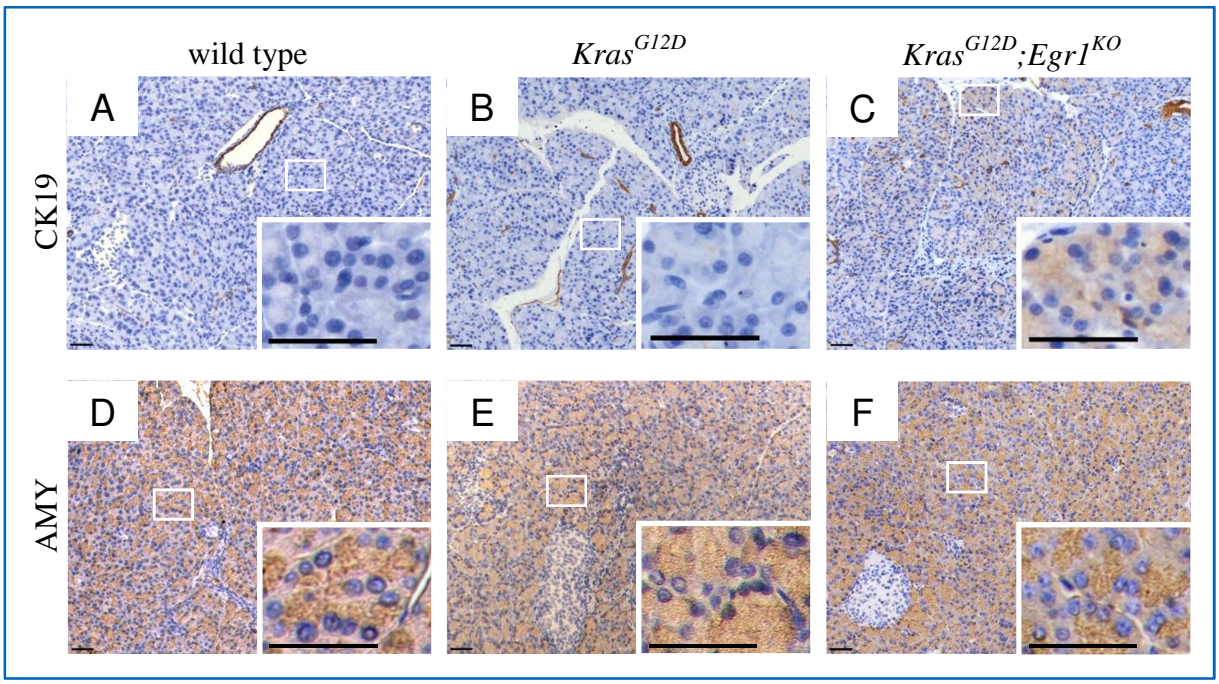

Figure 3.15: $Egr1^{KO}$ leads to elevated CK19 expression in the $Kras^{G12D}$ model. (A) – (C) Cytokeratin 19 staining of tissue slides of 4 weeks old wild type, $Kras^{G12D}$ and $Kras^{G12D};Egr1^{KO}$ mice. $Kras^{G12D}$ pancreata show a strong signal in normal ducts and pancreatic lesions, but not in acinar tissue. $Kras^{G12D};Egr1^{KO}$ samples exhibit an additional, cytoplasmic staining of acinar tissue. Wild type controls are only positive in normal pancreatic ducts. **(D) – (F)** Amylase staining of tissue slides of 4 weeks old wild type, $Kras^{G12D}$ and $Kras^{G12D};Egr1^{KO}$ mice. All samples exhibit a strong staining in acinar tissue (n = 3; scale bar represents 50 µm).

In addition to the *in vivo* studies, acinar cell transdifferentiation was investigated in *ex vivo* acinar explants of 5 weeks old $Kras^{G12D}$ and $Kras^{G12D};Egr1^{KO}$ mice. Bright field microscopy revealed that explants of both genotypes exhibited the same phenotype directly after isolation.

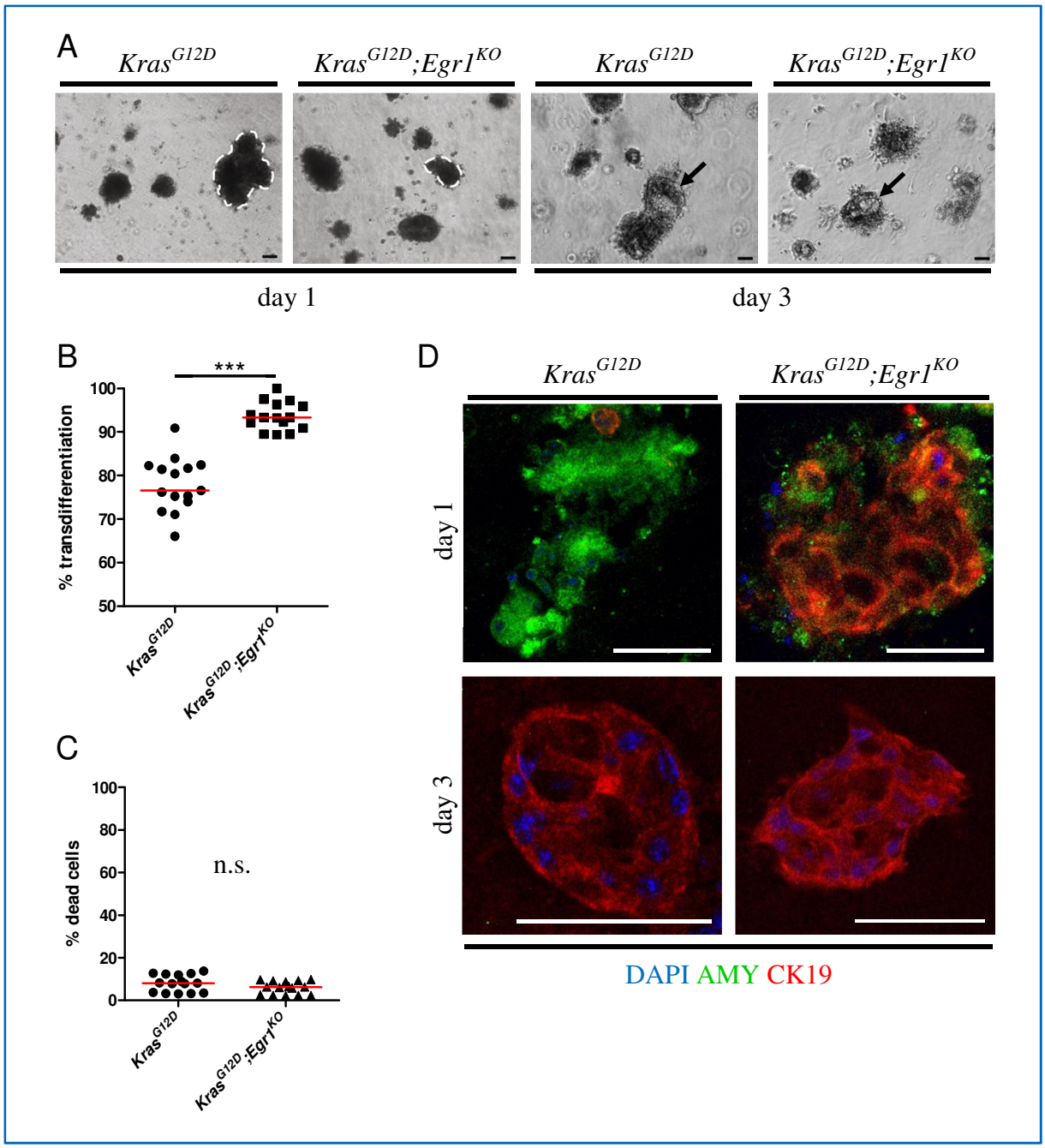

Figure 3.16: $Egr1^{KO}$ enhances acinar cell transdifferentiation in the $Kras^{G12D}$ model *ex vivo*. **(A)** Bright field microscopy of *ex vivo* acinar explants of $Kras^{G12D}$ and $Kras^{G12D};Egr1^{KO}$ pancreata. Directly after isolation (day 1), exclusively acinar cell clusters can be observed for both genotypes (dashed line). At day 3, most of the acinar clusters have transdifferentiated into duct-like structures (arrow; n = 3). **(B)** Percentage of transdifferentiated cell clusters at day 3. Each data point represents one well, with 3 randomly chosen fields counted per well and 3 – 5 wells per mouse. $Kras^{G12D};Egr1^{KO}$ samples exhibit highly significantly more duct-like structures than $Kras^{G12D}$ explants (n = 3; *** ≙ $p < 0.001$). **(C)** LDH assay at day 3, exhibiting no significant differences in cell mortality. Each data point represents one well (n = 3; n.s. ≙ not significant). **(D)** Confocal microscopy of immunofluorescence co-staining for Amylase and Cytokeratin 19 of acinar (day 1) and duct-like (day 3) clusters. scale bar represents 50 µm. Confocal microscopy was performed supported by Dr. Clara Lubeseder-Martellato.

After 3 days of culturing, samples of both genotypes showed transdifferentiated explants which had a duct-like phenotype (figure 3.16 A). Quantification of these transdifferentiated clusters showed that $Kras^{G12D};Egr1^{KO}$ samples exhibited a highly significantly increased rate of transdifferentiation compared to $Kras^{G12D}$ explants (figure 3.16 B), which was not a result of altered cell mortality (figure 3.16 C). Immunofluorescence co-staining of the acinar marker Amylase and the ductal marker Cytokeratin 19 revealed that explants of both genotypes exhibited high Amylase expression directly after isolation. Cytokeratin 19 was almost undetectable in $Kras^{G12D}$ acinar explants, except for single positive cells. However, $Kras^{G12D};Egr1^{KO}$ samples showed a strong Cytokeratin 19 signal, which mostly co-localised with Amylase, indicated by an orange to yellow, merged signal. At day 3, explants of both $Kras^{G12D}$ and $Kras^{G12D};Egr1^{KO}$ pancreata expressed exclusively Cytokeratin 19, while Amylase could not be detected (figure 3.16 D).

3.2.7 *Egr1*^{KO} does not enhance ADM formation in the *Tgfα* model

In order to investigate the impact of an *Egr1*^{KO} knockout in the *Tgfα* mouse model, in which ADM but not PanIN lesions form due to activation of EGFR without additional oncogenic KRAS, *Tgfα;Egr1*^{KO} mice were bred and analysed. H & E stained tissue slides of 4 weeks old *Tgfα* and *Tgfα;Egr1*^{KO} mice showed similar phenotypes without any obvious differences. Pancreata of both genotypes exhibited multiple ADM, but no PanIN lesions (figure 3.17 A - C). Consequently, quantification of Cytokeratin 19 positive ADM revealed no significant differences in lesion number (figure 3.17 E). The ratio of pancreas to body weight of both *Tgfα* and *Tgfα;Egr1*^{KO} mice was significantly elevated compared to wild type and *Egr1*^{KO} mice. Furthermore, this ratio was significantly higher in *Tgfα* compared to *Tgfα;Egr1*^{KO} mice; no significant differences were observed between wild type and *Egr1*^{KO} mice, though (figure 3.17 D).

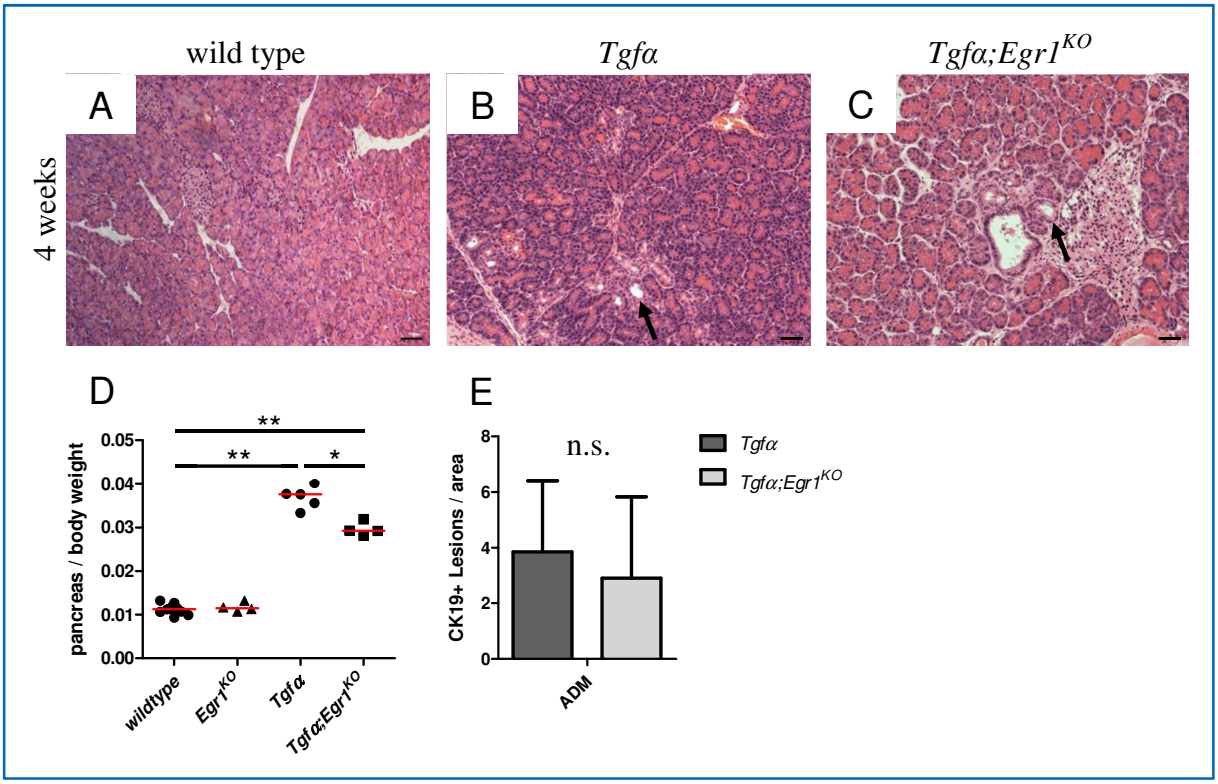

Figure 3.17: *Egr1*^{KO} does not enhance ADM formation in *Tgfα* mice. (A) – (C) H & E staining of tissue slides of 4 weeks old wild type, *Tgfα* and *Tgfα;Egr1*^{KO} mice. Pancreata of both genotypes exhibit multiple ADM (arrow; n = 3 – 4; scale bar represents 50 µm). **(D)** Pancreata of 4 weeks old *Tgfα* and *Tgfα;Egr1*^{KO} mice exhibit a significantly elevated ratio of pancreas to body weight compared to both wild type and *Egr1*^{KO} pancreata. Furthermore, this ratio was significantly higher in *Tgfα* compared to *Tgfα;Egr1*^{KO} mice. Ratios of wild type and *Egr1*^{KO} mice exhibited no significant differences (n = 4 – 14; * ≙ $p < 0.05$; ** ≙ $p < 0.01$). **(E)** Quantification of Cytokeratin 19 positive lesions in *Tgfα* and *Tgfα;Egr1*^{KO} mice. Data shown are average values with standard deviation of all counted areas, with 6 randomly chosen, counted fields per area and 3 counted areas per mouse, spaced by 100 µm each. The number of CK19 positive ADM was not significantly different in *Tgfα;Egr1*^{KO} pancreata compared to *Tgfα* samples of the same age (n = 3 – 4; n.s. ≙ not significant).

Since 4 weeks old *Kras*^{G12D};*Egr1*^{KO} mice exhibited a significantly higher number of ADM compared to *Kras*^{G12D} samples of the same age, it was further investigated which parameters might contribute to the fact that this was not the case for *Tgfα* and *Tgfα;Egr1*^{KO} pancreata. In the following, both CK19 and EGFR expression was analysed. Immunohistochemistry staining of tissue slides of 4 weeks old wild type, *Tgfα* and *Tgfα;Egr1*^{KO} mice showed a strong CK19 expression within ADM and normal ducts for all genotypes. However, the protein was not detectable within acinar tissues of these samples (figure 3.18 A - C). qPCR analysis of *Egfr* mRNA levels revealed that *Tgfα* samples exhibited a significantly increased *Egfr* expression compared to wild type pancreata. However, *Tgfα;Egr1*^{KO} samples expressed significantly less *Egfr* than *Tgfα* pancreata. No significant differences were observed between *Tgfα;Egr1*^{KO} and wild type samples (figure 3.18 D).

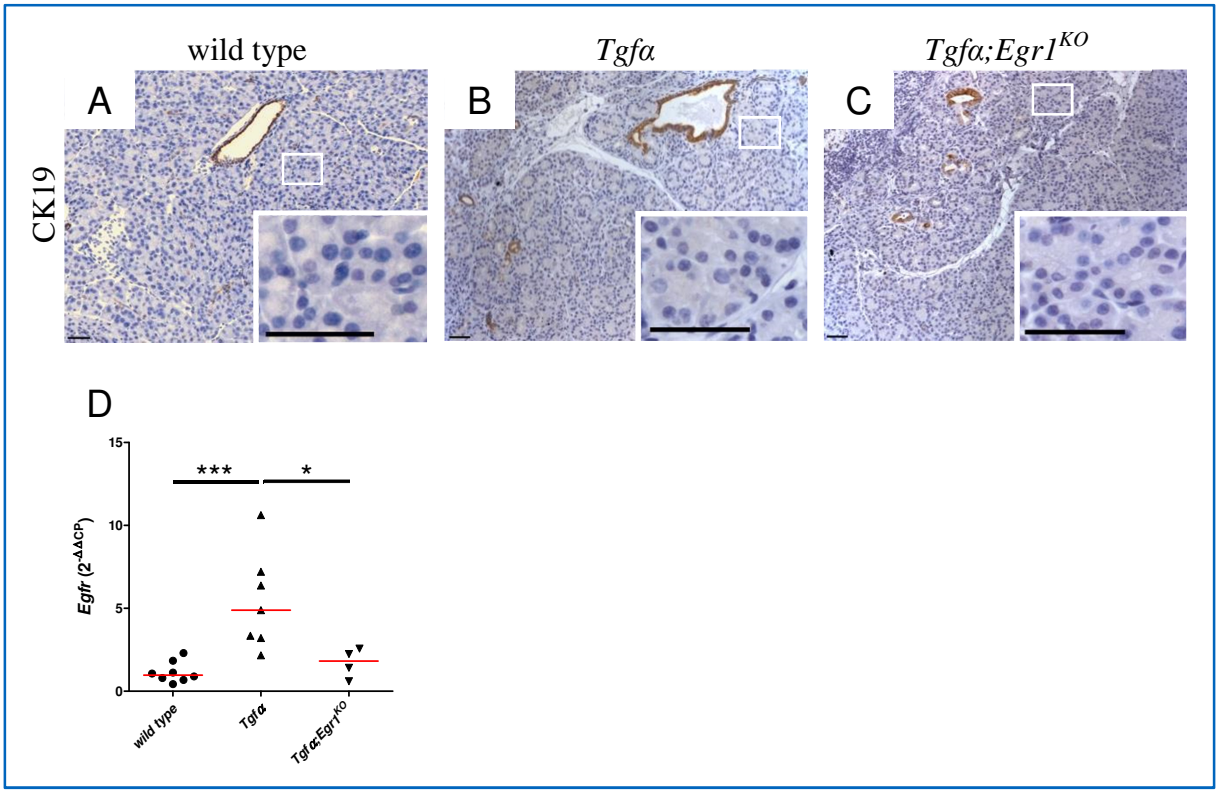

Figure 3.18: *Egr1*^{KO} leads to reduced EGFR expression in the *Tgfα* model. (A) – (C) Cytokeratin 19 staining of tissue slides of 4 weeks old wild type, *Tgfα* and *Tgfα;Egr1*^{KO} mice. Both *Tgfα* and *Tgfα;Egr1*^{KO} pancreata show a strong signal in normal ducts and pancreatic lesions, but not in acinar tissue. Wild type controls are only positive in normal pancreatic ducts. **(D)** qPCR analysis of *Egfr* mRNA expression of 4 weeks old wild type, *Tgfα* and *Tgfα;Egr1*^{KO} pancreata, showing a significantly higher *Egfr* expression level in *Tgfα* compared to both wild type and *Tgfα;Egr1*^{KO} samples. No differences were detected between wild type and *Tgfα;Egr1*^{KO} mice (n = 4 – 8; * ≙ $p < 0.05$; *** ≙ $p < 0.001$).

3.2.8 EGR1 binds to both *Egfr* and *Ck19* promoters

As a transcription factor, EGR1 controls and influences the expression of a variety of target genes. Regulation can take place directly or indirectly, thus binding to sites within the particular target gene or to other transcription factors, which influence expression of target genes in a second step. In $Kras^{G12D};Egr1^{KO}$ mice, CK19 was found to be upregulated in acinar tissue; further, EGFR was found to be downregulated in $Tgf\alpha;Egr1^{KO}$ pancreata. In the following, it was investigated whether EGR1 regulates these genes via direct binding of the corresponding promoter sequences. At first, putative binding sites of EGR1 within the

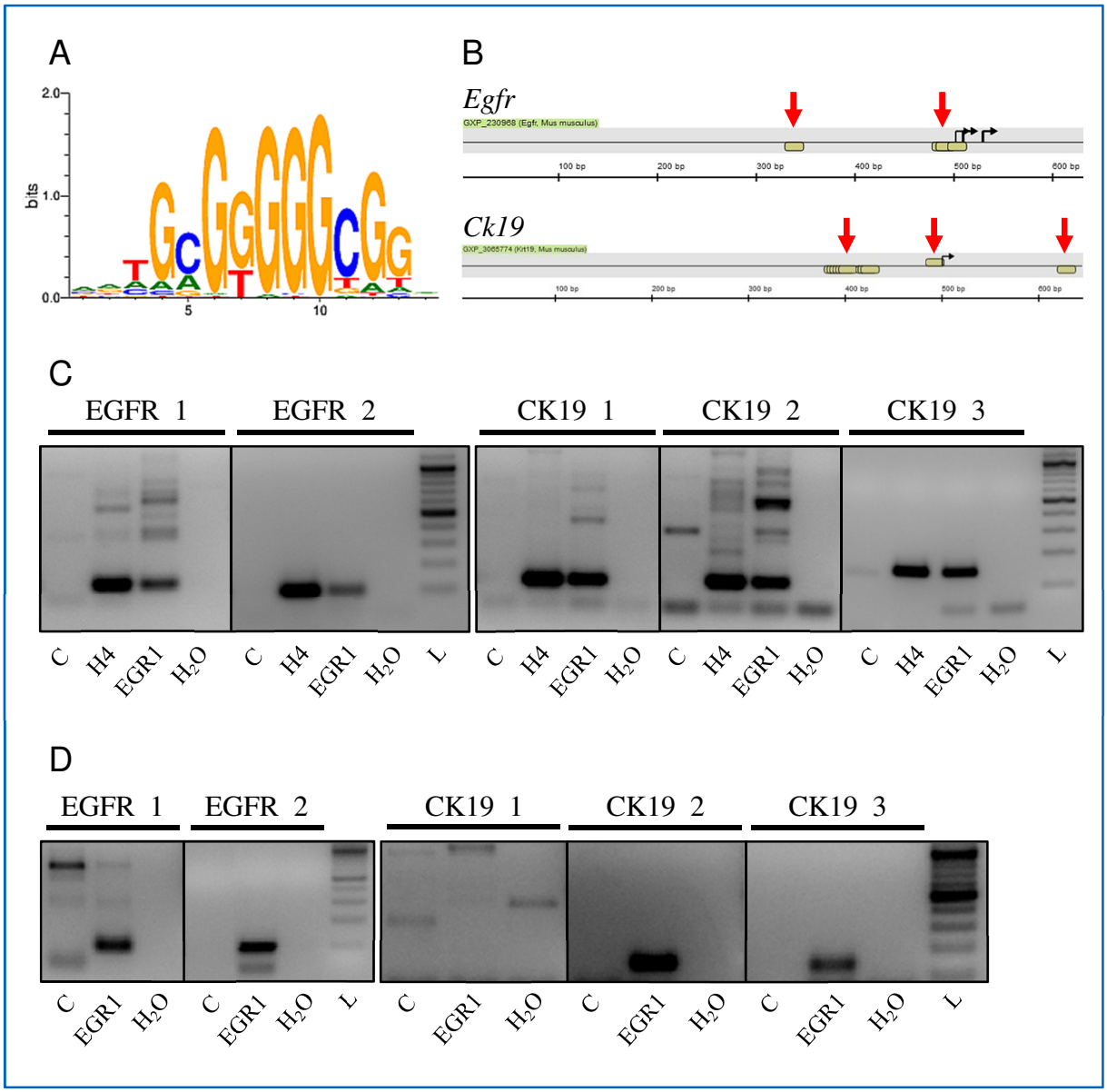

Figure 3.19: EGR1 binds to both *Egfr* and *Ck19* promoters. **(A)** The EGR1 binding site consensus sequence, schematic. **(B)** EGR family member binding sites within the promoters of *Egfr* and *Ck19*. Red arrows indicate EGR1 binding sites analysed via ChIP Assay. **(C)** ChIP Assay analysis of a wild type pancreas during induced acute pancreatitis, 4 h after the first cerulein injection. A Histone H4 antibody served as a positive control (H4), rabbit serum as a negative control (C). EGR1 binds to all *Egfr* and *Ck19* binding sites analysed. **(D)** ChIP Assay analysis of pancreatic tissue of a 7 days old *Tgfα* mouse. Rabbit serum served as a negative control (C). EGR1 binds to both *Egfr* binding sites analysed. Further, EGR1 binds to the *Ck19* binding sites 2 and 3, but not to site 1.

promoters of *Egfr* and *Ck19* were identified using the MatInspector software. Multiple repeats of the EGR1 consensus binding sequence (figure 3.19 A) were found in both promoters. Sites exhibiting high matrix similarity values (value > 0.8) were selected and primers enclosing these sequences were designed (figure 3.19 B); detailed sequence information can be found in the appendix. Subsequently, a ChIP Assay was performed using induced pancreatitis samples of wild type mice, 4 h after the first cerulein treatment, and pancreatic tissue of 7 days old *Tgfα* mice. Both types of samples were shown to express high amounts of EGR1, a prerequisite for a successful immunoprecipitation. PCR analysis revealed that EGR1 binds to both the *Egfr* and the *Ck19* promoter. Using induced pancreatitis samples, a signal was detected for all binding sites analysed (figure 3.19 C); in *Tgfα* pancreata, a signal was detected for *Egfr* sites 1 and 2 as well as *Ck19* sites 2 and 3, but not for *Ck19* site 1 (figure 3.19 D).

3.3 KLF5 IN ADM AND PANIN DEVELOPMENT

3.3.1 KLF5 is regulated via the EGFR – KRAS – MEK pathway

Another potential link between the EGFR – KRAS – MEK pathway and the observed phenotype of the *Mek1DD* model is the transcription factor KLF5, which is regulated via both MEK and EGR1 in other tissues (Kawai-Kowase *et al.,* 1999; Nandan *et al.,* 2004; Yang *et al.,* 2007). Analogue to the procedure exerted during the investigation of EGR1, the expression pattern of KLF5 was analysed first in several PDAC precursor models in order to elucidate its role during formation of pancreatic lesions as well as to confirm its mode of regulation - previously described for other murine tissues - within the pancreas. Immunohistochemistry staining of KLF5 on tissue slides of 4 weeks old wild type, *Mek1DD* and *Mek1DD;Egfr*$^{\Delta Panc}$ mice revealed that KLF5 was strongly expressed in nuclei of normal ducts of all investigated genotypes. Furthermore, both ADM and PanIN lesions of *Mek1DD* and *Mek1DD;Egfr*$^{\Delta Panc}$ samples were highly KLF5 positive. Normal acinar tissue exhibited KLF5 expression in most, but not all cells. In addition, the expression within acinar cells was not as strong as it was observed for pancreatic lesions (figure 3.20 A - C).

KLF5 was further investigated in 4 weeks old *Kras*^{G12D} and *Kras*^{G12D}*;Egfr*$^{\Delta Panc}$ mice to confirm its dependency on EGFR expression. Immunohistochemistry staining of *Kras*^{G12D} samples exhibited a strong signal for KLF5 in metaplastic lesions. In addition, virtually all nuclei of normal acinar tissue were positive, although the expression within these cells was weaker than in those of ADM. *Kras*^{G12D}*;Egfr*$^{\Delta Panc}$ samples were only KLF5 positive in normal pancreatic ducts; the same was true for wild type mice. Acinar tissue was completely negative in both genotypes (figure 3.21 A – C). Similar results were obtained during qPCR analysis of *Klf5* mRNA levels. Here, samples of *Kras*^{G12D} mice exhibited a significantly increased *Klf5*

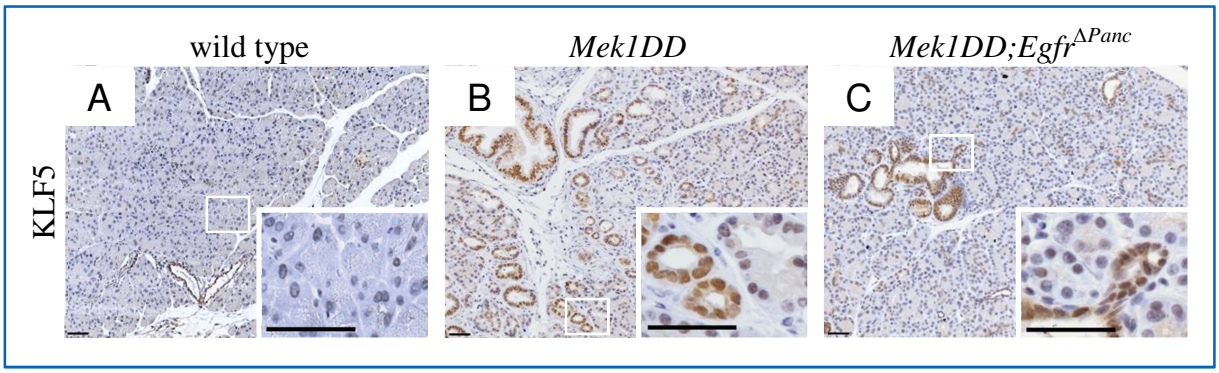

Figure 3.20: KLF5 is upregulated in pancreata of *Mek1DD* and *Mek1DD;Egfr*$^{\Delta Panc}$ mice. (A) – (C) Immunohistochemistry staining of KLF5 on tissue slides of 4 weeks old wild type, *Mek1DD* and *Mek1DD;Egfr*$^{\Delta Panc}$ mice, showing a strong nuclear signal in normal ducts of all samples. ADM and PanIN lesions are positive in *Mek1DD* and *Mek1DD;Egfr*$^{\Delta Panc}$ pancreata. Most of the normal acinar tissue of these mice is KLF5 positive, although less strong than pancreatic lesions (n = 4 - 7; scale bar represents 50 µm).

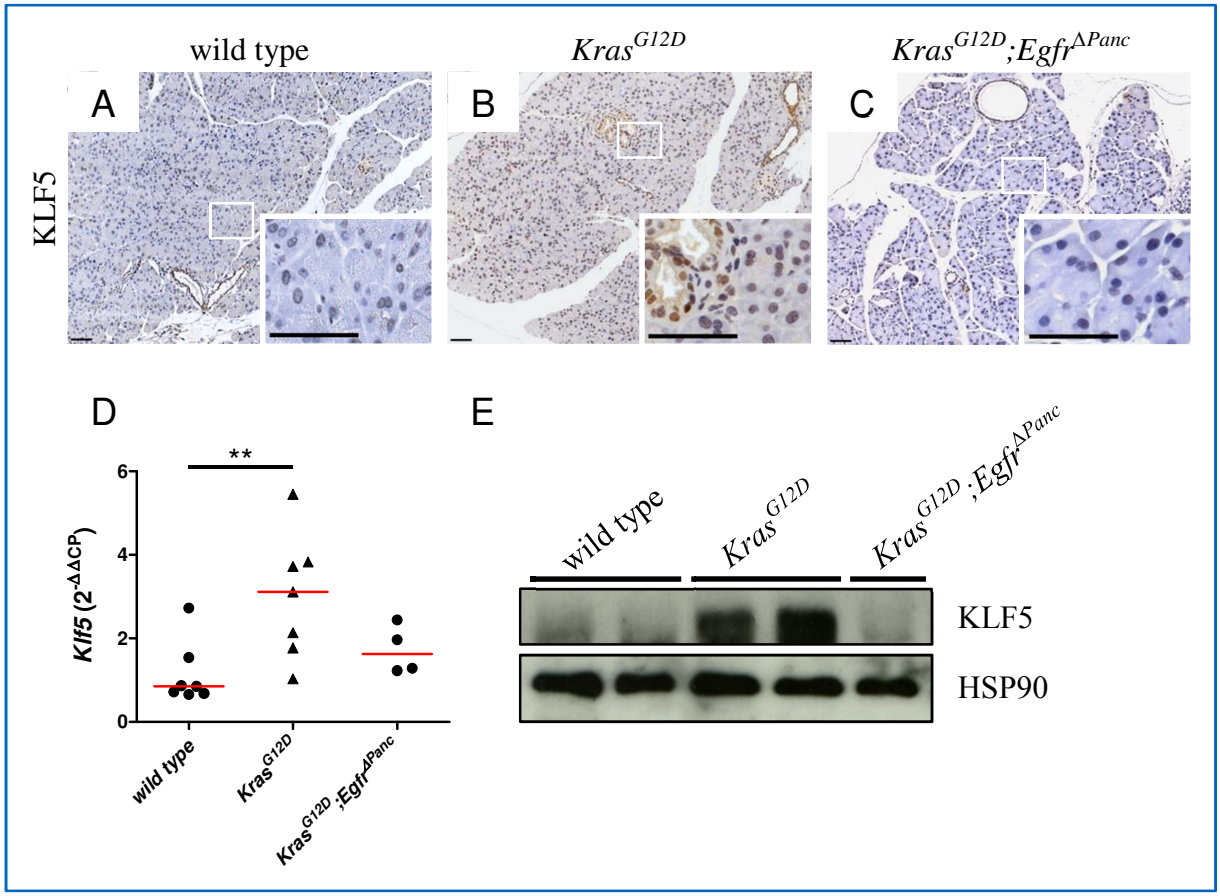

Figure 3.21: KLF5 is upregulated in pancreata of *Kras*^{G12D} but not *Kras*^{G12D};*Egfr*$^{\Delta Panc}$ mice. (A) – (C) Immunohistochemistry staining of KLF5 on tissue slides of 4 weeks old wild type, *Kras*^{G12D} and *Kras*^{G12D};*Egfr*$^{\Delta Panc}$ mice, exhibiting a strong nuclear staining in ADM of *Kras*^{G12D} samples. Nuclei of virtually all acinar cells are also positive, but less strong. *Kras*^{G12D};*Egfr*$^{\Delta Panc}$ pancreata only show KLF5 expression in normal ducts, while acinar tissue is completely negative (n = 4 – 5; scale bar represents 50 µm). **(D)** qPCR analysis of *Klf5* mRNA levels showing a significantly higher *Klf5* expression in *Kras*^{G12D} samples compared to those of wild type mice (n = 4 - 7; ** ≙ $p < 0.01$). **(E)** Western Blot analysis revealing a strong KLF5 expression in samples of *Kras*^{G12D} mice, while the protein was almost undetectable in both wild type and *Kras*^{G12D};*Egfr*$^{\Delta Panc}$ samples.

expression compared to wild type mice. The expression in *Kras*^{G12D};*Egfr*$^{\Delta Panc}$ pancreata neither showed a significant difference to wild type nor to *Kras*^{G12D} samples (figure 3.21 D). Western Blot analysis revealed a strong KLF5 signal for samples of *Kras*^{G12D} mice, while both wild type and *Kras*^{G12D};*Egfr*$^{\Delta Panc}$ pancreata exhibited almost no KLF5 expression (figure 3.21 E).

Immunohistochemistry staining of tissue slides of 4 weeks old *Tgfα* mice also showed strong KLF5 expression in metaplastic lesions. Again, acinar cells were positive, but less strong than the observed ADM. Wild type controls were negative except for normal pancreatic ducts, which were KLF5 positive in both genotypes (figure 3.22 A – B). qPCR analysis showed a significantly elevated *Klf5* mRNA expression in *Tgfα* pancreata compared to wild type samples (figure 3.22 C). Western Blot analysis revealed a strong KLF5 protein expression in *Tgfα* mice, whereas KLF5 was undetectable in wild type controls (figure 3.22 D).

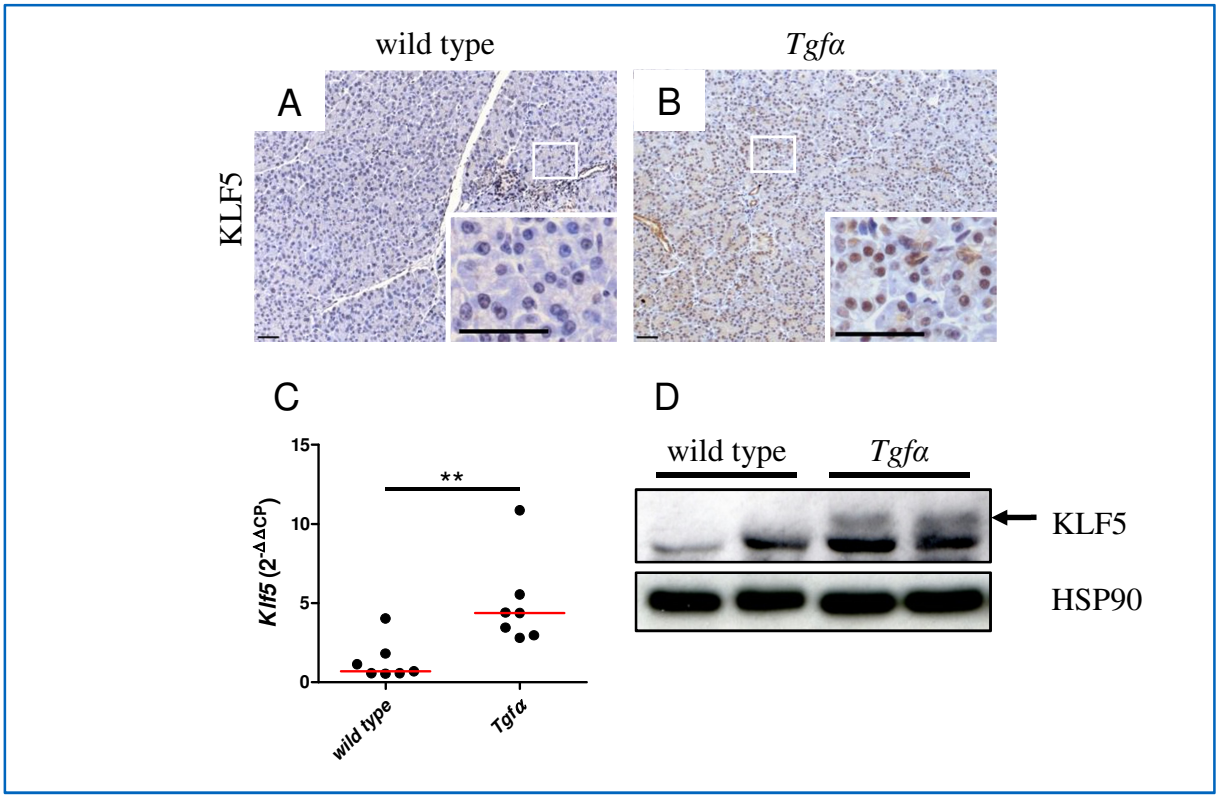

Figure 3.22: KLF5 is upregulated in pancreata of *Tgfα* mice. (A) – (B) Immunohistochemistry staining of KLF5 on tissue slides of 4 weeks old wild type and *Tgfα* mice, exhibiting a strong nuclear signal in ADM of *Tgfα* samples. Nuclei of virtually all acinar cells are also positive, but less strong. Wild type samples show no KLF5 expression in acinar tissue; normal pancreatic ducts were positive in both genotypes, though (n = 3; scale bar represents 50 µm). **(C)** qPCR analysis of *Klf5* mRNA levels showing a significantly higher *Klf5* expression in *Tgfα* samples compared to those of wild type mice (n = 7 – 8; ** ≙ $p < 0.01$). **(D)** Western Blot analysis revealing elevated KLF5 expression in *Tgfα* pancreata, while the protein was almost undetectable in wild type samples.

3.3.2 KLF5 is elevated during induced acute pancreatitis

Along with the analysis in mouse models, KLF5 expression was also investigated during cerulein induced acute pancreatitis in 6 weeks old wild type mice. Immunohistochemistry staining of KLF5 on tissue slides showed a strong signal in nuclei of all acinar cells 8 h after the first cerulein treatment. Untreated controls as well as samples obtained 72 h after the first injection were negative, except for normal pancreatic ducts (figure 3.23 A - C). qPCR analysis revealed that *Klf5* mRNA was significantly upregulated 4 h and 8 h after the first treatment compared to untreated controls. 24 h and 72 h after the first injection, the expression was down to levels of untreated samples again (figure 3.23 D). The same was observed during Western Blot analysis of KLF5 protein expression. Here, elevated KLF5 levels were detected 4 h after the first treatment compared to both untreated controls and samples obtained 72 h after the first injection. No difference was observed between the 72 h time point and untreated controls (figure 3.23 E).

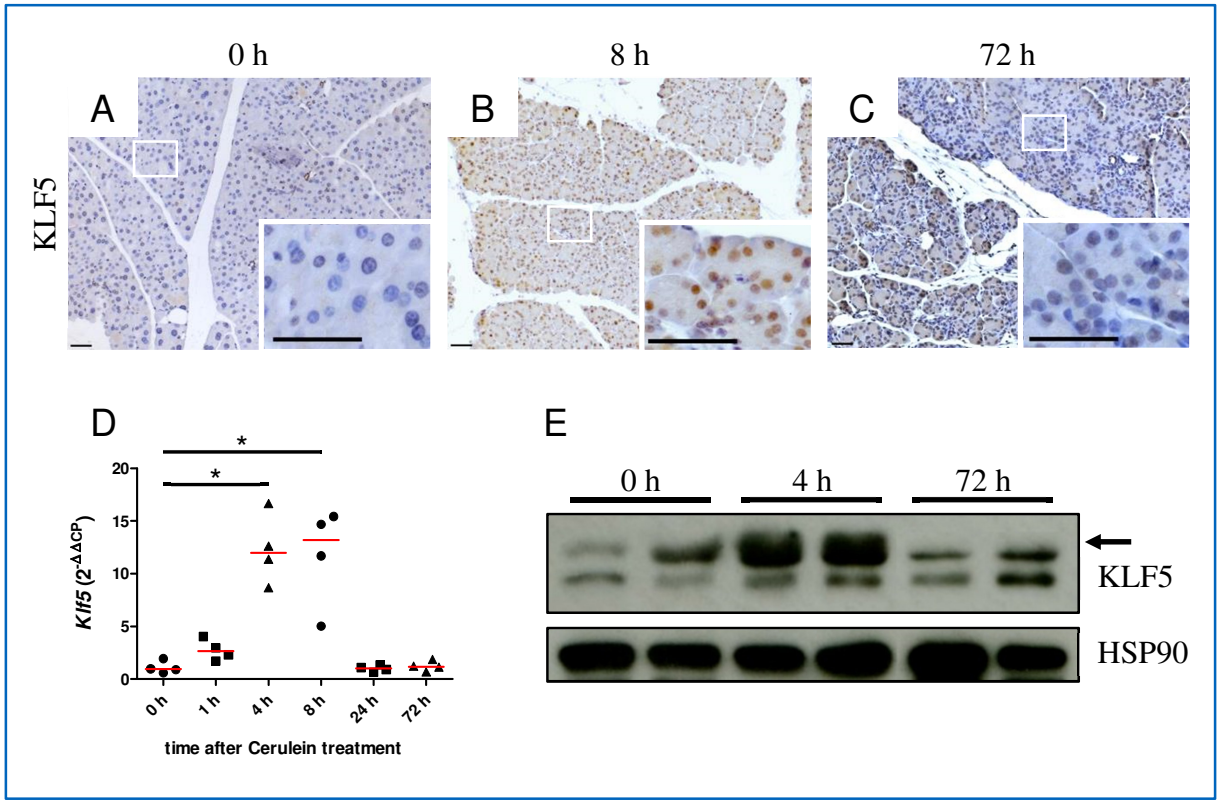

Figure 3.23: KLF5 is upregulated during cerulein induced acute pancreatitis. (A) – (C) Immunohistochemistry staining of KLF5, showing a strong nuclear staining in all acinar cells 8 h after the first injection, while untreated controls as well as samples obtained 72 h after the first injection were KLF5 negative (n = 4; scale bar represents 50 µm). **(D)** qPCR analysis of *Klf5* mRNA levels, showing a significant upregulation of *Klf5* expression 4 h and 8 h after the first injection compared to untreated samples. The expression is downregulated to wild type levels again 24 h and 72 h after the first injection (n = 4; * ≙ $p < 0.05$). **(E)** Western Blot analysis showing a strong upregulation of KLF5 4 h after the first cerulein treatment compared to both untreated controls and samples obtained 72 h after the first injection.

3.3.3 KLF5 is not regulated by EGR1

While both EGR1 and KLF5 have been described as being downstream of the EGFR – MEK pathway (Midgley and Khachigian, 2004; Khachigian, 2006; Hasan and Schafer, 2008;

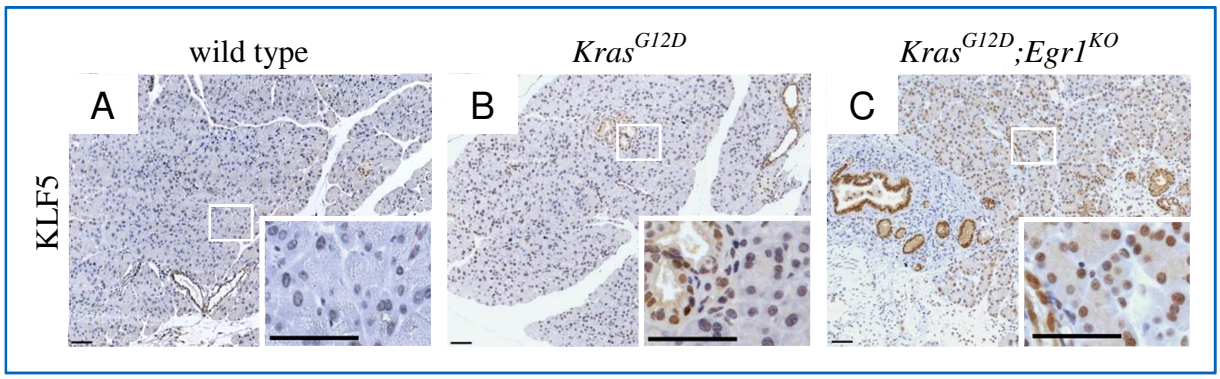

Figure 3.24: KLF5 is upregulated in pancreata of *Kras^{G12D};Egr1^{KO}* mice. (A) - (C) Immunohistochemistry staining of KLF5 on tissue slides of 4 weeks old wild type, *Kras^{G12D}* and *Kras^{G12D};Egr1^{KO}* mice showing strong KLF5 expression in pancreatic lesions as well as in normal acinar tissue of both *Kras^{G12D}* and *Kras^{G12D};Egr1^{KO}* pancreata (n = 4; scale bar represents 50 µm).

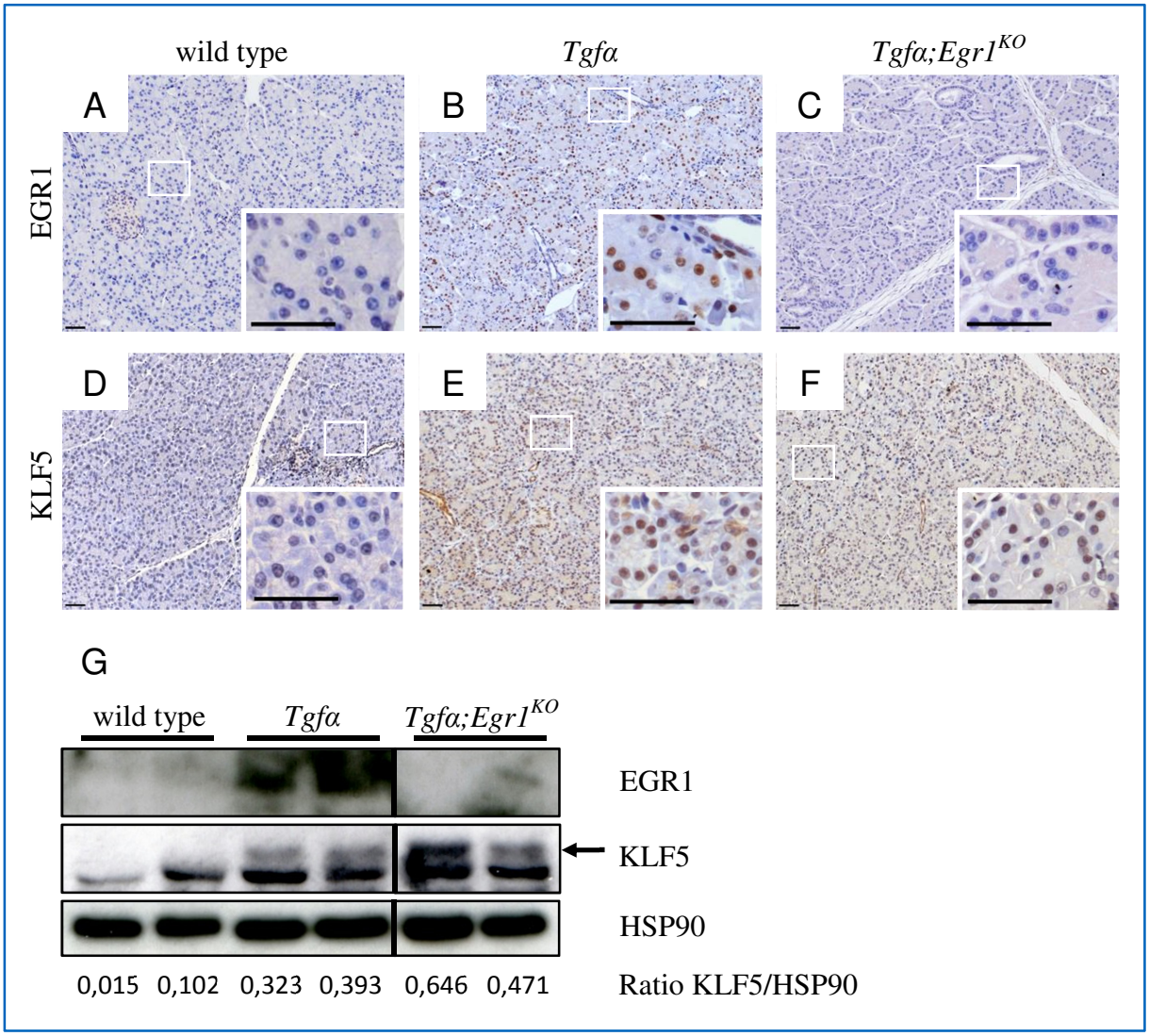

Figure 3.25: KLF5 is upregulated in pancreata of *Tgfα;Egr1*^{KO} mice. **(A) – (C)** Immunohistochemistry staining of EGR1 on tissue slides of 4 weeks old wild type, *Tgfα* and *Tgfα;Egr1*^{KO} mice, verifying the absence of EGR1 in *Tgfα;Egr1*^{KO} pancreata (n = 3 – 4; scale bar represents 50 µm). **(D) – (F)** KLF5 staining of the same samples. No obvious change in KLF5 expression can be observed for *Tgfα;Egr1*^{KO} pancreata compared to those of *Tgfα* mice (n = 3 – 4; scale bar represents 50 µm). **(G)** Western Blot analysis, showing a strong KLF5 expression in both *Tgfα* and *Tgfα;Egr1*^{KO} pancreata.

Kawai-Kowase *et al.,* 1999; Nandan *et al.,* 2004; Yang *et al.,* 2007), KLF5 acts downstream and is being regulated by EGR1 in other murine tissues (Kawai-Kowase *et al.,* 1999; Nandan *et al.,* 2004). Whether the same is the case for the murine pancreas was investigated by analysing KLF5 expression in both *Kras*^{G12D}*;Egr1*^{KO} and *Tgfα;Egr1*^{KO} mouse models as well as during cerulein-induced acute pancreatitis in *Egr1*^{KO} mice. Immunohistochemistry staining of tissue slides of 4 weeks old *Kras*^{G12D}*;Egr1*^{KO} mice showed no obvious difference in KLF5 expression compared to *Kras*^{G12D} samples. Pancreatic ducts, lesions and almost all acinar cells exhibited a strong nuclear staining (figure 3.24 A – C). Similar results were obtained for tissue slides of *Tgfα;Egr1*^{KO} mice. Although EGR1 was undetectable in these samples (figure 3.25 A – C), KLF5 expression remained unchanged and was still present in nuclei of most

acinar cells as well as all pancreatic lesions and ducts (figure 3.25 D – F). The same results were obtained during Western Blot analysis. Here, EGR1 was strongly expressed in *Tgfα* pancreata, while it was absent in *Tgfα;Egr1*^{KO} samples. KLF5 on the other hand was upregulated in samples of both genotypes, though the expression was higher in *Tgfα;Egr1*^{KO} pancreata (figure 3.25 G). In addition to these findings, KLF5 expression was investigated during induced acute pancreatitis in *Egr1*^{KO} mice. 6 weeks old mice were injected hourly i.p. with 50 ng of cerulein per g mouse weight, with a total of 4 injections. Wild type mice were treated simultaneously in the same manner and were used as positive controls. Samples were obtained 4 h after the first injection; untreated mice of both genotypes served as a control. qPCR analysis of wild type samples showed a significantly increased *Klf5* mRNA expression 4 h after the first cerulein treatment compared to untreated controls. *Egr1*^{KO} mice resembled these results: Klf5 was significantly upregulated at the 4 h time point compared to samples which were not injected (figure 3.26).

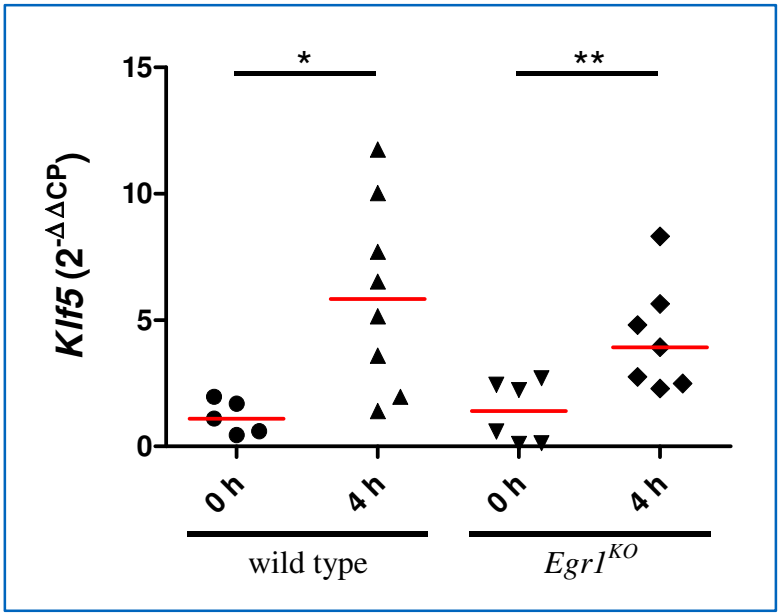

Figure 3.26: KLF5 is upregulated during induced acute pancreatitis in *Egr1*^{KO} pancreata. 6 weeks old wild type and *Egr1*^{KO} mice were injected i.p. hourly with 50 ng of cerulein per g mouse weight, with 4 injections in total. Samples were obtained before (0 h) and 4 h after the first injection. qPCR analysis shows that *Klf5* mRNA expression is significantly upregulated 4 h after the first cerulein treatment in both wild type and *Egr1*^{KO} samples compared to the corresponding untreated controls (n = 5 – 8; * ≙ p < 0.05; ** ≙ p < 0.01).

3.3.4 KLF5 induces the ductal marker CK19 *in vitro*

Given the fact that KLF5 is upregulated in several investigated pancreatic lesions and in ADM in particular, an *in vitro* overexpression assay was performed to analyse if KLF5 has an effect on proteins involved in metaplastic transition. The murine acinar cell line 266-6 was transfected with the pCAG-Klf5 overexpression vector and the mRNA expression levels of *Klf5*, *Ck19* and *Amy* were analysed via qPCR. Cells transfected with the vector pCAG served as a control. Further, a co-transfection with the vector pCAGGS-Cherry was performed in order to analyse the transfection efficiency. Fluorescence microscopy revealed that approx.

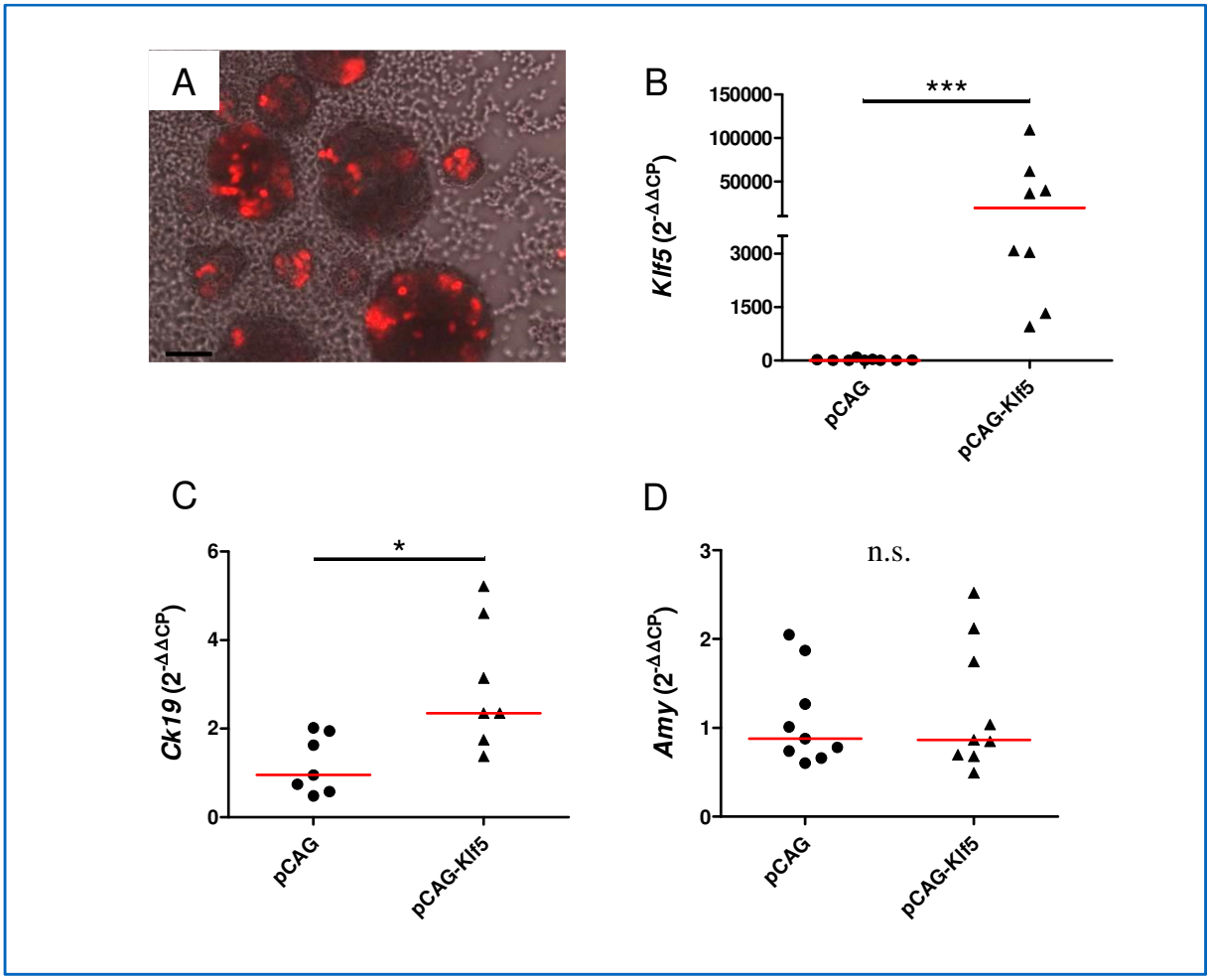

Figure 3.27: KLF5 induces the ductal marker CK19 *in vitro*. (A) Fluorescence microscopy of 266-6 cells co-transfected with the pCAG-Klf5 and the pCAGGS-Cherry vector. Scale bar represents 50 µm. **(B) – (D)** qPCR analysis of transfected 266-6 cells. *Klf5* (B) and *Ck19* (C) mRNA is significantly overexpressed in pCAG-Klf5 transfected cells compared to pCAG transfected controls. No significant difference can be observed for *Amy* expression (D; n = 7 – 9; * ≙ $p < 0.05$; *** ≙ $p < 0.001$).

30 % of the cells were transfected (figure 3.27 A). qPCR analysis showed that *Klf5* mRNA levels were significantly elevated in pCAG-Klf5 transfected cells compared to pCAG transfected controls (figure 3.27 B). These cells also exhibited elevated *Ck19* mRNA levels (figure 3.27 C); the expression of *Amy* mRNA remained unchanged, though (figure 3.27 D).

4 DISCUSSION

4.1 MEK1DD IS SUFFICIENT FOR ADM AND PANIN, BUT NOT PDAC FORMATION

Despite intense industrial and academic research efforts, PDAC is still a largely therapy-resistant, fatal disease and represents one of the most aggressive types of tumours known today (Kedia *et al.,* 2013). Its genetic background has been extensively studied and several pathways involved in PDAC formation have been identified. The most prominent gene is *Kras*, which can be found mutated in more than 90 % of all PDACs (Hezel, 2006). Consequently, genetically engineered mouse models expressing the mutated $KRAS^{G12D}$ have been shown to recapitulate the human disease and develop both PDAC and its precursors, ADM and PanIN lesions (Hingorani *et al.,* 2003). These lesions are highly positive for pERK and pAKT, hence $KRAS^{G12D}$ activates both the MEK – ERK and the PI3K – AKT pathway (Avraham and Yarden, 2011; Ardito *et al.,* 2012). Recently, it has been shown that EGFR ablation impairs the $KRAS^{G12D}$–induced phenotype, thus blocking PDAC precursor lesion initiation. $Kras^{G12D};Egfr^{\Delta Panc}$ mice were further shown to exhibit sustained AKT and STAT3 signalling, but reduced ERK activity. Pharmacological inhibition of MEK, responsible for ERK phosphorylation, likewise led to reduced ADM and PanIN development both *in vitro* and *in vivo* (Ardito *et al.,* 2012). These results support two major conclusions: first, EGFR is essential for oncogenic KRAS driven MEK activation; although other KRAS based pathways remain upregulated, $KRAS^{G12D}$ is not sufficient for reaching a critical ERK signalling threshold in the absence of EGFR. Second, MEK activity is needed for initial transdifferentiation processes, which cannot be replaced by active AKT or STAT3 signalling (Ardito *et al.,* 2012).

In this work, the role of MEK during PDAC initiation was further studied. In particular, a novel mouse model expressing a dominant active form of MEK, MEK1DD, was analysed and compared to the well-established $Kras^{G12D}$ as well as to the recently published $P110\alpha^{H1047R}$ model. A close look was taken at the types of lesions and signalling pathways in *Mek1DD* pancreata compared to those of $Kras^{G12D}$ and $P110\alpha^{H1047R}$ at different ages. MEK1DD was found to be sufficient for development of both ADM and PanIN lesions of all grades. The presence of PanIN lesions was further verified via staining for the PanIN markers MUC5,

CLDN18 and Alcian Blue, which were all found highly positive. Direct comparison of *Mek1DD* to *Kras*^{G12D} and *P110α*^{H1047R} pancreata revealed that lesion development starts earlier within *Mek1DD* mice. At an age of 4 weeks, the earliest time point analysed, a considerable quantity of ADM was already present within *Mek1DD* samples, highly significantly more than *Kras*^{G12D} pancreata exhibited. In addition, the number of PanIN1A lesions was also significantly higher in these mice. However, the quantities of higher-grade PanIN1B and PanIN2 lesions within *Mek1DD* pancreata were comparable to those of *Kras*^{G12D} mice. These results were further supported by a significantly increased pancreas to body weight index of *Mek1DD* mice, underlining the early occurrence of transforming effects within this genotype. Lesion development could furthermore not be impaired by an additional *Egfr* knockout; *Mek1DD;Egfr*$^{\Delta Panc}$ mice exhibited both ADM and PanIN lesions without any obvious differences compared to *Mek1DD* pancreata of the same age. These results additionally highlight the fact that MEK – ERK signalling and no other targets of EGFR are causing the observed phenotype.

Taken together, MEK1DD leads to early transformation effects, reflected in high ADM numbers as well as early PanIN development. These findings are furthermore independent of KRAS^{G12D} expression and therefore contribute to the recently proposed role for the MEK – ERK pathway as an essential mediator of initial transdifferentiation processes. Likewise, the fact that EGFR ablation in *Mek1DD* mice cannot impair the phenotype described supports the hypothesis that the blockage of lesion development reported for *Kras*^{G12D}*;Egfr*$^{\Delta Panc}$ pancreata is a result of insufficient or too low MEK/ERK activity.

Long term analysis of *Mek1DD*, *Kras*^{G12D} and *P110α*^{H1047R} mice revealed an increase of ADM and PanIN lesions at an age of 12 weeks for all genotypes. However, *Mek1DD* pancreata exhibited more lesions than those of *Kras*^{G12D} and *P110α*^{H1047R}, which was expectable given the early development of ADM and high-grade PanIN lesions of this genotype. At an age of 6 months, lesion development of both *Kras*^{G12D} and *P110α*^{H1047R} pancreata further advanced, while *Mek1DD* pancreata exhibited slightly less PanIN, but increasing ADM lesions. Hence, it can be assumed that the *Mek1DD* phenotype becomes regressive between three to six months. Moreover, end-point analysis revealed that *Mek1DD* mice do not develop PDAC. Preliminary data indicates that they exhibit a mean survival of approx. 498 days and therefore live longer than *Kras*^{G12D} and *P110α*^{H1047R} mice. *Mek1DD* mice develop ADM, PanIN lesions of all grades as well as IPMNs, but they rather have to be sacrificed due to the development of large cysts at this age and the resulting high overall suffering. In contrast, both *Kras*^{G12D} and *P110α*^{H1047R} mice do show PDAC development (Hingorani *et al.,* 2003; Eser *et al.,* 2013).

The incapability of *Mek1DD* to drive PDAC development was reversed by additional expression of mutated P53. *Mek1DD;P53^{R172H}* mice exhibit the same lesions observed in *Mek1DD* pancreata, but additionally develop PDAC. However, this process is slower than in an oncogenic KRAS expressing environment, since *Mek1DD;P53^{R172H}* mice exhibit a mean survival of approx. 290 days, while *Kras^{G12D};P53^{R172H}* mice have been reported to survive approx. 150 days (Hingorani *et al.,* 2005).

These data suggest that enhanced MEK – ERK signalling alone is not sufficient for PDAC development, though common precursor lesions develop early. ADM and PanIN lesions arise, but do not show progression after three to six months. The final transformation step towards tumour formation requires additional factors such as mutated P53. *Kras^{G12D}* mice do develop PDAC, but several other pathways aside the MEK – ERK signalling cascade are activated within this model. For example, KRAS regulates the PI3K – AKT – mTOR pathway, and AKT can be found highly active in pancreatic cancer (Maitra and Hruban, 2008). Recently, it has been shown that sustained PI3K signalling leads to ADM, PanIN and PDAC development; moreover, disruption of PI3K signalling via PDK1 ablation leads to blockage of PDAC development in *Kras^{G12D}* mice (Eser *et al.,* 2013). It can be assumed that MEK - ERK signalling strongly fosters initiation of metaplastic and neoplastic lesions, whereas PI3K signalling is essential for progression to PDAC. However, the MEK – ERK cascade and the PI3K – AKT pathway cannot be considered as completely independent, since many interdependencies exist (Steelman *et al.,* 2011; Niba *et al.,* 2013). Consequently, *Kras^{G12D}*, *Mek1DD* and *P110α^{H1047R}* mice were shown to highly express both active ERK and AKT without any obvious differences in expression strength between these genotypes, indicating that another target of PI3K might be the key factor driving PDAC. One putative candidate is RAC1, which is downstream of PI3K (Wertheimer *et al.,* 2012) and commonly overexpressed in pancreatic cancer (Karlsson *et al.,* 2009). Further, ablation of *Rac1* leads to impaired PDAC development via inhibition of cellular reorganization processes (Heid *et al.,* 2011). Differences in RAC1 activity in *Mek1DD* and *P110α^{H1047R}* pancreata should therefore be elucidated during future studies.

4.2 EGR1 EXHIBITS TUMOUR SUPPRESSOR QUALITIES IN THE PANCREAS

4.2.1 EGR1 is elevated during early metaplastic events

The transcription factor EGR1 has been investigated in many cell types and tissues, revealing a variety of different functions (Gitenay and Baron, 2009). In many reports, EGR1 plays a major role during cancer initiation and progression. The mode of influencing the course of this disease ranges from tumour suppression to oncogenic actions (Abdulkadir *et al.,* 2001; Krones-Herzig *et al.,* 2005; Gibbs *et al.,* 2008; Sun *et al.,* 2013). No studies have been reported concerning the role of EGR1 within the pancreas so far. However, prominent downstream targets of EGR1 are known to be PDAC related, including P53 and PTEN (Gitenay and Baron, 2009). In addition, EGR1 itself has been reported to be directly regulated by ELK1 and is therefore a target of the MEK – ERK signalling cascade (Khachigian, 2006; Hasan and Schafer, 2008). Given the recently reported need of MEK – ERK activity for initial transdifferentiation processes as well as the strong phenotype observed in *Mek1DD* mice, EGR1 is a potential key player in PDAC precursor development.

The regulation of EGR1 was investigated with the use of various mouse models. Within *Tgfα* mice, based on TGFα overexpression and therefore sustained EGFR signalling (Sandgren *et al.,* 1990), EGR1 was found highly expressed in most acinar and metaplastic cells. Additional *Egfr* ablation led to a complete blockage of EGR1 expression within these pancreata, except for infiltrating fibroblasts, where *Egfr* ablation did not take place and which were reported to strongly express EGR1 before (Bhattacharyya *et al.,* 2008). Hence, these findings represented a first hint that EGR1 is regulated via the EGFR – KRAS – MEK pathway in the pancreas. This theory was further supported by the fact that oncogenic KRAS was also sufficient for induction of EGR1 expression. $Kras^{G12D};Egfr^{\Delta Panc}$ pancreata were EGR1 negative, due to the fact that EGFR is essential for $KRAS^{G12D}$ driven MEK activation (Ardito *et al.,* 2012). Results obtained in *Mek1DD* mice, which exhibit sustained MEK - ERK signalling, ultimately verified this mode of regulation. Here, EGR1 was found highly expressed within pancreatic lesions, and expression could not be impaired by an additional *Egfr* ablation.

The functional role of EGR1 was first investigated via expression analysis. It was revealed that the quantity of normal acinar cells expressing EGR1 depended on the model the protein was investigated in. Acinar cells were almost completely negative in pancreata of $Kras^{G12D}$

mice, but frequently positive in *Mek1DD* samples. Given the early and strong development of ADM in *Mek1DD* pancreata, EGR1 positive acini could represent cells undergoing initial steps towards ductal reprogramming. This conclusion is supported by the fact that most acini of *Tgfα* pancreata, which exhibited already high quantities of ADM, were also strongly EGR1 positive. However, in all genotypes analysed EGR1 was mainly located within developed ADM, acinar cells adjacent to a newly formed ADM or acinar cells with beginning metaplasia. This was also the case for human samples, where positive cells were detected in ADM, additionally underlining a potential role of EGR1 in preneoplastic lesions. Furthermore, these samples exhibited positive cells in areas with fully transformed PDAC. In mice, not all developed ADM were positive, though, which contributes to the theory that EGR1 becomes upregulated only in an early, much defined point in time of ADM development. During cerulein induced pancreatitis, a widely used model for early metaplastic transition, EGR1 was already found highly upregulated one hour after the first injection, further highlighting the importance of EGR1 during early metaplastic events.

4.2.2 *Egr1*^{KO} drives PDAC in *Kras*^{G12D} mice by increasing cellular plasticity

The functional role of EGR1 during PDAC initiation and progression was further investigated in *Egr1* full knockout mice. *In vivo*, no effects on pancreatic development were observed. During e*x vivo* studies, *Egr1*^{KO} samples exhibited virtually no transdifferentiation and were almost completely insensitive to EGF treatment, whereas wild type acini transdifferentiated towards a duct-like phenotype. These findings might be a result of two mechanisms: first, *Egr1*^{KO} acinar explants expressed high amounts of AMY and CK19 simultaneously at day 5, since expression of CK19 had increased over time and with EGF treatment, while AMY expression remained at relatively high levels. Therefore, ductal and acinar markers were coexpressed within these explants, indicating an incomplete transdifferentiation initiation. Second, EGF is a ligand of EGFR and therefore induces EGFR dependent downstream signalling, resulting in transdifferentiation processes. Consequently, *Egfr* ablation blocks transdifferentiation of *ex vivo* acinar explants (Avraham and Yarden, 2011; Ardito *et al.,* 2012). Given the fact that it has been reported that EGR1 inhibition results in EGFR downregulation in colon cancer cell lines (Chen *et al.,* 2006a), it is highly likely that a reduction of EGFR expression, caused by absence of EGR1, ultimately leads to reduced transdifferentiation as well as to EGF insensitiveness. This theory is supported by the fact that EGFR is directly regulated by EGR1 within the pancreas, as it was shown during a ChIP

assay. Moreover, it was shown that EGFR expression was elevated in *Tgfα* pancreata, whereas an additional *Egr1* ablation was sufficient to completely reverse this effect and restore EGFR expression to wild type levels. Indeed, this downregulation of EGFR was not sufficient to rescue the *Tgfα* phenotype *in vivo*, though the slightly but significantly reduced pancreas to body weight index of *Tgfα;Egr1*^{KO} mice represents an evidence that the *Egr1* knockout runs contrary to the *Tgfα* phenotype. The finding that an equal quantity of ADM was present in *Tgfα* and *Tgfα;Egr1*^{KO} pancreata whereas EGF treated *Egr1*^{KO} acini do only exhibit minimal transdifferentiation can be explained by the fact that *Tgfα;Egr1*^{KO} pancreata exhibit wild type levels of EGFR, which is therefore still present and sustained EGFR signalling, even if reduced, can take place. *Egr1*^{KO} acini on the other side are not under the strong, EGFR promoting effects of TGFα overexpression prior to isolation. It can therefore be assumed that *Egr1*^{KO} acini exhibit an EGFR expression that is below wild type levels.

Under oncogenic KRAS expressing conditions, contrary results were obtained. *Kras*^{G12D}*;Egr1*^{KO} mice exhibited an accelerated development of preneoplastic lesions *in vivo* and *ex vivo*, accompanied by an increased pancreas to body weight index and early PDAC formation *in vivo*. Hence, it can be assumed that an additional activating factor accompanying an *Egr1* knockout is needed, which then ultimately drives PDAC initiation. EGR1 therefore exhibits typical characteristics of a tumour suppressor such as p53 or p16, which likewise only exhibit tumour enhancing effects if knocked out in an oncogene expressing environment (Bardeesy *et al.,* 2006). In *Tgfα;Egr1*^{KO} pancreata, it is likely that two effects antagonise each other: the ADM inhibiting effect caused by reduced EGFR expression, and loss of the tumour suppressor function conducted by EGR1. In *Kras*^{G12D}*;Egr1*^{KO} pancreata, it can be supposed that reduced EGFR levels do not exert strong tumour inhibiting effects. On the one hand, activating KRAS^{G12D} still leads to sustained signalling of other pathways, for example the AKT – mTOR pathway, even in complete absence of EGFR. On the other hand, *Egfr* ablation cannot completely block tumour formation caused by loss of other tumour suppressors, as it was shown in *Kras*^{G12D}*;P53*^{KO}*;Egfr*$^{\Delta Panc}$ mice, for example (Ardito *et al.,* 2012). The remaining question, on which mechanism the tumour suppressor function of EGR1 is based on, will be addressed in the following.

EGR1 has been extensively studied in the brain, one of the rare organs EGR1 can be found highly expressed in under normal conditions (Beckmann *et al.,* 1997). Here, it has been shown that EGR1 plays a critical role for a central principle of learning, neuronal plasticity. Hence, much has been published regarding this topic, reporting EGR1 as a cell type specific marker of plasticity (Ponomarev *et al.,* 2006; Lam *et al.,* 2009), regulating plasticity

associated downstream targets, thus stabilising neuronal activity (Li *et al.,* 2005). Consequently, *Egr1* ablation resulted in impaired long-term memory (Jones *et al.,* 2001). Within the pancreas, cellular plasticity has been described as strongly PDAC enhancing if activating factors such as $Kras^{G12D}$ are simultaneously expressed (Morris *et al.,* 2010). Increased cellular plasticity is further essential during tissue injury and wound healing and occurs during induced pancreatitis, for example (Fendrich *et al.,* 2008). Not only has it been reported that EGR1 is highly expressed in sites of injury where it exerts central functions during matrix remodelling and wound healing (Wu *et al.,* 2009; Dussmann *et al.,* 2011), but also has it been shown during this work that EGR1 is immediately and highly upregulated during induced acute pancreatitis. Further, it has been described elsewhere that the state of cellular plasticity and wound healing after cerulein induced injury is accompanied by coexpression of AMY and CK19 in acinar cells, followed by vanishing CK19 expression as regeneration proceeds (Fukuda *et al.,* 2012). During this work, AMY and CK19 coexpression has been observed repeatedly in the context of *Egr1* ablation: Within *ex vivo* acinar explants of $Egr1^{KO}$ pancreata, especially at day 5 without EGF treatment, within *ex vivo* acinar explants of $Kras^{G12D};Egr1^{KO}$ pancreata at day 1 as well as in acinar tissue of 4 weeks old $Kras^{G12D};Egr1^{KO}$ mice. This coeval expression of acinar and ductal markers indicates an intermediate state of these cells, though these still exhibit an acinar morphology. In addition, it has been shown during a ChIP assay that EGR1 directly regulates CK19 within the pancreas. The fact that EGR1 expression was predominantly found highly expressed in cells undergoing early stages of metaplasia further supports the theory that EGR1 is closely related to plasticity and cellular remodelling.

Taken together, there is strong evidence that EGR1 regulates cellular plasticity in the pancreas, most likely via additional factors, but also via direct regulation of the ductal marker CK19. Consequently, *Egr1* ablation leads to a dysregulation of this process, resulting in coexpression of acinar and ductal markers, thus driving these cells to an intermediate state with sustained high plasticity. As it has been reported for induced acute pancreatitis alike, this increased plasticity results in both enhanced tumour formation and progression in an activating factor expressing environment.

4.3 KLF5 IS ASSOCIATED WITH DUCTAL REPROGRAMMING

KLF5 is a DNA binding transcription factor and has been reported to be regulated via the MEK - ERK pathway (Nandan *et al.,* 2004; Yang *et al.,* 2007). Further, KLF5 promotes proliferation, transformation and is closely related to cancer initiation and progression (Chen *et al.,* 2006b; Dong and Chen, 2009). Consequently, a heterozygous knockout of *Klf5* was shown to be sufficient for reduction of tumour burden in colon cancer models (Nandan *et al.,* 2010). Since *Klf5* has been shown to be directly regulated via EGR1 in other murine cells and tissues (Kawai-Kowase *et al.,* 1999; Krones-Herzig *et al.,* 2003), it represents a potential mediator between EGR1 and its tumour suppressing effects within the pancreas.

The regulation of *Klf5* within the pancreas was investigated by analysing its expression in several mouse models. KLF5 was found highly upregulated in 4 weeks old *Tgfα* mice and in $Kras^{G12D}$ pancreata of the same age. However, additional *Egfr* ablation blocked KLF5 expression in $Kras^{G12D}$ mice. Given that EGFR has been reported to be essential for $Kras^{G12D}$ driven MEK activation (Ardito *et al.,* 2012), these results suggest that *Klf5* is a target of the MEK - ERK pathway. These findings were further supported by the fact that *Mek1DD* pancreata also exhibited strong KLF5 expression, which was not impaired by additional *Egfr* ablation. However, contrary to previous publications, KLF5 regulation was found to be EGR1 independent in the pancreas. *Egr1* ablation did neither change KLF5 expression in *Tgfα*, nor in $Kras^{G12D}$ mice. Further, induced acute pancreatitis in $Egr1^{KO}$ mice led to increased KLF5 levels, as it was the case in wild type controls alike.

KLF5 was found highly expressed in both ADM and PanIN lesions of *Tgfα*, $Kras^{G12D}$ and *Mek1DD* pancreata. Furthermore, it was detected in normal pancreatic ducts of all genotypes investigated including wild type controls. In addition, overexpression of KLF5 in acinar 266-6 cells led to an induction of the ductal marker CK19, strongly suggesting a role in regulation of ductal fate. Since KLF5 expression was elevated in most nuclei of normal acinar tissue of *Tgfα*, $Kras^{G12D}$ and *Mek1DD* pancreata, but not as strongly expressed as in lesions and ducts, it is likely that KLF5 expression increases as differentiation towards a ductal phenotype advances. If and how KLF5 actively participates in ductal transdifferentiation processes remains to be investigated in future studies.

4.4 CONCLUSION

During this work, the impact of MEK – ERK signalling in PDAC development was further elucidated. Not only was the importance of MEK activity during formation of PDAC progenitor lesions highlighted, but also were limitations identified. The incapacity of sustained MEK - ERK signalling to drive progenitor lesions towards PDAC formation shows the complexity of molecular crosstalk during tumour development. One putative candidate for pathways driving PDAC surely represents the PI3K - AKT - mTOR pathway. But, given that several publications have characterised intense crosstalk between these two pathways, further effort will be needed in order to dissect these interactions.

Downstream the MEK - ERK pathway, the transcription factor EGR1 was identified as a putative novel tumour suppressor within the pancreas. Though results obtained with the use of several mouse models were not uniform, it became clear that an *Egr1* knockout in a $Kras^{G12D}$ expressing environment results in highly enhanced tumour formation. The hypothesis that increased cellular plasticity triggers this enhancement may not be the only, but a most likely mechanism. Further studies will have to shed light on additional effects of EGR1. However, the investigations performed during this work have made it clear that EGR1 is a key player during PDAC initiation and progression.

Though KLF5 regulation was shown to be most likely independent of EGR1 in the pancreas, KLF5 was confirmed to be another participant of the MEK - ERK pathway. The exact function KLF5 carries out has still to be characterised, but the data obtained already allows the conclusion that it is associated with lesion development and might turn out as an important PDAC affecting factor.

Taken as a whole, the present study investigated three important factors, each participating in the MEK - ERK pathway at a particular level. Given the high impact on PDAC initiation and progression these proteins have, each by the use of most diverse mechanisms, gives an impression about the complexity of all pathways orchestrating together in cellular regulation.

5 OUTLOOK

Signalling differences between *Mek1DD* and *P110α*^{H1047R} mice will be further investigated during future studies. These will focus on RAC1, a potential key factor of tumour development. In a first step, RAC1 activity will be analysed in both *Mek1DD* and *P110α*^{H1047R} pancreata. Should RAC1 be found highly active in *P110α*^{H1047R}, but not in *Mek1DD* samples, *P110α*^{H1047R}*;Rac1*$^{\Delta Panc}$ mice will be bred in a second step, which should clarify if PDAC development in *P110α*^{H1047R} mice is *Rac1* dependent. Likewise, *Mek1DD;Rac1*^{G12V} mice will be analysed in order to investigate if dominant active RAC1 is sufficient to drive PDAC formation in a *Mek1DD* expressing environment.

The exact mechanisms enhancing tumour formation in *Kras*^{G12D}*;Egr1*^{KO} mice will be further studied. The importance of cellular plasticity during this process will be verified by analysing additional plasticity related factors in both *Kras*^{G12D} and *Kras*^{G12D}*;Egr1*^{KO} mice. Since regulation of cellular plasticity is critical during tissue regeneration and repair, it will be of particular interest to investigate molecular and histological differences between wild type and *Egr1*^{KO} mice during long term induced acute pancreatitis.

Future studies concerning KLF5 will focus on its functional role during PDAC development. Overexpression of KLF5 in *ex vivo* acinar explants could show if the protein actively participates in ductal differentiation. Investigation of models holding a pancreas specific deletion of KLF5 could ultimately clarify its impact during malignant transformation *in vivo*.

6 LITERATURE

Abdulkadir, S.A.; Qu, Z.; Garabedian, E.; Song, S. K.; Peters, T. J.; Svaren, J.; Carbone, J. M.; Naughton, C. K.; Catalona, W. J.; Ackerman, J. J.; Gordon, J. I.; Humphrey, P. A.; Milbrandt, J.*, et al. (*2001). Impaired prostate tumorigenesis in Egr1-deficient mice. Nat. Med. *7*, 101-107.

Abremski, K.; Wierzbicki, A.; Frommer, B.; Hoess, R. H. (1986). Bacteriophage P1 Cre-loxP site-specific recombination. Site-specific DNA topoisomerase activity of the Cre recombination protein. J. Biol. Chem. *261*, 391-396.

Adam, P.J.; Regan, C. P.; Hautmann, M. B.; Owens, G. K. (2000). Positive- and negative-acting Kruppel-like transcription factors bind a transforming growth factor beta control element required for expression of the smooth muscle cell differentiation marker SM22alpha in vivo. J. Biol. Chem. *275*, 37798-37806.

Adler, G.; Hupp, T.; Kern, H. F. (1979). Course and spontaneous regression of acute pancreatitis in the rat. Virchows Arch A Pathol Anat Histol *382*, 31-47.

Aichler, M.; Seiler, C.; Tost, M.; Siveke, J.; Mazur, P. K.; Da Silva-Buttkus, P.; Bartsch, D. K.; Langer, P.; Chiblak, S.; Dürr, A.; Höfler, H.; Klöppel, G.; Müller-Decker, K.; Brielmeier, M.; Esposito, I.*, et al. (*2012). Origin of pancreatic ductal adenocarcinoma from atypical flat lesions: a comparative study in transgenic mice and human tissues. J. Pathol. *226*, 723-734.

Albores-Saavedra, J.; Weimersheimer-Sandoval, M.; Chable-Montero, F.; Montante-Montes de Oca, Daniel; Hruban, R. H.; Henson, D. E. (2008). The foamy variant of pancreatic intraepithelial neoplasia. Ann Diagn Pathol *12*, 252-259.

Alessi, D.R.; Saito, Y.; Campbell, D. G.; Cohen, P.; Sithanandam, G.; Rapp, U.; Ashworth, A.; Marshall, C. J.; Cowley, S. (1994). Identification of the sites in MAP kinase kinase-1 phosphorylated by p74raf-1. EMBO J. *13*, 1610-1619.

Ardito, C.M.; Grüner, B. M.; Takeuchi, K. K.; Lubeseder-Martellato, C.; Teichmann, N.; Mazur, P. K.; DelGiorno, K. E.; Carpenter, E. S.; Halbrook, C. J.; Hall, J. C.; Pal, D.; Briel, T.; Herner, A.; Trajkovic-Arsic, M.; Sipos, B.*, et al. (*2012). EGF Receptor Is Required for KRAS-Induced Pancreatic Tumorigenesis. Cancer Cell *22*, 304-317.

Avraham, R.; Yarden, Y. (2011). Feedback regulation of EGFR signalling: decision making by early and delayed loops. Nat Rev Mol Cell Biol *12*, 104-117.

Bardeesy, N.; Aguirre, A. J.; Chu, G. C.; Cheng, K.-H.; Lopez, L. V.; Hezel, A. F.; Feng, B.; Brennan, C.; Weissleder, R.; Mahmood, U.; Hanahan, D.; Redston, M. S.; Chin, L.; DePinho, R. A.*, et al. (*2006). Both p16(Ink4a) and the p19(Arf)-p53 pathway constrain progression of pancreatic adenocarcinoma in the mouse. Proc. Natl. Acad. Sci. U.S.A. *103*, 5947-5952.

Barreto, S.; Thomas, T.; Mah, L. (2012). Systematic review of diet in the pathogenesis of acute pancreatitis: A tale of too much or too little? Saudi J Gastroenterol *18*, 310.

Beckmann, A.M.; Davidson, M. S.; Goodenough, S.; Wilce, P. A. (1997). Differential expression of Egr-1-like DNA-binding activities in the naive rat brain and after excitatory stimulation. J. Neurochem. *69*, 2227-2237.

Bhattacharyya, S.; Chen, S.-J.; Wu, M.; Warner-Blankenship, M.; Ning, H.; Lakos, G.; Mori, Y.; Chang, E.; Nihijima, C.; Takehara, K.; Feghali-Bostwick, C.; Varga, J.*, et al. (*2008). Smad-independent transforming growth factor-beta regulation of early growth response-1 and sustained expression in fibrosis: implications for scleroderma. Am. J. Pathol. *173*, 1085-1099.

Bhattacharyya, S.; Fang, F.; Tourtellotte, W.; Varga, J. (2013). Egr-1: new conductor for the tissue repair orchestra directs harmony (regeneration) or cacophony (fibrosis). J. Pathol. *229*, 286-297.

Bort, R.; Martinez-Barbera, J. P.; Beddington, Rosa S P; Zaret, K. S. (2004). Hex homeobox gene-dependent tissue positioning is required for organogenesis of the ventral pancreas. Development *131*, 797-806.

Campbell, N.A.; Reece, J. B. (2006). Biologie (München u.a: Pearson).

Carrière, C.; Young, A. L.; Gunn, J. R.; Longnecker, D. S.; Korc, M. (2009). Acute pancreatitis markedly accelerates pancreatic cancer progression in mice expressing oncogenic Kras. Biochem. Biophys. Res. Commun. *382*, 561-565.

Chen, A.; Xu, J.; Johnson, A. C. (2006a). Curcumin inhibits human colon cancer cell growth by suppressing gene expression of epidermal growth factor receptor through reducing the activity of the transcription factor Egr-1. Oncogene *25*, 278-287.

Chen, C.; Benjamin, M. S.; Sun, X.; Otto, K. B.; Guo, P.; Dong, X.-Y.; Bao, Y.; Zhou, Z.; Cheng, X.; Simons, J. W.; Dong, J.-T.*, et al. (*2006b). KLF5 promotes cell proliferation and tumorigenesis through gene regulation and the TSU-Pr1 human bladder cancer cell line. Int. J. Cancer *118*, 1346-1355.

Chen, C.; Sun, X.; Ran, Q.; Wilkinson, K. D.; Murphy, T. J.; Simons, J. W.; Dong, J.-T. (2005). Ubiquitin-proteasome degradation of KLF5 transcription factor in cancer and untransformed epithelial cells. Oncogene *24*, 3319-3327.

Collins, M.A.; Bednar, F.; Zhang, Y.; Brisset, J.-C.; Galbán, S.; Galbán, C. J.; Rakshit, S.; Flannagan, K. S.; Adsay, N. V.; Pasca di Magliano, Marina (2012). Oncogenic Kras is required for both the initiation and maintenance of pancreatic cancer in mice. J. Clin. Invest. *122*, 639-653.

Conkright, M.D.; Wani, M. A.; Anderson, K. P.; Lingrel, J. B. (1999). A gene encoding an intestinal-enriched member of the Krüppel-like factor family expressed in intestinal epithelial cells. Nucleic Acids Res. *27*, 1263-1270.

Derynck, R.; Roberts, A. B.; Winkler, M. E.; Chen, E. Y.; Goeddel, D. V. (1984). Human transforming growth factor-alpha: precursor structure and expression in E. coli. Cell *38*, 287-297.

Desai, B.M.; Oliver-Krasinski, J.; De Leon, Diva D; Farzad, C.; Hong, N.; Leach, S. D.; Stoffers, D. A. (2007). Preexisting pancreatic acinar cells contribute to acinar cell, but not islet beta cell, regeneration. J. Clin. Invest. *117*, 971-977.

Dong, J.-T.; Chen, C. (2009). Essential role of KLF5 transcription factor in cell proliferation and differentiation and its implications for human diseases. Cell. Mol. Life Sci. *66*, 2691-2706.

Downward, J. (2003). Targeting RAS signalling pathways in cancer therapy. Nat. Rev. Cancer *3*, 11-22.

Du, J.X.; Bialkowska, A. B.; McConnell, B. B.; Yang, V. W. (2008). SUMOylation regulates nuclear localization of Krüppel-like factor 5. J. Biol. Chem. *283*, 31991-32002.

Dussmann, P.; Pagel, J. I.; Vogel, S.; Magnusson, T.; Zimmermann, R.; Wagner, E.; Schaper, W.; Ogris, M.; Deindl, E. (2011). Live in vivo imaging of Egr-1 promoter activity during neonatal development, liver regeneration and wound healing. BMC Dev. Biol. *11*, 28.

Edlund, H. (2002). Pancreatic organogenesis--developmental mechanisms and implications for therapy. Nat. Rev. Genet. *3*, 524-532.

Ehrengruber, M.U.; Muhlebach, S. G.; Söhrman, S.; Leutenegger, C. M.; Lester, H. A.; Davidson, N. (2000). Modulation of early growth response (EGR) transcription factor-dependent gene expression by using recombinant adenovirus. Gene *258*, 63-69.

Eser, S.; Reiff, N.; Messer, M.; Seidler, B.; Gottschalk, K.; Dobler, M.; Hieber, M.; Arbeiter, A.; Klein, S.; Kong, B.; Michalski, C. W.; Schlitter, A. M.; Esposito, I.; Kind, A. J.; Rad, L.*, et al. (*2013). Selective requirement of PI3K/PDK1 signaling for Kras oncogene-driven pancreatic cell plasticity and cancer. Cancer Cell *23*, 406-420.

Everhart, J.; Wright, D. (1995). Diabetes mellitus as a risk factor for pancreatic cancer. A meta-analysis. JAMA *273*, 1605-1609.

Fendrich, V.; Esni, F.; Garay, Maria Veronica R; Feldmann, G.; Habbe, N.; Jensen, J. N.; Dor, Y.; Stoffers, D.; Jensen, J.; Leach, S. D.; Maitra, A.*, et al. (*2008). Hedgehog signaling is required for effective regeneration of exocrine pancreas. Gastroenterology *135*, 621-631.

Fjällskog, M.-L.H.; Lejonklou, M. H.; Oberg, K. E.; Eriksson, B. K.; Janson, E. T. (2003). Expression of molecular targets for tyrosine kinase receptor antagonists in malignant endocrine pancreatic tumors. Clin. Cancer Res. *9*, 1469-1473.

Flisikowska, T.; Kind, A.; Schnieke, A. (2013). The new pig on the block: modelling cancer in pigs. Transgenic Res. *22*, 673-680.

Fuchs, C.S.; Colditz, G. A.; Stampfer, M. J.; Giovannucci, E. L.; Hunter, D. J.; Rimm, E. B.; Willett, W. C.; Speizer, F. E. (1996). A prospective study of cigarette smoking and the risk of pancreatic cancer. Arch. Intern. Med. *156*, 2255-2260.

Fukuda, A.; Morris, J. P.; Hebrok, M. (2012). Bmi1 is required for regeneration of the exocrine pancreas in mice. Gastroenterology *143*, 821-31.e1-2.

Gapstur, S.M.; Gann, P. H.; Lowe, W.; Liu, K.; Colangelo, L.; Dyer, A. (2000). Abnormal glucose metabolism and pancreatic cancer mortality. JAMA *283*, 2552-2558.

Gibbs, J.D.; Liebermann, D. A.; Hoffman, B. (2008). Egr-1 abrogates the E2F-1 block in terminal myeloid differentiation and suppresses leukemia. Oncogene *27*, 98-106.

Gitenay, D.; Baron, V. T. (2009). Is EGR1 a potential target for prostate cancer therapy? Future Oncology *5*, 993-1003.

Grant, B.D.; Donaldson, J. G. (2009). Pathways and mechanisms of endocytic recycling. Nat. Rev. Mol. Cell Biol. *10*, 597-608.

Hadjantonakis, A.-K.; Pirity, M.; Nagy, A. (2008). Cre recombinase mediated alterations of the mouse genome using embryonic stem cells. Methods Mol. Biol. *461*, 111-132.

Han, W.; Lo, H.-W. (2012). Landscape of EGFR signaling network in human cancers: Biology and therapeutic response in relation to receptor subcellular locations. Cancer Letters *318*, 124-134.

Hanahan, D. (1983). Studies on transformation of Escherichia coli with plasmids. J. Mol. Biol. *166*, 557-580.

Hasan, R.N.; Schafer, A. I. (2008). Hemin upregulates Egr-1 expression in vascular smooth muscle cells via reactive oxygen species ERK-1/2-Elk-1 and NF-kappaB. Circ. Res. *102*, 42-50.

Hebrok, M.; Kim, S. K.; Melton, D. A. (1998). Notochord repression of endodermal Sonic hedgehog permits pancreas development. Genes Dev. *12*, 1705-1713.

Heid, I.; Lubeseder–Martellato, C.; Sipos, B.; Mazur, P. K.; Lesina, M.; Schmid, R. M.; Siveke, J. T. (2011). Early Requirement of Rac1 in a Mouse Model of Pancreatic Cancer. Gastroenterology *141*, 719-730.e7.

Hezel, A.F. (2006). Genetics and biology of pancreatic ductal adenocarcinoma. Genes & Development *20*, 1218-1249.

Hingorani, S.R.; Petricoin, E. F.; Maitra, A.; Rajapakse, V.; King, C.; Jacobetz, M. A.; Ross, S.; Conrads, T. P.; Veenstra, T. D.; Hitt, B. A.; Kawaguchi, Y.; Johann, D.; Liotta, L. A.; Crawford, H. C.; Putt, M. E.*, et al. (*2003). Preinvasive and invasive ductal pancreatic cancer and its early detection in the mouse. Cancer Cell *4*, 437-450.

Hingorani, S.R.; Wang, L.; Multani, A. S.; Combs, C.; Deramaudt, T. B.; Hruban, R. H.; Rustgi, A. K.; Chang, S.; Tuveson, D. A. (2005). Trp53R172H and KrasG12D cooperate to promote chromosomal instability and widely metastatic pancreatic ductal adenocarcinoma in mice. Cancer Cell *7*, 469-483.

Jackson, E.L.; Willis, N.; Mercer, K.; Bronson, R. T.; Crowley, D.; Montoya, R.; Jacks, T.; Tuveson, D. A. (2001). Analysis of lung tumor initiation and progression using conditional expression of oncogenic K-ras. Genes Dev. *15*, 3243-3248.

Jensen, J.N.; Cameron, E.; Garay, Maria Veronica R; Starkey, T. W.; Gianani, R.; Jensen, J. (2005). Recapitulation of elements of embryonic development in adult mouse pancreatic regeneration. Gastroenterology *128*, 728-741.

Jones, M.W.; Errington, M. L.; French, P. J.; Fine, A.; Bliss, T. V.; Garel, S.; Charnay, P.; Bozon, B.; Laroche, S.; Davis, S. (2001). A requirement for the immediate early gene Zif268 in the expression of late LTP and long-term memories. Nat. Neurosci. *4*, 289-296.

Karlsson, R.; Pedersen, E. D.; Wang, Z.; Brakebusch, C. (2009). Rho GTPase function in tumorigenesis. Biochim. Biophys. Acta *1796*, 91-98.

Karreth, F.A.; Tuveson, D. A. (2009). Modelling oncogenic Ras/Raf signalling in the mouse. Current Opinion in Genetics & Development *19*, 4-11.

Kawaguchi, Y.; Cooper, B.; Gannon, M.; Ray, M.; MacDonald, R. J.; Wright, C. V. (2002). The role of the transcriptional regulator Ptf1a in converting intestinal to pancreatic progenitors. Nat. Genet. *32*, 128-134.

Kawai-Kowase, K.; Kurabayashi, M.; Hoshino, Y.; Ohyama, Y.; Nagai, R. (1999). Transcriptional activation of the zinc finger transcription factor BTEB2 gene by Egr-1 through mitogen-activated protein kinase pathways in vascular smooth muscle cells. Circ. Res. *85*, 787-795.

Kedia, P.; Gaidhane, M.; Kahaleh, M. (2013). Technical Advances in Endoscopic Ultrasound (EUS)-Guided Tissue Acquisition for Pancreatic Cancers: How Can We Get the Best Results with EUS-Guided Fine Needle Aspiration? Clin Endosc *46*, 552-562.

Khachigian, L.M. (2006). Early growth response-1 in cardiovascular pathobiology. Circ. Res. *98*, 186-191.

Koera, K.; Nakamura, K.; Nakao, K.; Miyoshi, J.; Toyoshima, K.; Hatta, T.; Otani, H.; Aiba, A.; Katsuki, M. (1997). K-ras is essential for the development of the mouse embryo. Oncogene *15*, 1151-1159.

Kopp, J.L.; Dubois, C. L.; Hao, E.; Thorel, F.; Herrera, P. L.; Sander, M. (2011). Progenitor cell domains in the developing and adult pancreas. cc *10*, 1921-1927.

Kota, S.; Krishna, S.; Lakhtakia, S.; Modi, K. (2013). Metabolic pancreatitis: Etiopathogenesis and management. Indian J Endocr Metab *17*, 799.

Krones-Herzig, A.; Adamson, E.; Mercola, D. (2003). Early growth response 1 protein, an upstream gatekeeper of the p53 tumor suppressor, controls replicative senescence. Proc. Natl. Acad. Sci. U.S.A. *100*, 3233-3238.

Krones-Herzig, A.; Mittal, S.; Yule, K.; Liang, H.; English, C.; Urcis, R.; Soni, T.; Adamson, E. D.; Mercola, D. (2005). Early growth response 1 acts as a tumor suppressor in vivo and in vitro via regulation of p53. Cancer Res. *65*, 5133-5143.

Kubo, A.; Shinozaki, K.; Shannon, J. M.; Kouskoff, V.; Kennedy, M.; Woo, S.; Fehling, H. J.; Keller, G. (2004). Development of definitive endoderm from embryonic stem cells in culture. Development *131*, 1651-1662.

Lam, B.; Zhang, W.; Enticknap, N.; Haggis, E.; Cader, M. Z.; Chawla, S. (2009). Inverse regulation of plasticity-related immediate early genes by calcineurin in hippocampal neurons. J. Biol. Chem. *284*, 12562-12571.

Larusch, J.; Whitcomb, D. C. (2012). Genetics of pancreatitis with a focus on the pancreatic ducts. Minerva Gastroenterol Dietol *58*, 299-308.

Lee, C.G.; Cho, S. J.; Kang, M. J.; Chapoval, S. P.; Lee, P. J.; Noble, P. W.; Yehualaeshet, T.; Lu, B.; Flavell, R. A.; Milbrandt, J.; Homer, R. J.; Elias, J. A.*, et al. (*2004). Early growth response gene 1-mediated apoptosis is essential for transforming growth factor beta1-induced pulmonary fibrosis. J. Exp. Med. *200*, 377-389.

Lee, S.L.; Tourtellotte, L. C.; Wesselschmidt, R. L.; Milbrandt, J. (1995). Growth and differentiation proceeds normally in cells deficient in the immediate early gene NGFI-A. J. Biol. Chem. *270*, 9971-9977.

Li, L.; Carter, J.; Gao, X.; Whitehead, J.; Tourtellotte, W. G. (2005). The neuroplasticity-associated arc gene is a direct transcriptional target of early growth response (Egr) transcription factors. Mol. Cell. Biol. *25*, 10286-10300.

Liu, C.; Rangnekar, V. M.; Adamson, E.; Mercola, D. (1998). Suppression of growth and transformation and induction of apoptosis by EGR-1. Cancer Gene Ther. *5*, 3-28.

Lo, H.-W.; Hsu, S.-C.; Ali-Seyed, M.; Gunduz, M.; Xia, W.; Wei, Y.; Bartholomeusz, G.; Shih, J.-Y.; Hung, M.-C. (2005). Nuclear interaction of EGFR and STAT3 in the activation of the iNOS/NO pathway. Cancer Cell *7*, 575-589.

Logsdon, C.D.; Ji, B. (2009). Ras Activity in Acinar Cells Links Chronic Pancreatitis and Pancreatic Cancer. Clinical Gastroenterology and Hepatology *7*, S40.

Löhr, M.; Klöppel, G.; Maisonneuve, P.; Lowenfels, A. B.; Lüttges, J. (2005). Frequency of K-ras mutations in pancreatic intraductal neoplasias associated with pancreatic ductal adenocarcinoma and chronic pancreatitis: a meta-analysis. Neoplasia *7*, 17-23.

Luria, S.E.; Burrous, J. W. (1957). Hybridization between Escherichia coli and Shigella. J. Bacteriol. *74*, 461-476.

Maitra, A.; Hruban, R. H. (2008). Pancreatic Cancer. Annu. Rev. Pathol. Mech. Dis. *3*, 157-188.

McConnell, B.B.; Ghaleb, A. M.; Nandan, M. O.; Yang, V. W. (2007). The diverse functions of Krüppel-like factors 4 and 5 in epithelial biology and pathobiology. Bioessays *29*, 549-557.

McCracken, K.W.; Wells, J. M. (2012). Molecular pathways controlling pancreas induction. Seminars in Cell & Developmental Biology *23*, 656-662.

McCubrey, J.A.; Steelman, L. S.; Chappell, W. H.; Abrams, S. L.; Wong, E. W.; Chang, F.; Lehmann, B.; Terrian, D. M.; Milella, M.; Tafuri, A.; Stivala, F.; Libra, M.; Basecke, J.; Evangelisti, C.; Martelli, A. M.*, et al. (*2007). Roles of the Raf/MEK/ERK pathway in cell growth, malignant transformation and drug resistance. Biochimica et Biophysica Acta (BBA) - Molecular Cell Research *1773*, 1263-1284.

Means, A.L. (2005). Pancreatic epithelial plasticity mediated by acinar cell transdifferentiation and generation of nestin-positive intermediates. Development *132*, 3767-3776.

Means, A.L.; Ray, K. C.; Singh, A. B.; Washington, M. K.; Whitehead, R. H.; Harris, R. C.; Wright, Christopher V E; Coffey, R. J.; Leach, S. D. (2003). Overexpression of heparin-binding EGF-like growth factor in mouse pancreas results in fibrosis and epithelial metaplasia. Gastroenterology *124*, 1020-1036.

Mfopou, J.K.; Groote, V. de; Xu, X.; Heimberg, H.; Bouwens, L. (2007). Sonic Hedgehog and Other Soluble Factors from Differentiating Embryoid Bodies Inhibit Pancreas Development. Stem Cells *25*, 1156-1165.

Michaud, D.S.; Giovannucci, E.; Willett, W. C.; Colditz, G. A.; Fuchs, C. S. (2001). Coffee and alcohol consumption and the risk of pancreatic cancer in two prospective United States cohorts. Cancer Epidemiol. Biomarkers Prev. *10*, 429-437.

Midgley, V.C.; Khachigian, L. M. (2004). Fibroblast growth factor-2 induction of platelet-derived growth factor-C chain transcription in vascular smooth muscle cells is ERK-dependent but not JNK-dependent and mediated by Egr-1. J. Biol. Chem. *279*, 40289-40295.

Miettinen, H.M.; Huuskonen, H.; Partanen, A.-M.; Miettinen, P.; Tuomisto, J. T.; Pohjanvirta, R.; Tuomisto, J. (2004). Effects of epidermal growth factor receptor deficiency and 2,3,7,8-tetrachlorodibenzo-p-dioxin on fetal development in mice. Toxicol. Lett. *150*, 285-291.

Milbrandt, J. (1987). A nerve growth factor-induced gene encodes a possible transcriptional regulatory factor. Science *238*, 797-799.

Miller, J.H. (1972). Experiments in Molecular Genetics. Cold Spring Harbour Laboratory Press.

Morris, J.P.; Cano, D. A.; Sekine, S.; Wang, S. C.; Hebrok, M. (2010). β-catenin blocks Kras-dependent reprogramming of acini into pancreatic cancer precursor lesions in mice. J. Clin. Invest. *120*, 508-520.

Mulkeen, A.-L.; Yoo, P.-S.; Cha, C. (2006). Less common neoplasms of the pancreas. World J. Gastroenterol. *12*, 3180-3185.

Myung, E.; Park, Y.-L.; Kim, N.; Chung, C.-Y.; Park, H.-B.; Park, H.-C.; Myung, D.-S.; Kim, J.-S.; Cho, S.-B.; Lee, W.-S.; Joo, Y.-E.*, et al. (*2013). Expression of early growth response-1 in human gastric cancer and its relationship with tumor cell behaviors and prognosis. Pathol. Res. Pract. *209*, 692-699.

Nakhai, H.; Sel, S.; Favor, J.; Mendoza-Torres, L.; Paulsen, F.; Duncker, Gernot I W; Schmid, R. M. (2007). Ptf1a is essential for the differentiation of GABAergic and glycinergic amacrine cells and horizontal cells in the mouse retina. Development *134*, 1151-1160.

Nandan, M.O.; Ghaleb, A. M.; McConnell, B. B.; Patel, N. V.; Robine, S.; Yang, V. W. (2010). Krüppel-like factor 5 is a crucial mediator of intestinal tumorigenesis in mice harboring combined ApcMin and KRASV12 mutations. Mol. Cancer *9*, 63.

Nandan, M.O.; McConnell, B. B.; Ghaleb, A. M.; Bialkowska, A. B.; Sheng, H.; Shao, J.; Babbin, B. A.; Robine, S.; Yang, V. W. (2008). Krüppel-like factor 5 mediates cellular transformation during oncogenic KRAS-induced intestinal tumorigenesis. Gastroenterology *134*, 120-130.

Nandan, M.O.; Yoon, H. S.; Zhao, W.; Ouko, L. A.; Chanchevalap, S.; Yang, V. W. (2004). Krüppel-like factor 5 mediates the transforming activity of oncogenic H-Ras. Oncogene *23*, 3404-3413.

Natarajan, A.; Wagner, B.; Sibilia, M. (2007). The EGF receptor is required for efficient liver regeneration. Proc. Natl. Acad. Sci. U.S.A. *104*, 17081-17086.

Navolanic, P.M.; Steelman, L. S.; McCubrey, J. A. (2003). EGFR family signaling and its association with breast cancer development and resistance to chemotherapy (Review). Int. J. Oncol. *22*, 237-252.

Niba, E.; Nagaya, H.; Kanno, T.; Tsuchiya, A.; Gotoh, A.; Tabata, C.; Kuribayashi, K.; Nakano, T.; Nishizaki, T. (2013). Crosstalk between PI3 Kinase/PDK1/Akt/Rac1 and Ras/Raf/MEK/ERK Pathways Downstream PDGF Receptor. Cell Physiol Biochem *31*, 905-913.

Ohnishi, S.; Laub, F.; Matsumoto, N.; Asaka, M.; Ramirez, F.; Yoshida, T.; Terada, M. (2000). Developmental expression of the mouse gene coding for the Krüppel-like transcription factor KLF5. Dev. Dyn. *217*, 421-429.

Oishi, Y.; Manabe, I.; Tobe, K.; Tsushima, K.; Shindo, T.; Fujiu, K.; Nishimura, G.; Maemura, K.; Yamauchi, T.; Kubota, N.; Suzuki, R.; Kitamura, T.; Akira, S.; Kadowaki, T.; Nagai, R.*, et al. (*2005). Krüppel-like transcription factor KLF5 is a key regulator of adipocyte differentiation. Cell Metab. *1*, 27-39.

Olive, K.P.; Tuveson, D. A.; Ruhe, Z. C.; Yin, B.; Willis, N. A.; Bronson, R. T.; Crowley, D.; Jacks, T. (2004). Mutant p53 gain of function in two mouse models of Li-Fraumeni syndrome. Cell *119*, 847-860.

Ornitz, D.M.; Palmiter, R. D.; Messing, A.; Hammer, R. E.; Pinkert, C. A.; Brinster, R. L. (1985). Elastase I promoter directs expression of human growth hormone and SV40 T antigen genes to pancreatic acinar cells in transgenic mice. Cold Spring Harb. Symp. Quant. Biol. *50*, 399-409.

Otsuki, M. (2013). Criteria for the diagnosis and severity stratification of acute pancreatitis. WJG *19*, 5798.

Paigen, B.; Morrow, A.; Brandon, C.; Mitchell, D.; Holmes, P. (1985). Variation in susceptibility to atherosclerosis among inbred strains of mice. Atherosclerosis *57*, 65-73.

Pan, F.C.; Wright, C. (2011). Pancreas organogenesis: From bud to plexus to gland. Dev. Dyn. *240*, 530-565.

Ponomarev, I.; Maiya, R.; Harnett, M. T.; Schafer, G. L.; Ryabinin, A. E.; Blednov, Y. A.; Morikawa, H.; Boehm, S. L.; Homanics, G. E.; Berman, A. E.; Berman, A.; Lodowski, K. H.; Bergeson, S. E.; Harris, R. A.*, et al. (*2006). Transcriptional signatures of cellular plasticity in mice lacking the alpha1 subunit of GABAA receptors. J. Neurosci. *26*, 5673-5683.

Prado, C.L.; Pugh-Bernard, A. E.; Elghazi, L.; Sosa-Pineda, B.; Sussel, L. (2004). Ghrelin cells replace insulin-producing beta cells in two mouse models of pancreas development. Proc. Natl. Acad. Sci. U.S.A. *101*, 2924-2929.

Rachagani, S.; Senapati, S.; Chakraborty, S.; Ponnusamy, M. P.; Kumar, S.; Smith, L. M.; Jain, M.; Batra, S. K. (2011). Activated KrasG12D is associated with invasion and metastasis of pancreatic cancer cells through inhibition of E-cadherin. Br J Cancer *104*, 1038-1048.

Reichert, M.; Rustgi, A. K. (2011). Pancreatic ductal cells in development, regeneration, and neoplasia. J. Clin. Invest. *121*, 4572-4578.

Rukstalis, J.M.; Habener, J. F. (2007). Snail2, a mediator of epithelial-mesenchymal transitions, expressed in progenitor cells of the developing endocrine pancreas. Gene Expr. Patterns *7*, 471-479.

Sadr-Azodi, O.; Andrén-Sandberg, Å.; Orsini, N.; Wolk, A. (2012). Cigarette smoking, smoking cessation and acute pancreatitis: a prospective population-based study. Gut *61*, 262-267.

Sambrook, J.; Russell, D. (1989). Molecular Cloning: A Laboratory Manual. Cold Spring Harbour Laboratory Press.

Sanada, Y.; Hirose, Y.; Osada, S.; Tanaka, Y.; Takahashi, T.; Yamaguchi, K.; Yoshida, K. (2010). Immunohistochemical study of claudin 18 involvement in intestinal differentiation during the progression of intraductal papillary mucinous neoplasm. Anticancer Res. *30*, 2995-3003.

Sandgren, E.P.; Luetteke, N. C.; Palmiter, R. D.; Brinster, R. L.; Lee, D. C. (1990). Overexpression of TGF alpha in transgenic mice: induction of epithelial hyperplasia, pancreatic metaplasia, and carcinoma of the breast. Cell *61*, 1121-1135.

Schoenberg, M.H.; Birk, D.; Beger, H. G. (1995). Oxidative stress in acute and chronic pancreatitis. Am. J. Clin. Nutr. *62*, 1306S-1314S.

Shen, M.M. (2007). Nodal signaling: developmental roles and regulation. Development *134*, 1023-1034.

Shields, J.M.; Christy, R. J.; Yang, V. W. (1996). Identification and characterization of a gene encoding a gut-enriched Krüppel-like factor expressed during growth arrest. J. Biol. Chem. *271*, 20009-20017.

Shindo, T.; Manabe, I.; Fukushima, Y.; Tobe, K.; Aizawa, K.; Miyamoto, S.; Kawai-Kowase, K.; Moriyama, N.; Imai, Y.; Kawakami, H.; Nishimatsu, H.; Ishikawa, T.; Suzuki, T.; Morita, H.; Maemura, K.*, et al. (*2002). Krüppel-like zinc-finger transcription factor KLF5/BTEB2 is a target for angiotensin II signaling and an essential regulator of cardiovascular remodeling. Nat. Med. *8*, 856-863.

Slack, J.M. (1995). Developmental biology of the pancreas. Development *121*, 1569-1580.

Sogawa, K.; Imataka, H.; Yamasaki, Y.; Kusume, H.; Abe, H.; Fujii-Kuriyama, Y. (1993). cDNA cloning and transcriptional properties of a novel GC box-binding protein, BTEB2. Nucleic Acids Res. *21*, 1527-1532.

Song, S.Y.; Gannon, M.; Washington, M. K.; Scoggins, C. R.; Meszoely, I. M.; Goldenring, J. R.; Marino, C. R.; Sandgren, E. P.; Coffey, R. J.; Wright, C. V.; Leach, S. D.*, et al. (*1999). Expansion of Pdx1-expressing pancreatic epithelium and islet neogenesis in transgenic mice overexpressing transforming growth factor alpha. Gastroenterology *117*, 1416-1426.

Sphyris, N.; Logsdon, C. D.; Harrison, D. J. (2005). Improved retention of zymogen granules in cultured murine pancreatic acinar cells and induction of acinar-ductal transdifferentiation in vitro. Pancreas *30*, 148-157.

Srinivasan, L.; Sasaki, Y.; Calado, D. P.; Zhang, B.; Paik, J. H.; DePinho, R. A.; Kutok, J. L.; Kearney, J. F.; Otipoby, K. L.; Rajewsky, K. (2009). PI3 kinase signals BCR-dependent mature B cell survival. Cell *139*, 573-586.

Steele, C.W.; Jamieson, N. B.; Evans, T R J; McKay, C. J.; Sansom, O. J.; Morton, J. P.; Carter, C. R. (2013). Exploiting inflammation for therapeutic gain in pancreatic cancer. Br J Cancer *108*, 997-1003.

Steelman, L.S.; Franklin, R. A.; Abrams, S. L.; Chappell, W.; Kempf, C. R.; Bäsecke, J.; Stivala, F.; Donia, M.; Fagone, P.; Nicoletti, F.; Libra, M.; Ruvolo, P.; Ruvolo, V.; Evangelisti, C.; Martelli, A. M.*, et al. (*2011). Roles of the Ras/Raf/MEK/ERK pathway in leukemia therapy. Leukemia *25*, 1080-1094.

Steelman, L.S.; Pohnert, S. C.; Shelton, J. G.; Franklin, R. A.; Bertrand, F. E.; McCubrey, J. A. (2004). JAK/STAT, Raf/MEK/ERK, PI3K/Akt and BCR-ABL in cell cycle progression and leukemogenesis. Leukemia *18*, 189-218.

Sternberg, N.; Hamilton, D. (1981). Bacteriophage P1 site-specific recombination. I. Recombination between loxP sites. J. Mol. Biol. *150*, 467-486.

Sun, R.; Chen, X.; Yang, V. W. (2001). Intestinal-enriched Krüppel-like factor (Krüppel-like factor 5) is a positive regulator of cellular proliferation. J. Biol. Chem. *276*, 6897-6900.

Sun, T.; Tian, H.; Feng, Y.-G.; Zhu, Y.-Q.; Zhang, W.-Q. (2013). Egr-1 promotes cell proliferation and invasion by increasing β-catenin expression in gastric cancer. Dig. Dis. Sci. *58*, 423-430.

Taneyhill, L.; Pennica, D. (2004). Identification of Wnt responsive genes using a murine mammary epithelial cell line model system. BMC Dev. Biol. *4*, 6.

Ulrich, A.B.; Schmied, B. M.; Standop, J.; Schneider, M. B.; Pour, P. M. (2002). Pancreatic cell lines: a review. Pancreas *24*, 111-120.

Untergasser, A.; Nijveen, H.; Rao, X.; Bisseling, T.; Geurts, R.; Leunissen, Jack A M (2007). Primer3Plus, an enhanced web interface to Primer3. Nucleic Acids Res. *35*, W71-4.

Van der Weyden, L.; Adams, D. J.; Bradley, A. (2002). Tools for targeted manipulation of the mouse genome. Physiol. Genomics *11*, 133-164.

Wagner, M.; Greten, F. R.; Weber, C. K.; Koschnick, S.; Mattfeldt, T.; Deppert, W.; Kern, H.; Adler, G.; Schmid, R. M. (2001). A murine tumor progression model for pancreatic cancer recapitulating the genetic alterations of the human disease. Genes Dev. *15*, 286-293.

Wang, G.-J. (2009). Acute pancreatitis: Etiology and common pathogenesis. WJG *15*, 1427.

Wang, S.-C.; Nakajima, Y.; Yu, Y.-L.; Xia, W.; Chen, C.-T.; Yang, C.-C.; McIntush, E. W.; Li, L.-Y.; Hawke, D. H.; Kobayashi, R.; Hung, M.-C.*, et al. (*2006). Tyrosine phosphorylation controls PCNA function through protein stability. Nat. Cell Biol. *8*, 1359-1368.

Warshaw, A.L.; Fernández-del Castillo, C. (1992). Pancreatic carcinoma. N. Engl. J. Med. *326*, 455-465.

Wells, J.M.; Melton, D. A. (2000). Early mouse endoderm is patterned by soluble factors from adjacent germ layers. Development *127*, 1563-1572.

Wertheimer, E.; Gutierrez-Uzquiza, A.; Rosemblit, C.; Lopez-Haber, C.; Sosa, M. S.; Kazanietz, M. G. (2012). Rac signaling in breast cancer: a tale of GEFs and GAPs. Cell. Signal. *24*, 353-362.

Wu, M.; Melichian, D. S.; de la Garza, Mauricio; Gruner, K.; Bhattacharyya, S.; Barr, L.; Nair, A.; Shahrara, S.; Sporn, Peter H S; Mustoe, T. A.; Tourtellotte, W. G.; Varga, J.*, et al. (*2009). Essential roles for early growth response transcription factor Egr-1 in tissue fibrosis and wound healing. Am. J. Pathol. *175*, 1041-1055.

Yang, Y.; Goldstein, B. G.; Nakagawa, H.; Katz, J. P. (2007). Kruppel-like factor 5 activates MEK/ERK signaling via EGFR in primary squamous epithelial cells. The FASEB Journal *21*, 543-550.

Yeo, C.J.; Cameron, J. L.; Lillemoe, K. D.; Sohn, T. A.; Campbell, K. A.; Sauter, P. K.; Coleman, J.; Abrams, R. A.; Hruban, R. H. (2002). Pancreaticoduodenectomy with or without distal gastrectomy and extended retroperitoneal lymphadenectomy for periampullary adenocarcinoma, part 2: randomized controlled trial evaluating survival, morbidity, and mortality. Ann. Surg. *236*, 355-66; discussion 366-8.

Yoshitomi, H.; Zaret, K. S. (2004). Endothelial cell interactions initiate dorsal pancreas development by selectively inducing the transcription factor Ptf1a. Development *131*, 807-817.

Zhou, Q.; Law, A. C.; Rajagopal, J.; Anderson, W. J.; Gray, P. A.; Melton, D. A. (2007). A Multipotent Progenitor Domain Guides Pancreatic Organogenesis. Developmental Cell *13*, 103-114.

Zhu, N.; Gu, L.; Findley, H. W.; Chen, C.; Dong, J.-T.; Yang, L.; Zhou, M. (2006). KLF5 Interacts with p53 in Regulating Survivin Expression in Acute Lymphoblastic Leukemia. Journal of Biological Chemistry *281*, 14711-14718.

7 APPENDIX

7.1 VECTOR MAPS

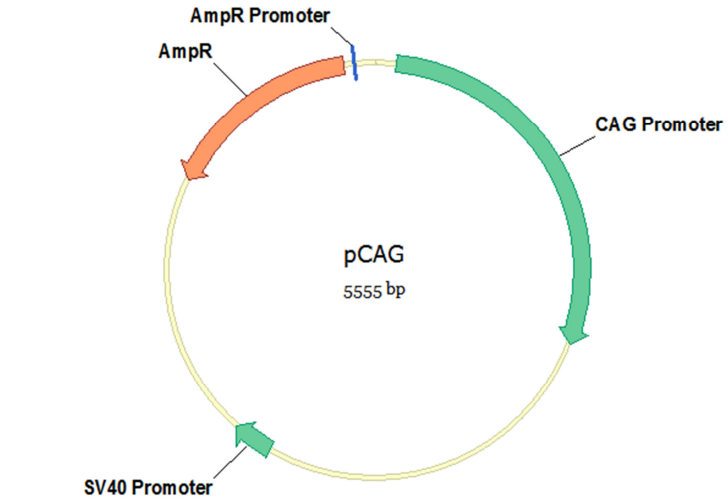

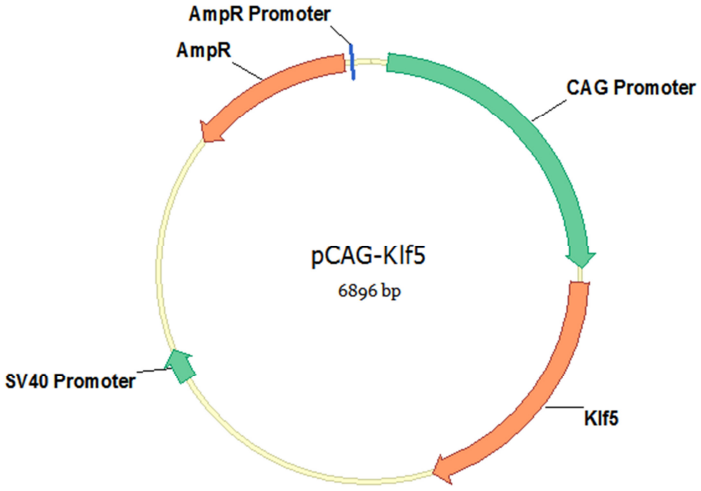

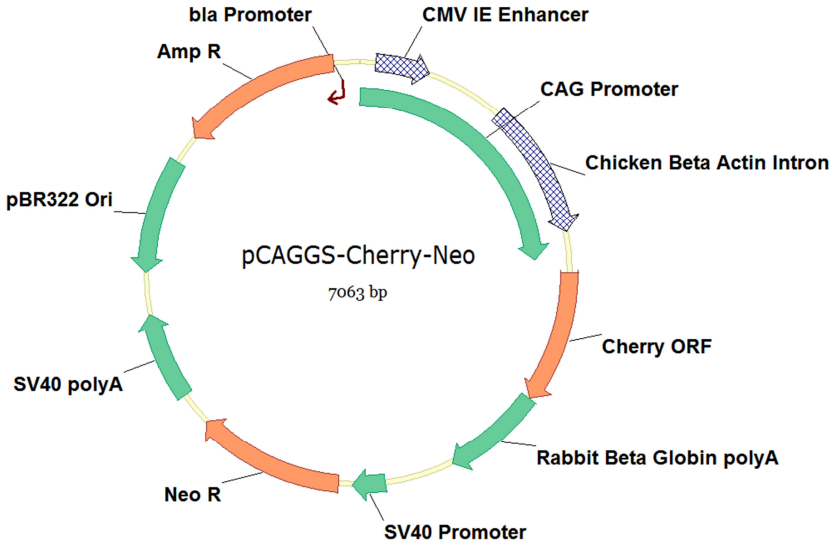

7.2 CHIP ASSAY SEQUENCES

7.2.1 EGR1 Binding Sites in *Egfr*

Name	Matrix	Start	End	C. Sim.	M. Sim.	Sequence
GXP_230968(Egfr/mouse)	V$EGR1.02	328	346	1,000	0,907	ggctctgggggcgagttct
GXP_230968(Egfr/mouse)	V$EGR1.04	477	495	0,881	0,876	gcgggaggaggagggacta

Table 7.1: EGR1 binding sites in *Egfr*. The core similarity (C. Sim.) evaluates the match of the target sequence and the core consensus sequence of EGR1. The matrix similarity (M. Sim.) evaluates the overall match of the target sequence and the consensus binding sequence of EGR1. A value of 1 equals 100 %.

Sequence GXP_230968:

```
  1 CCCGCCTCTG CCTGTGCTGT TGGAAACTGC TGCCAAGTCA GCCTGACCCT TCTGAGATCC
 61 TGGAGAAGTT ATGGAGAATA CGTGAACAGC GTCCCCACCT GTGTTATTCT CCAACCTGTG
121 CTCTGTGGTT GGACAGTTTG TAACCGAGGT GGTCCAGAGT TGTTTGGTTA ATTGAAAGAA
181 AGGAAGGAAG AAGGTGGGAG ACAGAGGGAA GGAAGGAGGG GACCCTGGCA TAGATTGGCT
241 GGACTTCCTA GGTCCTGAAA TGCAGCGGAG CGGAGTCCCC TCAGAAATTA ACTCCAAAGG
301 CCACCCACTG ACCCGCTGCA CACAGCCAGA ACTCGCCCCC AGAGCCTTGT CTAGTGGTGG
361 CCAAGGCCAT CCACCACCAC CTTCCGGTCA CTGCCTGCTT TCGATCCTCG CGGAGAGCGC
421 TTCCTCTCTC CTGACATTCT CCTCCTCTTC GCTCCTCTGG ATCCCTCCTC CTTCTTTAGT
481 CCCTCCTCCT CCCGCCCAGC CTCCCCCAGT CCCGACCCGA GCTAACTAGA CGTCTGGGCA
541 GCCCCAGCGC AACGCGCAGC AGCCTCCCTC CTCTTCTTCC CGCACTGTGC GCTCCTCCTG
601 GGCTAGGGCG TCTGGATCGA GTCCCGGAGG CTACCGCCTC CCAGACAGAC GACAGGTCAC
661 CTGGACGCGA GCCTGTGTCC GGGTCTCGTC GTTGCCGGCG CAGTCACTGG GCACAACCGT
721 GGGACTCCGT CTGTCTCGGA
```

Primers ChIP EGFR for / rev 1 Primers ChIP EGFR for / rev 2

7.2.2 EGR1 Binding Sites in *Ck19*

Name	Matrix	Start	End	C. Sim.	M. Sim.	Sequence
GXP_219993(Krt19/mouse)	V$EGR1.02	484	502	1,000	0,904	gtgggctggggcggggcag
GXP_219993(Krt19/mouse)	V$EGR1.02	620	638	1,000	0,883	tgttgaaggggcgggtatc
GXP_3065774(Krt19/mouse)	V$EGR1.04	378	396	0,881	0,888	ggaggaggaggaggaggcc
GXP_3065774(Krt19/mouse)	V$EGR1.04	381	399	0,881	0,883	ggaggaggaggaggaggag
GXP_3065774(Krt19/mouse)	V$EGR1.04	384	402	0,881	0,883	ggaggaggaggaggaggag
GXP_3065774(Krt19/mouse)	V$EGR1.04	387	405	0,881	0,883	ggaggaggaggaggaggag
GXP_3065774(Krt19/mouse)	V$EGR1.04	390	408	0,881	0,883	agaggaggaggaggaggag
GXP_3065774(Krt19/mouse)	V$EGR1.04	393	411	0,881	0,882	aggagaggaggaggaggag
GXP_3065774(Krt19/mouse)	V$EGR1.04	413	431	0,881	0,918	ggaggaggggaggagaag
GXP_3065774(Krt19/mouse)	V$EGR1.04	416	434	0,839	0,875	gaaggaggaggggaggag

Table 7.2: EGR1 binding sites in *Ck19*. The core similarity (C. Sim.) evaluates the match of the target sequence and the core consensus sequence of EGR1. The matrix similarity (M. Sim.) evaluates the overall match of the target sequence and the consensus binding sequence of EGR1. A value of 1 equals 100 %.

Sequence GXP_219993:

```
  1 TAGAGGTCTT GTTAAGTGCG TCTTGAGACT TGGGCAGGGA AGGGTGGAGG TGTCTTGGTG
 61 GGGGTGAGGG TCGAGTTTCT GAGCTGGGTC AGCCATGCTT CAGATTGAGC ATTTAGCAGG
121 AGTGTAAAGA AGCCACTTTG GTGGCCTAGT GTTCCCTGCA GCTGTACCTA TTGCCACCTA
181 GGACATTGTG GCAGCAGGGT GGGGCAACCT TGTCTCAGAA AGTCAGGAAG CCTGGAGCTT
241 AACTGCACGA ATTATTATCA CAAGGAGGGA GGGATTTATT AACATTATTC CAGAGGGGGC
301 ACTCTCAGAG TAAGTCACTG AGTTGGGGCT CAGAGGGGTG TGATTTCTAA GGGTGTCAAA
361 TTCCTGGAGG TTTTAAAGGG CCAGAGTGAT ATCGTCACTC CGGAAGTTAG AGTTGTCTAA
421 GCCTGTGTAG TAAGGGGCTG AAGGGCCAGA AAAGGGACGT GACATGTTGG CAGTAGCTTT
481 GGAGTGGGCT GGGGCGGGGC AGCTCTGGGA AGGACTGAGA CCTCTGGCTC CTGGGAGGGG
541 AGAGGTAGGA GCAGAATCGC CAGGAATTGA CCAATGGGGA AAGAGCCCAT ATTTGCACTC
601 TGGGAGCTTG GAAATTTCTG ATACCCGCCC CTTCAACATC TCCATCCCCC TTCCCGCCCC
661 GGGCATAAAA AGCCACAGGT GAGGGCCTTG TCACTCCTCC TGCGGCCAGC AGTTCTCAGA
721 CCTGCGTCCC TTTTTCCTTC GCTCTGGTCT CCCTCCTCAT CATGACTTCC TATAGCTATC
781 GCCAGACCTC AGCTATGTCT TCCTTTGGGG GTACGGGCGG GGGTTCAGTA CGCATTGGGT
841 CAGGGGGTGT TTTCCGCGCA CCC
```

Primers ChIP CK19 for / rev 1 Primers ChIP CK19 for / rev 2

Sequence GXP_3065774:

```
  1 GGAGAGTCTC CACGGGAGAG CCGGGCTTGG GAGGTGATCT TGGCTCTCTT CAGGAGGCAC
 61 GTGACCTCAG ACAACTCGCC TCGCTTCTCT GAGCCCTTGG ATTGGAGCAG CCTTTCCTGT
121 TGTTGGGAGG CTATTGTTAA GATTCACCAG ACAAAGGAGC CCATGGCCCT GTGTATTGGG
181 AAAATGTGAA TTAAACAGAG TTAGACAATA CTATTCGCGA TTATAATTAT GACAATCATA
241 TACTATTTAA TACTAATAAC ATTATATGAT AAAATAATAA TAACAAAGCA ATTTGAGTGG
301 TAACTATTAG CCAGGTGCTC TGATTAAGCC CTGCACAAGC ACATCCCATT GATTCCTTTA
361 AATAACGCCA TGAAACAGGC CTCCTCCTCC TCCTCCTCCT CCTCCTCTCC TCCTTCTCCT
421 CCCCCTCCTC CTTCTTCTCC TCCTCCTCAA TTTACAAATG AGACAAGTTT CCATGGCCTC
481 TAGTACTTGT GCATGGTAGA TTTAAAAGTC AGCTAGAGCC ACCAGTGTTA ACTCTTATGG
541 ACAAGTTCTT TCTCACAAGT TTCTCATCAC AGCTTTGTGT GTGTGTGTGT GGGGGGGGGG
601 T
```

Primers ChIP CK19 for / rev 3

Curriculum Vitae

Persönliche Daten

Name:	Thomas Briel
Geburtsdatum:	04.04.1984
Geburtsort:	Frankenberg (Eder)
Staatsangehörigkeit:	deutsch

Hochschulbildung

10/2011 – 2016 **Bachelorstudium Wirtschaftswissenschaften**
FernUniversität in Hagen

04/2010 – 02/2015 **Promotion zum Dr. rer. nat.**
Klinikum rechts der Isar der Technischen Universität München
Dissertation: *"The Role of EGFR / KRAS Downstream Targets MEK, EGR1 and KLF5 in Pancreatic Cancer Initiation and Progression"*

10/2007 – 11/2009 **Masterstudium Biologie**
Technische Universität München
Master Thesis: *"Conditional Porcine Cancer Models - Reporter Pigs in Biomarker Analysis"*

10/2004 – 08/2007 **Bachelorstudium Biowissenschaften**
Westfälische Wilhelms-Universität Münster
Bachelor Thesis: *„Velvet in Fusarium fujikuroi: Lokalisationsstudien und Molekulare Analysen zur Wirkungsweise des Globalen Regulators"*

Schulbildung

08/2000 – 06/2003 **Gymnasium Edertalschule, Frankenberg (Eder)**
Leistungsfächer: Mathematik und Physik
Abschluss: Allgemeine Hochschulreife

08/1994 – 06/2000 **Gymnasialzweig, Gesamtschule Battenberg**

Zivildienst

08/2003 – 05/2004 **Lebenshilfewerk Waldeck-Frankenberg e.V.**
Betreuung von Behinderten, Fahrdienst sowie Bürotätigkeiten

Danksagungen

Mein erster, ganz besonderer Dank gebührt Frau Prof. Angelika Schnieke, die meine akademische Entwicklung seit meinem ersten Studientag an der TU München begleitet hat. Neben Vorlesungen, Seminaren, einem Forschungspraktikum und meiner Masterarbeit hat sie sich sofort bereiterklärt, als meine Doktormutter meine Promotion zu betreuen. In diesem Zusammenhang auch noch einmal ganz besonderen Dank an den Lehrstuhl für Biotechnologie der Nutztiere, die mich noch immer herzlich mit Kaffee und guten Gesprächen empfangen wenn mich mein Weg dorthin führt.

Ganz herzlichen Dank an Prof. Dr. med. Jens Siveke für die Aufnahme am Klinikum rechts der Isar, die Möglichkeit, an der Schnittstelle zwischen Biologie und Medizin forschen zu können sowie eine diskussionsreiche Betreuung meiner Arbeit.

Vielen herzlichen Dank an Dr. Clara Lubeseder-Martellato für die Einführung in die Tücken der Azinusisolation und die besonders gute Zusammenarbeit während der Arbeit am Ardito & Grüner Paper. Die äußerst konstruktiven Diskussionen meiner *Egr1* Ergebnisse sowie die wissenschaftliche Begeisterung darüber waren oft sehr motivierend.

Der größte Dank gebührt meinen Freunden in der Heimat sowie meinen „Laborfreunden“ Christin, Nicole, Marc und Anja für die schöne Zeit, die moralische Unterstützung, Feiern, Biergartenbesuchen, Schlagergarten, Zwischenfällen auf großen Schnecken und Kaffeetrinken. Das „Triumvirat“ wird mir hierbei in besonderer Erinnerung bleiben.

Besonderer Dank ebenfalls an meinen Freund Florian für seine immerwährende Unterstützung, seinen Rat und sein Verständnis für komplexe Promotionsprobleme.

Vielen Dank außerdem an meine gesamte Arbeitsgruppe für die gute Zusammenarbeit während der letzten 4 ½ Jahre.

Des Weiteren vielen Dank an meine ganze Familie, meinen Vater Horst und meine Mutter Monika für die moralische Fernunterstützung per Telefon und bei meinen Heimatbesuchen, sowie meinem Bruder Matthias für seine Unterstützung und seine herzlichen Empfänge daheim.

Hiermit versichere ich, dass ich die vorliegende Dissertation selbst, sowie ausschließlich unter Verwendung der angegebenen Hilfsmittel und Quellen erstellt habe. Diese Dissertation wurde weder ganz noch teilweise für eine Prüfung an einer anderen Hochschule eingereicht.

Thomas Briel

München, 07.07.2014